

An Analysis of the Sailing Efficiency of the Junk Yacht *Boleh*: Individual Research Project

Jonathan Happs

(4) 23268743

2013

Abstract

The Junk Yacht *Boleh*, designed and built by Cmdr. R.A. Kilroy DSC RN in 1949, is currently undergoing a major restoration in Portsmouth, UK. This is being organised by a charity set up for the purpose, the *Boleh* Trust. Consequently there is renewed interest in this historic vessel, and particularly in her unique original rig and sail plan. This report provides an assessment of the efficiency and efficacy of this rig through comprehensive wind tunnel testing of a model at 5:31 of full scale, in the University of Southampton's 7'x5' wind tunnel.

From the investigations full scale global loads on the rig are presented for a range of wind speeds representing a likely operational envelope for the vessel. Issues with the design of the rig are identified and discussed, and the results are compared against data from literature for alternative rig designs. Provisional optimum sailing attitudes are presented, along with approximate predictions of the speed of the vessel under sail. The results are concluded to be of reasonable accuracy.

Additional investigations of the interaction between multiple lifting surfaces are undertaken using Computational Fluid Dynamics (CFD).

This report is submitted in partial fulfilment of the requirements for the Degree of
Master of Engineering, Faculty of Engineering and the Environment
University of Southampton

Project academic supervisor:
Professor P. A. Wilson BSc CEng DSc FRINA

Contents

| | | |
|----------|---|-----------|
| 1 | Introduction | 1 |
| 1.1 | Overview of the project | 1 |
| 1.2 | Exploration of the question | 1 |
| 1.3 | Structure of the project and report | 2 |
| 2 | Theoretical background and literature review | 2 |
| 2.1 | Introduction | 2 |
| 2.2 | Introduction to aerofoil theory | 4 |
| 2.2.1 | Lift and Drag | 4 |
| 2.2.2 | Flow around an object | 5 |
| 2.3 | Geometry and Physics of Yacht Sailing | 6 |
| 2.3.1 | Drive force from sails | 7 |
| 2.3.2 | 2D sail shape | 8 |
| 2.3.3 | Flow over sails | 8 |
| 2.3.4 | Constraints of Finite Sails | 8 |
| 2.3.5 | Interaction between sails | 9 |
| 2.4 | Scaling methods | 11 |
| 2.5 | Sail types and preliminary estimates | 13 |
| 3 | Wind tunnel experiments | 17 |
| 3.1 | Aims of the Investigations | 17 |
| 3.1.1 | Identifying optimum sailing conditions | 17 |
| 3.1.2 | Estimating forces on the rig | 17 |
| 3.1.3 | Identifying issues in the design | 18 |
| 3.2 | Preparation for the experiments | 18 |
| 3.2.1 | Construction of the model | 18 |
| 3.2.2 | Planning of the experiments | 19 |
| 3.3 | Experimental procedure and results | 19 |
| 3.3.1 | Theoretical investigations | 25 |
| 3.4 | Conclusions of the wind tunnel experiments | 26 |
| 4 | Numerical investigations | 28 |
| 4.1 | Aims of the Numerical Investigations | 28 |
| 4.2 | Procedure and results of the experiments | 28 |
| 4.3 | Conclusions of the numerical investigations | 32 |
| 5 | Conclusions | 33 |
| 6 | Further work | 34 |
| 7 | Bibliography | 35 |

| | | |
|----------|---|-----------|
| A | Appendices | 38 |
| A.1 | Computational fluid dynamics | 38 |
| A.1.1 | Introduction | 38 |
| A.1.2 | Basic theory | 38 |
| A.1.3 | RANS CFD | 38 |
| A.1.4 | Turbulence models | 40 |
| A.2 | Time plan | 41 |
| A.3 | Experimental model | 41 |
| A.3.1 | Heel angle derivation | 43 |
| A.3.2 | Derivation of heeling moment | 44 |
| A.3.3 | Sail area calculation | 50 |
| A.3.4 | Images of wind tunnel model construction | 50 |
| A.4 | Physical experiment planning and data | 55 |
| A.4.1 | Calculation of Reynolds numbers for the heel program | 55 |
| A.4.2 | Justification of mismatched Reynolds numbers in the physical experiments | 56 |
| A.4.3 | Testing matrix for the experiments | 57 |
| A.4.4 | Notes on use of the equipment and calibration | 59 |
| A.4.5 | Plots of experimental data | 64 |
| A.4.6 | Comparative plots of theoretical and experimental data | 89 |
| A.5 | Computational fluid dynamics experiments | 92 |
| A.5.1 | Notes on conducting experiments using computational fluid dy- namics | 106 |
| A.5.2 | Global force data | 109 |
| A.6 | Glossary | 111 |

Word Count:

9621

List of Figures

| | | |
|----|--|----|
| 1 | Structures of the project and report | 3 |
| 2 | Diagram of lift components | 4 |
| 3 | Lift vectors over a two dimensional wing | 5 |
| 4 | Forces on a 2D aerofoil | 5 |
| 5 | Development of the boundary layer over a sail | 6 |
| 6 | Diagram of the vector components of sail force | 7 |
| 7 | Lift vectors over a three dimensional wing | 9 |
| 8 | Diagram of vortices shed from a 3D aerofoil | 9 |
| 9 | Diagram of circulation around interacting sails | 10 |
| 10 | Diagram of pressure distribution around sails | 10 |
| 11 | Diagram of streamlines around sails | 11 |
| 12 | Changing flow regimes with increasing Reynolds number | 13 |
| 13 | Bermudan rigged sailing yachts racing in the Solent, author's photo . . | 14 |
| 14 | <i>Boleh</i> sailing with her original rig | 15 |
| 15 | A Junk rigged ship | 15 |
| 16 | Variation of lift and drag coefficients with aspect ratio | 16 |
| 17 | Plot showing the effect of turbulent transition on the Lift and Drag . . | 21 |
| 18 | The model during testing | 22 |
| 19 | Sail deformation due to wishbone battens | 24 |
| 20 | Issues with the sheeting angle of the jib | 25 |
| 21 | Sail plans used in the data in Fig.41 | 26 |
| 22 | An example test envelope | 27 |
| 23 | Mesh used for CFD investigations | 28 |
| 24 | An example of CFD | 39 |
| 25 | Gant chart of tasks for this project | 42 |
| 26 | Estimated graph of heel angle against wind speed | 44 |
| 27 | Lines plan of the Junk Yacht <i>Boleh</i> | 50 |
| 28 | Producing the initial components of the model | 52 |
| 29 | Assembly and fairing of the hull | 52 |
| 30 | Finishing the hull | 53 |
| 31 | The original design of <i>Boleh's</i> rig | 53 |
| 32 | Sail components | 54 |
| 33 | The author inspecting the model prior to testing | 54 |
| 34 | Comparison of true and apparent wind angles | 59 |
| 35 | Schematic of the dynamometer set up used in the experiments | 60 |
| 36 | Connection between model and dynamometers | 60 |
| 37 | Experimental setup for the physical experiments, upright condition . . | 61 |
| 38 | Control lines and detailed rig modelling | 62 |
| 39 | Calibration of the experimental equipment | 63 |

| | | |
|----|--|----|
| 40 | Approximate polar velocity plot | 64 |
| 41 | Test envelopes for comparison of the results | 65 |
| 42 | Plot of close-hauled condition | 66 |
| 43 | Plot of close-hauled condition | 66 |
| 44 | Plot of close-hauled condition | 67 |
| 45 | Plot of close-hauled condition | 67 |
| 46 | Plot of on-wind condition | 68 |
| 47 | Plot of on-wind condition | 68 |
| 48 | Plot of on-wind condition | 69 |
| 49 | Plot of fetching condition | 69 |
| 50 | Plot of fetching condition | 70 |
| 51 | Plot of fetching condition | 70 |
| 52 | Plot of off-wind condition | 71 |
| 53 | Plot of off-wind condition | 72 |
| 54 | Plot of off-wind condition | 72 |
| 55 | Plot of close-reach condition | 73 |
| 56 | Plot of close-reach condition | 73 |
| 57 | Plot of close-reach condition | 74 |
| 58 | Plot of reaching condition | 74 |
| 59 | Plot of reaching condition | 75 |
| 60 | Plot of reaching condition | 75 |
| 61 | Plot of downwind condition | 76 |
| 62 | Plot of downwind condition | 76 |
| 63 | Plot of downwind condition | 77 |
| 64 | Heeled, AWA 20 degrees | 78 |
| 65 | Heeled, AWA 20 degrees | 79 |
| 66 | Heeled, AWA 20 degrees | 79 |
| 67 | Heeled, AWA 30 degrees | 80 |
| 68 | Heeled, AWA 30 degrees | 80 |
| 69 | Heeled, AWA 30 degrees | 81 |
| 70 | Heeled, AWA 40 degrees | 81 |
| 71 | Heeled, AWA 40 degrees | 82 |
| 72 | Heeled, AWA 40 degrees | 82 |
| 73 | Heeled, AWA 50 degrees | 83 |
| 74 | Heeled, AWA 50 degrees | 83 |
| 75 | Heeled, AWA 50 degrees | 84 |
| 76 | Heeled, AWA 60 degrees | 84 |
| 77 | Heeled, AWA 60 degrees | 85 |
| 78 | Heeled, AWA 80 degrees | 86 |
| 79 | Heeled, AWA 80 degrees | 87 |

| | | |
|-----|--|-----|
| 80 | Heeled, AWA 100 degrees | 87 |
| 81 | Heeled, AWA 100 degrees | 88 |
| 82 | Heeled, AWA 120 degrees | 88 |
| 83 | Heeled, AWA 120 degrees | 89 |
| 84 | Comparison of driving forces with theory | 90 |
| 85 | Comparison of lift coefficient with theory | 90 |
| 86 | Comparison of Drag coefficient with theory | 91 |
| 87 | Mesh dependency analysis | 92 |
| 88 | Plot of transverse velocity against span wise position over a foil | 92 |
| 89 | Comparison of pressures along three streamlines | 95 |
| 90 | Detail of meshing in the slot between foils, base case | 96 |
| 91 | Detail of meshing in the slot between foils, configuration 2 | 96 |
| 92 | Detail of meshing in the slot between foils, configuration 4 | 97 |
| 93 | Cross section of the moderate-fine mesh | 97 |
| 94 | Cross section of pressures at mid span, configuration 1 | 98 |
| 95 | Cross section of pressures at half span, configuration 1 | 98 |
| 96 | Cross section of pressures at full span, configuration 1 | 98 |
| 97 | Cross section of pressures at mid span, configuration 2 | 99 |
| 98 | Detail of pressure difference within a slot | 99 |
| 99 | Cross section of pressures at full span, configuration 3 | 100 |
| 100 | Cross section of pressures at full span, configuration 4 | 100 |
| 101 | Cross section of pressures at mid span, control configuration | 101 |
| 102 | Cross section of velocities at mid span, configuration 1 | 101 |
| 103 | Comparison of wing tip vortices visualised using streamlines | 103 |
| 104 | Cross section of transverse velocities at mid span, configuration 1 | 104 |
| 105 | Cross section of transverse velocities at half span, configuration 1 | 104 |
| 106 | Cross section of transverse velocities at full span, configuration 1 | 105 |
| 107 | Cross section of transverse velocities at 120% of full span, configuration 1 | 105 |
| 108 | Isometric view of the unstructured mesh geometry | 106 |
| 109 | Cross section of unstructured mesh with sails visible | 107 |
| 110 | Issues meshing sails | 107 |
| 111 | Sails in a block mesh | 108 |
| 112 | Block mesh incoherence | 108 |
| 113 | Diagram of the parts of a sail | 110 |

List of Tables

| | | |
|----|--|-----|
| 1 | Overall dimensions of the wind tunnel model | 19 |
| 2 | Matrix of optimum sailing angles | 22 |
| 3 | Systematic variations in position of the lower foil | 29 |
| 4 | Main area derivation. Factor refers to the model-full scale conversion . | 51 |
| 5 | Jib area derivation | 51 |
| 6 | Main centroid derivation | 51 |
| 7 | Jib centroid derivation | 51 |
| 8 | Reynolds numbers at various wind speeds | 56 |
| 9 | List of fundamental physical units | 56 |
| 10 | Matrix of test conditions | 58 |
| 11 | Table of average global forces on the rig | 109 |

Nomenclature

| | | |
|--------------|-------|--|
| $^{\circ}$ | | angle in degrees |
| ∞ | | designates a property of undisturbed flow |
| μ | | dynamic viscosity |
| ρ | | fluid density |
| A | | area |
| A_F | | sheeting angle of the foresail (jib) |
| A_M | | sheeting angle of the mainsail |
| AR | | aspect ratio, of height squared to area |
| AWA | | Apparent Wind Angle |
| C | | chord length used to non-dimensionalise the geometry of the CFD experiments |
| C_F | | force coefficient, see Section 2.4 |
| h | | height |
| knt | | abbreviation for knots, nautical miles per hour |
| ms^{-1} | | meters per second |
| l | | length |
| L | | length dimension |
| M | | mass dimension |
| M_a | | the Mach number, see Section 2.4 |
| N | | Newtons of force |
| p | | static pressure |
| R_N | | the Reynolds number, see Section 2.4 |
| T | | time dimension |
| U | | flow speed |
| x_{centre} | | distance from centroid of area to origin |
| x_{mmt} | | moment arm in the x direction |
| y^+ | | a non-dimensional factor critical in insuring accurate representation of boundary layer phenomena in CFD simulations |
| y_{centre} | | distance from centroid of area to origin |
| y_{mmt} | | moment arm in the y direction |

Acknowledgements

The author is indebted to many people for the successful completion of this work, not least the *Boleh* Trust, who commissioned the work and have been helpful and generous throughout the process. Particular thanks go to the Directors and staff of the Trust, and to Graham Westbrook, for their advice, patience and the loan of many documents which were hugely important in beginning the research.

The author would like to thank Professor Wilson for his advice, support and guidance as academic supervisor for the project. Others at the University whose assistance has been invaluable include Dave Cardwell, Dave Marshall and Andrew Claughton at the Wolfson Unit, without whose assistance the wind tunnel experiments could not have been a success, and the many research assistants at the Department of Ship Science who gave up their time to advise on the mysteries of Computational Fluid Dynamics.

Additional thanks must go to the online L^AT_EX community, without whom this report would have been considerably less readable.

Finally, thanks to the author's family and friends for their support and assistance in so many ways throughout the project.

“Dealing with the theory of yacht behaviour is risky. . . sailing boats naturally belong to the fair sex and are, therefore, largely unpredictable, their behaviour being very difficult to analyse indeed.”

C.A. Marchaj, *Sailing Theory and Practice* 1964

1 Introduction

1.1 Overview of the project

This report focusses on obtaining estimations, through the use of scale experiments in a wind tunnel, of the forces that can be expected from the full scale sailing rig of the Junk Yacht *Boleh*. This data is crucial when designing appropriate scantlings for the yacht, and in estimating the speeds and distances that might be achieved by the vessel in particular conditions. This latter information has implications on classification, and on the operational profile, impacting on stores, auxiliary power provision, and numerous other factors.

It is hoped that this information will be of value to the *Boleh* Trust in a number of ways, ranging from the ongoing design of the vessel during restoration, to finding a suitable operational profile for the vessel and planning voyages during her future work as a Sail Training vessel. Accordingly, parts of this report are worded in such a way that it is intended to be accessible to those with less theoretical background. The information may also be of use to other parties interested in sail design or in this unique rig in particular, in that it provides the first known fully scientific investigation into the efficacy of this design.

In this work it is fortunate that parallel work is being undertaken to establish the hydrodynamic resistance of the vessel. It has therefore been possible to validate the results of the experiments against approximate measurements taken aboard the vessel when sailing prior to the restoration, using a similar sail plan, in addition to comparison with data on alternative rigs taken from literature.

1.2 Exploration of the question

In the initial stages of the project four aims were identified;

1. Conduct an investigation into the underlying physics of sailing, and produce a literature review of the results.
2. Produce a physical scale model of the hull and original rig, test this in a wind tunnel to identify the best sailing attitudes and estimate the induced forces at full scale.
3. Investigate the practicalities of the designed rig. Note and analyse any practicality issues that are identified during the tests.
4. Undertake CFD and other investigations to validate the results of the wind tunnel experiments.

In February 2012 the University of Southampton was approached by the *Boleh* Trust to answer a series of questions about the eponymous vessel, which is under restoration by the Trust. A number of meetings were arranged, in which the key questions, summarised in the second and third points above, were identified and selected for investigation.

In order to investigate the full scale forces, it was decided that the author should produce an accurate, physical scale model of the vessel and subject it to testing in a wind tunnel. From these observations, measurements could be made to answer the issues raised. This method also allowed investigation of the third point, practical issues within the design, in the way that only physical models can achieve.

1.3 Structure of the project and report

In order to promote understanding of the development and structure of the project, a PERT chart is presented in Fig.1 showing the main aspects of the investigation, ranked in chronological order. A flow chart of this report is also shown for clarity. Clear identification of the aims and requirements of the project were key to maintaining logic and order in the results, and it is hoped that this figure will aid comprehension of the report and its conclusions.

In addition to the information in this report, a CD is provided containing all source files, data, and programs listed, used or produced in the production of this work, along with plots and images. Therefore it is considered unnecessary to reproduce large quantities of data within the report, and that which is given is heavily condensed.

2 Theoretical background and literature review

2.1 Introduction

The majority of sailing craft, including *Boleh*, have their sails arranged in a ‘fore and aft’ rig. Various types of rig exist, with different characters, but the basic principles remain the same.

To allow the craft to move towards the wind, each individual sail is designed to act as an aerofoil, in that they produce a suction force called lift, which pulls the craft forwards. The sails must be set at an angle of attack to the incident airflow (wind), generating lift and drag, which are perpendicular and parallel to the airflow respectively. This is shown in Fig.2. These force vectors can then be resolved into components parallel and perpendicular to the direction of travel. The keel produces a reaction against the side force, and the forward force drives the boat. At angles

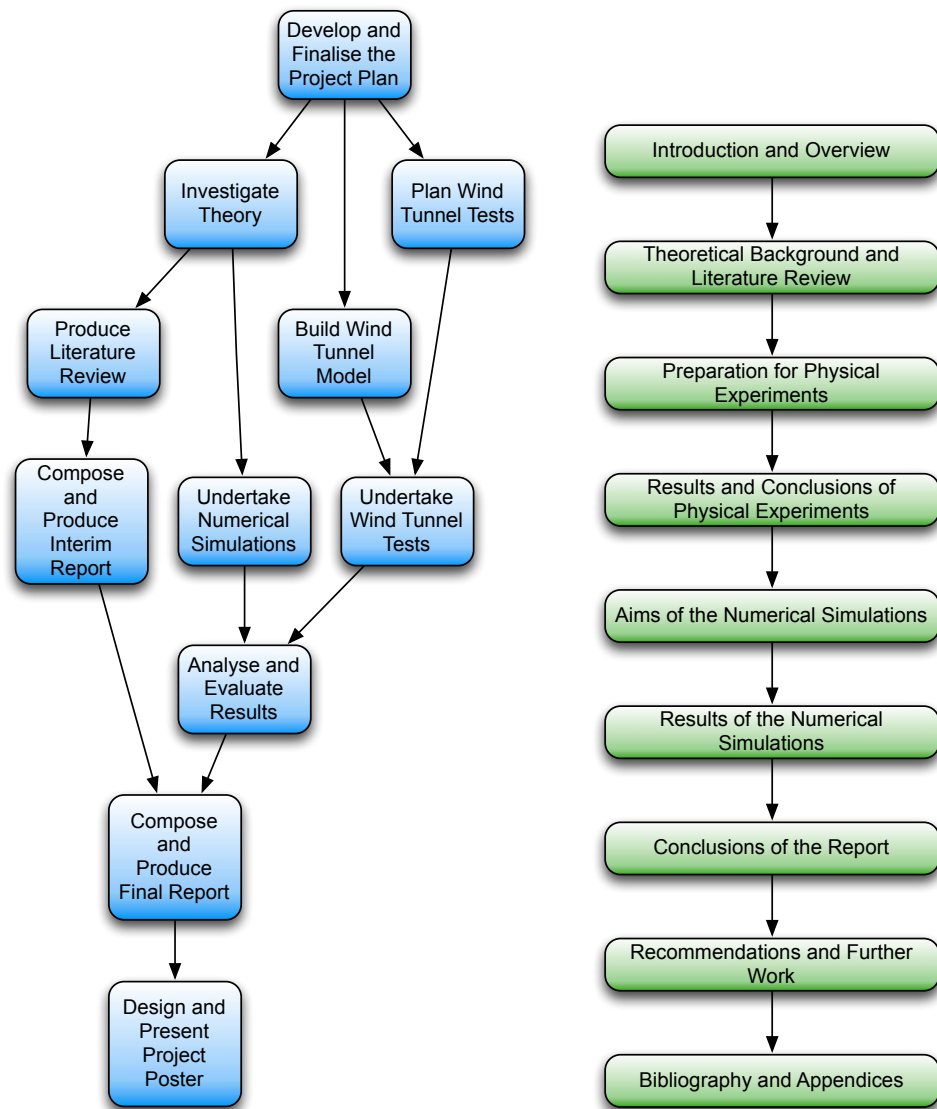


Figure 1: In blue, a PERT chart for major aspects of the project, and in green a flow diagram of the structure of this report

between 45° and 135° of the true wind angle, the forward force is mostly lift. (Slight, 1999) At angles of $135^\circ \rightarrow 180^\circ$, the sail acts as a virtually pure drag device. Since the sail generates lift at right angles to the flow, it cannot pull directly into the wind. However, most vessels can proceed in any direction outside of $\pm 45^\circ$ of the true wind.

Clearly then, to understand more about *Boleh's* rig it is necessary to have some understanding of aerofoils.

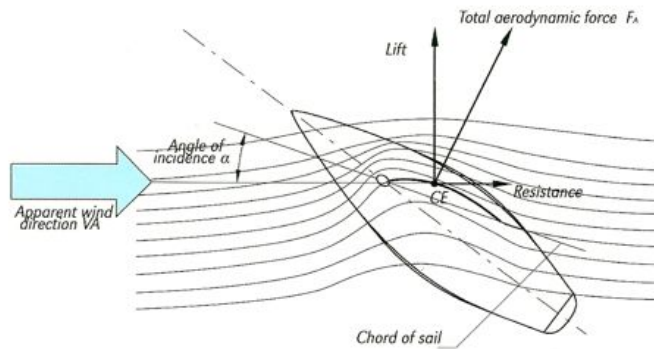


Figure 2: Diagram of lift components, taken from Fossati (2009)

2.2 Introduction to aerofoil theory

2.2.1 Lift and Drag

Imagine you could see the direction of flow in a fluid as a series of paths moving through space. These are called streamlines. As the fluid flows around an object due to relative motion, the streamlines are bent, to allow the object through. From Newton's laws of motion, this change in direction requires a force on the fluid, and hence produces an equal and opposite force on the object, which is experienced as pressure. Clearly, for a streamline to describe some section of a circular arc, a constant force is required, resulting in suction towards the 'outside' of the arc, and 'pressure' towards the centre. The tighter the radius of the arc, the greater the pressure force. (Larsson, 2013)

From the diagram of streamlines shown in Fig.3 it can be seen that the flow must curve away at the nose of the aerofoil, producing a pressure force. It must then curve back towards the foil further down the length, (or 'chord') of the object, resulting in a suction force. The relative pressure at every point on the surface produces a force, each infinitesimal force with its own magnitude and direction. This is shown in the lower diagram in Fig.3. The sum of these can be considered as a single 'aerodynamic force', acting at a point known as the 'centre of pressure', and this is what we see acting on the object. (Kay, 1971)

Aerofoils have a net circulation of flow around them, ie. the flow is faster over one

surface than the other. Therefore the acceleration, and hence the decrease in pressure is greater on one side than the other, resulting in a component of the net force perpendicular to the flow. This is the lift, as shown in Fig.4. Circulation can be achieved by positioning the object at an ‘angle of attack’ to the flow, or by designing the object to be asymmetrical on a plane perpendicular to the lift direction. Most commonly it is a combination of both.

The presence of the object in the flow causes additional drag due to viscosity, (Kay, 1971) acting in the plane of the flow. The resulting force vectors are shown in Fig.4.

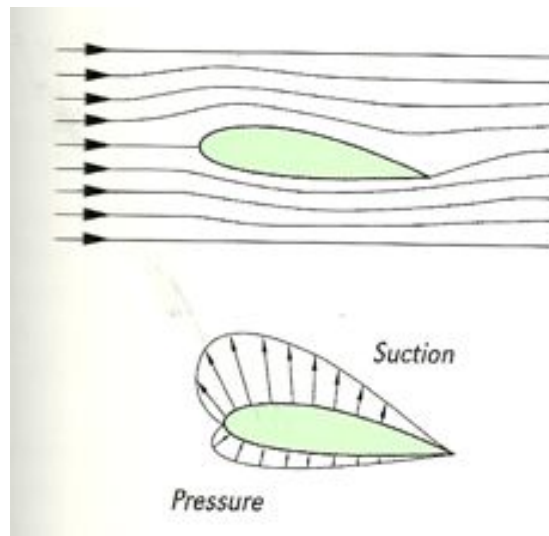


Figure 3: Lift vectors over a two dimensional wing, taken from Fossati (2009)

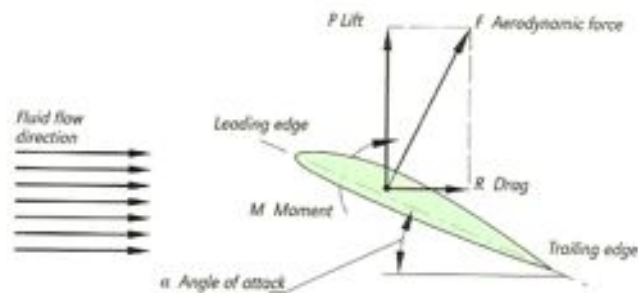


Figure 4: Forces on a 2D aerofoil, taken from Fossati (2009)

2.2.2 Flow around an object

Close to any object, the fluid flow U must be zero. The region of varying flow between the object and the ‘ordinary’ free stream flow U_∞ , is called the boundary layer. In most cases, the outer edge of the boundary layer is considered to be when $U = 0.9U_\infty$

Boundary layers can be either laminar, (where the flow is parallel to the surface, and the velocity increases smoothly with distance h from the surface) or turbulent. Turbulence is “highly erratic flow, in which a mass of small eddies are present in a

flow field, with velocities varying rapidly in space and time.” (Claughton et al., 2006). Flow over an object is normally assumed to begin as laminar, with rises in pressure (termed ‘adverse pressure gradient’), sudden changes in shape, and roughness in the surface all serving to ‘trip’ the boundary layer into turbulence. The additional flows due to turbulence absorb energy, increasing drag.

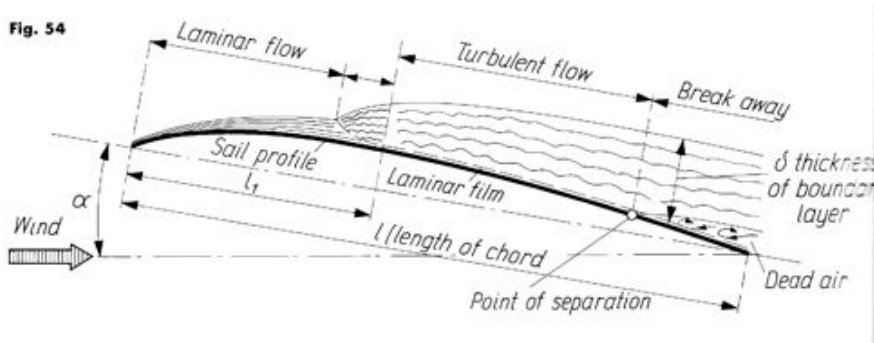


Figure 5: Development of the boundary layer over a sail, taken from Marchaj (1964)

Additionally, the flow over an object may separate, which is a different phenomenon. Large adverse pressure gradients cause the flow to detach completely from the object, the gap being filled by ‘recirculating’ air, which sometimes travels in the opposite direction to the free stream. (Claughton et al., 2006) Due to the more complex velocities involved, any flow generally becomes turbulent once separated. The typical development of a boundary layer through these phenomena is shown in Fig.5.

Increasing lift on a foil means increasing the difference between the extremes of pressure, and so leads to more severe pressure gradients. This leads to the instigation and growth of separated flow on the low pressure (upper) surface. Since the strength of the adverse pressure gradient required to cause separation from an aerofoil decreases with increasing distance from the leading edge, separation generally begins at the trailing edge. It can however be instigated from the leading edge in thin, highly cambered aerofoils, such as sails. As the flow separates further, the lift reaches a maximum, before falling off sharply with a simultaneous and large increase in drag. (Claughton et al., 2006) The foil is now ‘stalled’, with no connection to the pressure field which generated its lift.

2.3 Geometry and Physics of Yacht Sailing

Yachts move through a balance of aerodynamic and hydrodynamic forces. The sails and keel both generate lift, which combine to drive the boat forwards, not just in the direction of the wind. A full description of the forces involved is beyond the scope of this work, but the basics are covered below.

2.3.1 Drive force from sails

When pointing to windward, sails are designed to act as aerofoils, producing lift and drag. The resultant of these forces has a component in the forward direction, which provides the drive. (Campbell, 1997) This drive force is the summation of a number of vectors as shown in Fig.6.

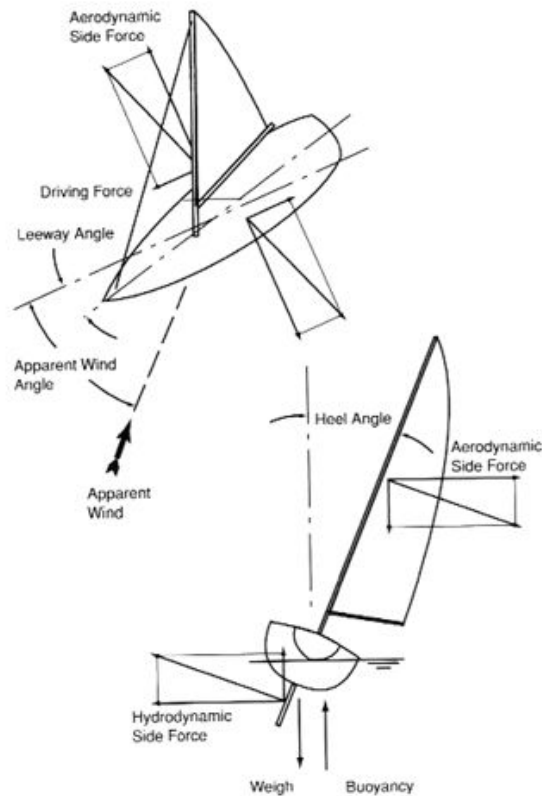


FIGURE 15.14 Force systems acting on a sail boat.

Figure 6: Diagram of the vector components of sail force, taken from Barlow et al. (1999)

The lift acting on the sails can be resolved into forward and lateral components, along the direction of travel. As the vessel is pulled through the water by the forward component, it slips sideways because of the lateral component. This slip, called leeway, causes an angle of attack between the keel and the water. Consequently, the keel also acts as an aerofoil, producing lift and drag again resolved into forward and lateral components. These, along with the drag of the hull, counteract the sails. The result is dynamic balance, with the vessel having forward motion at an angle of leeway to the centreline of the yacht. (Marchaj, 1964)

Because the aerodynamic force acts on the sails, above the centre of gravity, and the hydrodynamic force acts on the keel which is below it, there is a moment acting to roll the yacht. As a vessel rolls, its centre of buoyancy moves, but its centre of mass does not. This provides the couple which maintains a balanced angle of heel. (Marchaj, 1964)

2.3.2 2D sail shape

Sails act as an aerofoil of negligible thickness. Since the range of angles of attack at which an aerofoil can be efficiently operated is dependent on the radius of the leading edge of the foil, (Claughton et al., 2006) sails are particularly sensitive to angle of attack. However, most sails have an advantage over other aerofoils in that, being soft, they flex automatically to an extent, which can account for small variations in angle of attack, for example in different areas of the sail.

Varying the camber, or ‘belly’ of a sail alters the lift and drag generated, as discussed by Fossati (2009). A yacht’s crew can therefore take advantage of the flexible nature of sails to alter the properties of their ‘aerofoil’ manually to suit the conditions, for example, reducing camber to improve lift at high angles of attack, or increasing camber to increase lift off the wind.

2.3.3 Flow over sails

There are a number of limitations placed on sails by practical design, particularly support. Sails must be supported vertically in order to catch the wind, generally in the form of a mast at their leading edge. This bluff body induces very early onset turbulence and often significant separation at the leading edge of the sail, on the downwind (low pressure) side, leading to a reduction in efficiency. (Kay, 1971). However, Claughton et al. (2006) note that this flow can re-attach, and the resulting separation ‘bubble’ need not adversely affect performance. Indeed, as discussed in section 2.2.2, maximum lift is achieved when some separation is present in the flow, at less than the critical level. A small amount of separation can therefore sometimes result in improved performance, discussed in greater detail by Wellicome (2012).

2.3.4 Constraints of Finite Sails

As with any foil, the finite length of sails has implications which limit its performance. Since any non-infinite foil has ends, the pressure difference producing the lift is able to ‘leak’ from the windward (high pressure) side, to the leeward side. Consequently, there is a pressure gradient along the span of the foil on both surfaces, and some component of the flow over each surface is directed outward from the centre on the windward face, and towards the leeward centre. (Claughton et al., 2006) This change in direction disturbs the flow, reducing lift away from the centre of the foil, as shown in Fig.7.

The transverse flow reaches maximum velocity at the tips, the head and foot in the case of a sail, and the resulting circulation results in vortices being shed, as shown

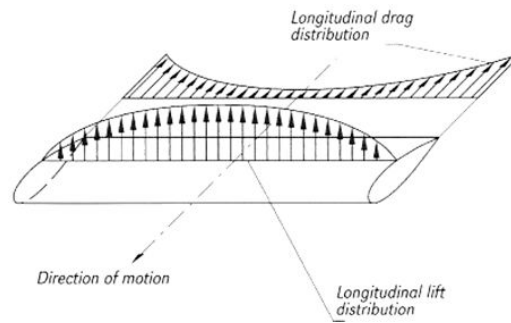


Figure 7: *Lift vectors over a three dimensional wing, taken from Fossati (2009)*

in Fig.8. These create considerable ‘induced’ drag, due to the energy dissipated. (Marchaj, 1964)

Additionally, there is a net flow over the trailing edge, or leech of the sail towards the low pressure face, called upwash. This is a manifestation of the circulation which produces the lift. In effect, this circulation reduces the angle of incidence of the local flow compared to that of the free stream far from the foil, which has the effect of rotating the lift angle. (Claughton et al., 2006) A component of lift is therefore now in the downstream direction, and is effectively additional ‘induced drag’. The maximum efficiency now attainable is for the total induced drag to equal the profile (pressure) drag. (Claughton et al., 2006) As the lift increases from this case, the induced drag increases far in excess of the 2D profile drag, and consequently the efficiency ratio of lift to drag reduces markedly.

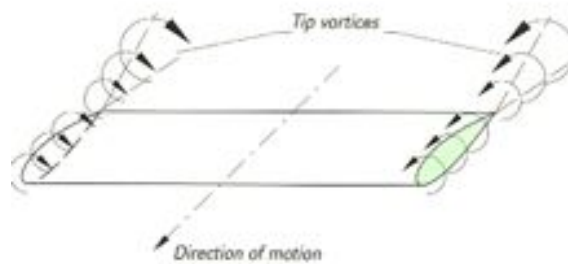


Figure 8: *Diagram of vortices shed from a 3D aerofoil, taken from Fossati (2009)*

2.3.5 Interaction between sails

Sails set in close proximity to each other will both act in air flow modified by the presence of the other sail(s), due to the circulation effects discussed above. The angle of attack of the forward sails is increased, but that of the sail(s) aft is reduced, reducing the efficiency of those sails.

An apparently separate effect is that, if the sails are close together, the flow from the forward sail will reduce separation on the aft. (Claughton et al., 2006) Early

CFD experiments conducted by Gentry (1973) with an analogue field plotter showed that both effects can be understood by examining the circulation around the sails, disproving the popular ‘Venturi effect’ theory of the ‘slot effect’.

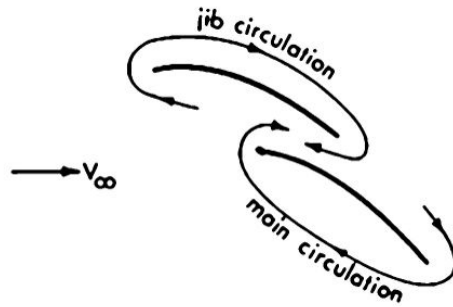


Figure 9: Diagram of circulation around interacting sails, taken from Gentry (1973)

The circulation around the leading and trailing sails oppose in the slot, leading to a local increase in pressure, and decrease in flow rate, as shown in Fig.9. In theory, this should increase the pressure on the low pressure side of the main, reducing its efficiency. However, in real life the pressure peak at this point is so high and sudden due to the thinness of the sail (Fig.10) that the flow generally separates at otherwise good angles of attack. The interaction with the jib delays the onset of separation along the chord of the mainsail, increasing the available lift. (Claughton et al., 2006) Thus the mainsail is more efficient in the presence of the jib than without it. Meanwhile, the pressure is increased on the windward face of the jib, increasing its efficiency.

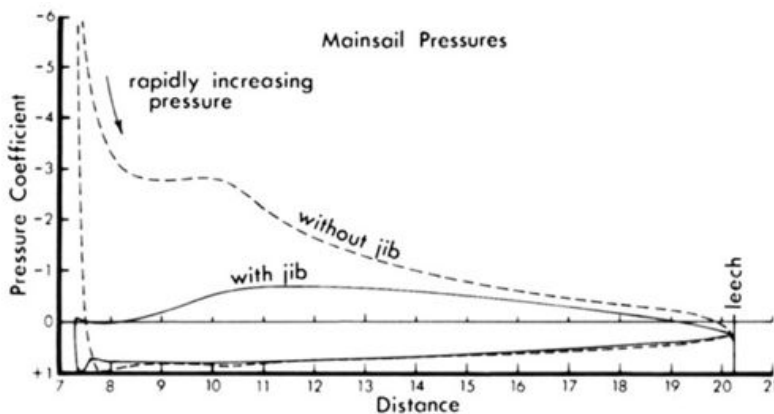


Figure 10: Diagram of the pressure distribution on a main/jib arrangement overlaid on those of a single sail, taken from Gentry (1973)

As can be seen from Fig.11, a very simple way to visualise this is that the two sails combine to form one large one, at a higher angle of attack. However, were a single sail used in this position, it would stall. The slot delays the onset of separation, increasing lift without destroying the air flow. This effect is used to great effect in the take off and landing flaps of aircraft, which can often be seen when flying in a commercial airliner.

The key practical implications of this for sailors are given by Kay (1971) and Gentry

(1973), summarised as follows:

- The Genoa sheeting angle has little effect on the heeling force but causes a considerable decrease in drive if set too hard.
- The Mainsail sheeting angle has little effect on the drive force but considerably increases the heeling force if set too hard. Hence one should spill wind from the mainsail to reduce heel.

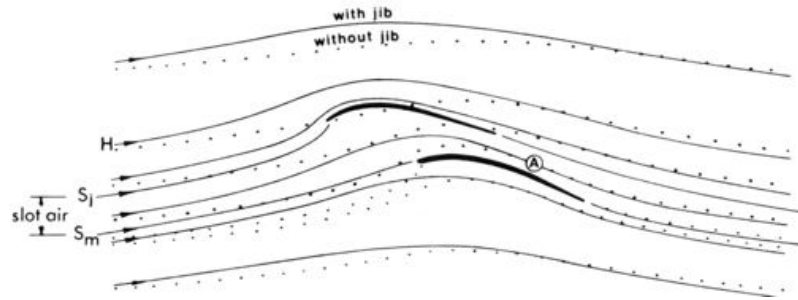


Figure 11: *Diagram of the streamlines around a main/jib arrangement overlaid on those of a single sail, taken from Gentry (1973)*

2.4 Scaling methods

To find an analytical solution to a fluid flow problem requires the solution to a complex system of Partial Differential Equations (PDEs). The equations of many common practical problems are considered analytically unsolvable using current methods. The most time-honoured, and many would say still the most reliable, means of solution is to measure equivalent forces on a scale model of the problem, and analyse the flow in a controlled environment. As Barlow et al. (1999) describe, it is relatively simple to arrive at a set of non-dimensional coefficients, which are unique to a specific situation but independent of scale. These coefficients can be obtained from a small scale experiment, and then scaled to find the forces due to the problem of interest.

Barlow et al. (1999) give the Reynolds number,

$$R_N = \frac{\rho_\infty U_\infty l}{\mu_\infty}$$

as the “primary similarity parameter of interest when planning experiments for Mach numbers less than ~ 0.3 when the geometry is fixed.” l is the reference length, U the relative flow speed, ρ the density of the fluid and μ the dynamic viscosity. The subscript ∞ denotes a value measured far from the object.

In this case, the maximum wind speed used in testing was $6.5m s^{-1}$, and the assumed

equivalent wind speed was 10.7ms^{-1} . The Mach Number for air is given by,

$$M_a = \frac{U}{\sqrt{\frac{1.4p}{\rho}}}$$

where U is the speed of flow, p the static pressure and ρ the density of the air. This corresponds to an experimental Mach Number $M_a \approx 0.0190$ and a full scale Mach Number $M_a \approx 0.0312$. Since sonic effects are considered negligible in any case where $M_a \leq 0.3$, the Mach Number will not be considered in this work.

Experiments are carried with a fluid of known properties, on a model of known dimensions, from which the Reynolds number can be calculated. Variables measured during the experiment must then be converted to separate non-dimensional coefficients. For example in the case of forces, the force coefficient,

$$C_F = \frac{F}{\frac{1}{2}\rho_\infty AU_\infty^2}$$

is used to convert the dimension dependent force F to the dimension independent coefficient C_F .

Provided the experiment has geometry exactly matching the problem, and the same Reynolds number, the force coefficient can be converted back using the full scale values to find the required force. Put another way, for geometrically similar systems, “Each solution of the non-dimensional system for a value of the Reynolds number provides a result that applies for every combination of the four involved quantities that give that particular Reynolds number” (Barlow et al., 1999)

However, there are numerous effects which cause inaccuracies in wind tune experiments. Most of these can be classified either as scale effects, or geometrical effects. (Barlow et al., 1999) Scale effects occur when the Reynolds number, for a variety of possible reasons, does not match that of the full scale. Other discrepancies are caused by inexact geometry of the model. In some cases, this cannot be avoided since “Reynolds number effects on small items are too great even if they could be accurately constructed” Barlow et al. (1999) and so are generally best left out.

Barlow et al. (1999) notes that “The effects [of the pressure pattern on an object] can be profound on essentially all areas of interest” and depend largely on the geometry. Consequently it is extremely desirable to conduct tests at Reynolds numbers which correspond to full scale values. However, this is ‘seldom feasible’ and consequently attempts must be made to replicate the flow regime in the full scale Reynolds number using other means.

The transition to turbulence is one key aspect of the flow regime, and this can be artificially induced to occur where required, by the introduction of a sharp disturbance

such as a wire or a strip of sand at the required point. This allows experiments to be conducted at less than the required Reynolds number. Transition is discussed in more detail in Appendix A.4.1 However, separation, which is also Reynolds number dependent, is less easily controlled. It is consequently always desirable to use a Reynolds number as close as possible to the real case. The importance of transition, and its partial control over separation, is shown in Fig.12.

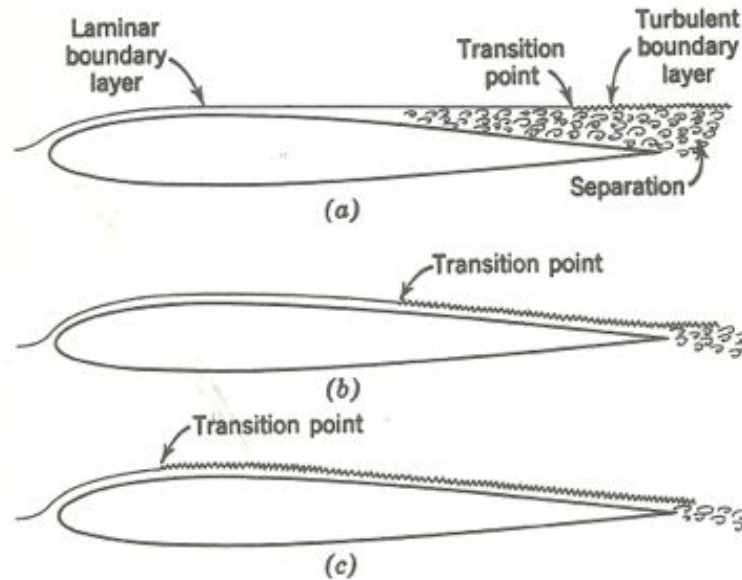


Figure 12: Changing flow regimes with increasing Reynolds number, and corresponding forward movement of the transition point along the chord of an airfoil, taken from Barlow et al. (1999)

Other non-dimensional numbers, such as the Prandtl Number are also key in describing certain physical problems. However, since the Prandtl Number deals with temperature variation which is deemed negligible in this work, these will not be considered.

2.5 Sail types and preliminary estimates

This project is concerned only with the unique sail configuration used in *Boleh's* rig. However, in justifying the research it is worth comparing this with other configurations in more regular use. The terms used in describing sails are covered in the glossary in Appendix A.6.

It is clear from examining Slight (1999) that the most common configuration used on modern sailing vessels of *Boleh's* size is the Bermudan sloop rig of two roughly triangular sails, as shown in Fig.13. In general terms, *Boleh's* rig, shown in Fig.14 is very similar. However, Kilroy (1951) describes the design as influenced heavily by the 'Junk' rigged vessels of the China Seas, both in hull and sail plan. This is shown primarily in the large external 'wishbone battens' on the lower half of the mainsail,

which were intended to promote an efficient camber, as well as for practical purposes when the crew wish to reduce the sail area. However, this is at cost of significant drag.



Figure 13: *Bermudan rigged sailing yachts racing in the Solent, author's photo*

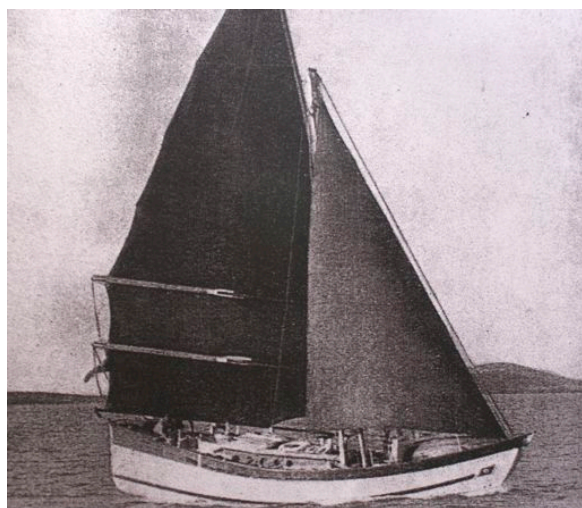
An additional advantage of the battens, however, comes from the extra sail area made possible in the roach, due to the greater stiffness in the leech. This sail area for a given height is key in determining the best operating conditions of the sail, and is best examined through the aspect ratio:

$$AR = \frac{h^2}{A}$$

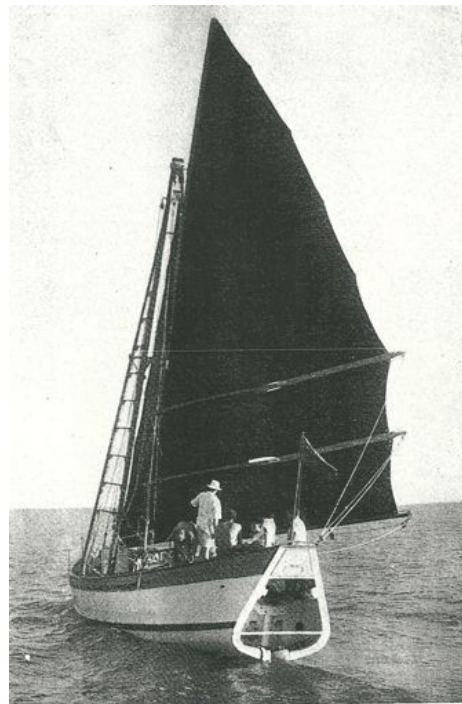
where h is the luff length of the sail and A its total area. The larger the aspect ratio, the more efficient the sail will be at small angles of attack, i.e. upwind. Smaller aspect ratios are correspondingly more efficient at high angles of attack. This is shown graphically in Fig.16, with high aspect ratio rigs delivering high lift to drag ratios at small angles of incidence, and the optimum angle increasing with reducing aspect ratio. Another example of this is in bird's wings. Those that glide long distances, such as albatrosses, must be able to fly efficiently as close to zero angle of incidence as possible, and have long, slender wings. However soaring birds such as vultures and condors utilise the rising air of thermals. For them, the angle of attack is much greater, and consequently their wings have a much smaller aspect ratio.

In *Boleh's* rig, other major deviations from the norm such as replacing the mast with a double A-frame 'Quadrupole' arrangement, and the use of a sliding gunter in the mast, are expected to introduce significant parasitic drag to the configuration.

Unfortunately, though Kilroy (1951) gives details of the practical difficulties found in using the wishbone battens, there is little discussion of their effectiveness in promoting a suitable camber in the sail, or in the suitability of the rig to various sailing attitudes, only that of the vessel as a whole. There has been no opportunity until now to estimate the efficiency of the rig scientifically or compare it to alternatives. As (Howlett, 1974)



(a) *Leaving Singapore*



(b) *Christmas 1949*

Figure 14: *Boleh sailing with her original rig, taken from Kilroy (1951)*



HONG KONG JUNK

Figure 15: *A Junk rigged ship, given as a source of inspiration by Kilroy (1951)*

notes: “The changes in sail force... [due to] what might at first be thought minor changes in geometry are surprisingly large... As the sail plan is progressively made more complicated the general effect is to reduce its aerodynamic effectiveness”, and correspondingly it is expected that this more complex rig will be less effective than that of a modern yacht. However, it is important for the Trust to be able to assertion if, and to what extent, this is the case.

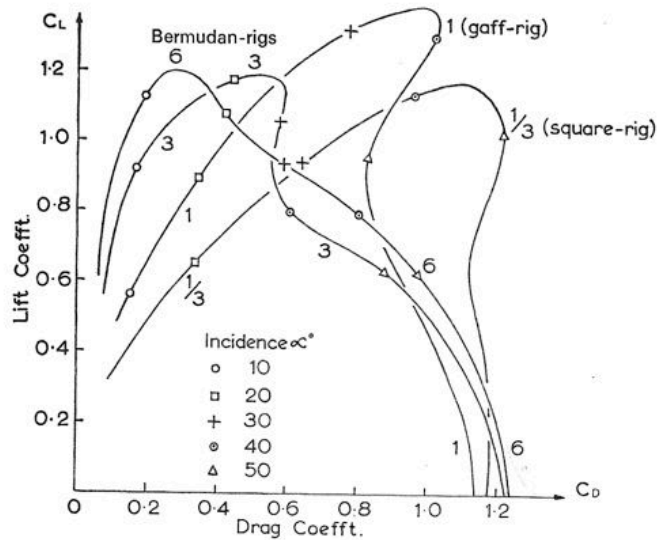


Figure 16: Variation of lift and drag coefficients with sail aspect ratio. Taken from Kay (1971)

3 Wind tunnel experiments

3.1 Aims of the Investigations

In the introduction, two main aims of the wind tunnel experiments were identified;

- Produce a physical scale model of the hull and original rig, test this in a wind tunnel to identify the best sailing attitudes and estimate the induced forces at full scale.
- Investigate the practicalities of the designed rig. Note and analyse any practicality issues that are identified during the tests.

These aims will now be expanded to aid comprehension of the reasoning and method of the experiments.

3.1.1 Identifying optimum sailing conditions

When navigating a sailing vessel on the sea, a large number of variables, such as tide, sea state and current have an effect on the performance of the vessel. This can make it difficult to optimise one variable, for example, the optimum sailing angle, since other variables conflict. This is particularly the case on a vessel with which the crew are unfamiliar. Consequently it can very useful to have information on the character of a vessel which can be used a basis when predicting the vessel's behaviour.

In the long term, knowledge of the optimum sailing attitude for this rig is also of importance, due to the rig's unique nature. Since this sail plan has been used only on one hull, it is impossible to separate the performance of the hull when sailing from that of the sails. For example, though *Boleh* is described as being "not fast to windward" (Kilroy, 1951), it is impossible to state categorically whether this is due to her unusual bluff bow shape, or the equally unusual sails. By testing the sails in isolation from the hydrodynamics of the hull, it is hoped the performance of the rig specifically can be better understood.

3.1.2 Estimating forces on the rig

Boleh is currently being restored at considerable cost, and to an exacting standard, through the work of professional Naval Architects, shipwrights and others. It is important that this is done with an understanding of the forces on the sails, since these determine the scantlings of the masts and all their supports, and also have critical implications for the speed, stability, and endurance of the vessel. In conjunction with comprehensive information on the hydrodynamic resistance of the yacht when sailing,

the drive and heel forces produced by the sails can be used to predict the speed of the vessel in any given conditions.

3.1.3 Identifying issues in the design

Given the cost of alterations and retrofits to any vessel, it is vital that any issues with the design which might occur at sea are identified and dealt with at the design stage, or at the latest during construction. Though this vessel has sailed many thousand miles, with this and other sailing rigs, it was considered pertinent to use the opportunity of the tests to search for any problems in construction and testing of the model which may also be likely to occur during the rebuild and operation of the vessel. Since the original rig (on which that under investigation was based) does not survive, there is no other opportunity to physically identify problems with the design. In addition, though plans of the original rig exist, it was subject to multiple structural failures, and Kilroy (1951) gave the opinion that a major re-design using alternative materials would be necessary, for the wishbone booms in particular, to be a success.

3.2 Preparation for the experiments

There are various complications involved in model testing. Perhaps the greatest difficulty is noted by Kay (1971) in that “if the size of the model is too small then the required wind velocity to ensure similarity by constance of Reynolds number R_N is so great that soft sails are difficult to use”; they are likely to tear. However, as discussed by Marchaj (1964) “Tests on solid sails cannot, of course, be completely successful as they cannot simulate fabric sails” particularly in terms of flexibility. As a consequence rigid models are generally used only in extreme cases.

In this case it was decided to replicate the entire rig as accurately as possible, including the use of fabric sails. Accurate replication of the rig was key since it was expected that there would be a high level of parasitic drag in the design which would strongly affect the results, as well as for the identification of any design issues. The geometry of the hull was also modelled in order to replicate the flow regime over the sails as accurately as possible.

3.2.1 Construction of the model

The wind tunnel model was constructed at a scale of 5:31 as described in Appendix A.3. The approximate principle dimensions of the model are given in Table 1.

The model was built as an accurate geometrical representation of the vessel including masts, control lines, wishbones and deck arrangement, in order to fully replicate the

Table 1: Overall dimensions of the wind tunnel model

| Length (m) | Beam(m) | Draft (below floor) (m) | Height (above floor) (m) |
|------------|---------|-------------------------|--------------------------|
| 1.856 | 0.598 | 0.086 | 1.729 |

entire flow regime around the vessel and simulate a realistic sailing condition for feasibility checks.

3.2.2 Planning of the experiments

In addition to the production of the model, a number of other preparations were required before the experiment could be undertaken. An appropriate testing matrix for the experiment was devised with reference to Barlow et al. (1999) among others. A range of wind speed from $1.0ms^{-1} \rightarrow 6.5ms^{-1}$, and apparent wind angles between $20^\circ \rightarrow 130^\circ$. Sheeting angles were varied from an assumed base angle to find an optimum in each case. Measurements were taken upright and at 10° of heel, for the reasons discussed in Appendix A.3.1. The frontal air drag due to the rigging with sails in the stowed position was also measured, since this is of interest when motoring.

In order to identify appropriate base sheeting angles for the test, particular use was made of observations by Kay (1971) regarding sheeting angles. The optimum foresail sheeting angle (A_F) for maximum drive force at all angles of AWA (Apparent Wind Angle relative to the centreline of the yacht) from $12^\circ \rightarrow 30^\circ$ was found in this text to be 12.5° . The optimum main sheeting angle A_M was found to be 0° relative to the centreline for $\beta = 12^\circ \rightarrow \approx 20^\circ$, and 5° for $\beta = 21^\circ \rightarrow 30^\circ$.

Unfortunately, there is no description of the exact sail plan or conditions used in that experiment. However, this agrees closely with experiments with generic mainsail/foresail experiments such as Gentry (1973), and Marchaj (1962). Therefore, these values were considered appropriate as a start point in designing the experiment. The testing matrix used in the experiments is given in Appendix A.4.3. The experiments consisted of a total of 710 separate runs including tare tests, conducted over 5 days.

3.3 Experimental procedure and results

The experiments were conducted in the low-speed section of the University of Southampton's 7x5 wind tunnel. This has dimensions of 4.6m wide, 3.7m high and 3.7m long, and is capable of a maximum wind speed of $9ms^{-1}$. (Booth, 2007) The model therefore clearly satisfies the requirement by Razenback and Mairs (1997) that 'the width or height of the model should not exceed 80% that of the test section'. The experimental set-up is shown and described in Appendix A.4.4. Due to the size of the model, it had to be raised slightly above its natural waterline to fit. However, since the air seal

between hull and tunnel floor remained, this was not considered a significant issue, as in the work of Booth (2007).

Average forces on the sailing rig were measured by seven separate dynamometers, and the results automatically resolved into drive and heeling forces. This was done for a number of different wind speeds to quantify any changes in the capability of the rig over the range, and the routine repeated over a range of sheeting and apparent wind angles. To evaluate the accuracy of the experimental data, repeat runs were carried out on a sample of the data. In order to repeat runs in an efficient fashion, results were recorded into a spreadsheet during the experiment and analysed in real time. Consequently general trends could be noted and unusual results repeated to confirm their validity. For each test, tare runs were carried out with sails detached from the rig, to find the lift and drag forces due to the remainder of the experimental set up.

For each run, readings of the pressure and temperature of the air were taken. Wind speeds were then corrected to Standard Temperature and Pressure (STP) for comparison, to give greater accuracy in comparing results between tests. Consequently, results are given for an equivalent, rather than measured wind speed, and there is some scatter in the wind speeds, due to variations especially in temperature, during testing. However, had this not been done this scatter would instead have manifested as an error in the results.

The results were then input to the Wolfson MTIA unit's *Wind Correct* software (version 16.03.07). This program corrected for experimental inaccuracies by removing the measured tare forces, and applying a blockage correction. The method used for this is claimed by the Wolfson unit to be derived from the work of Claughton et al. (2006). However given that testing is not the focus of this work it is not surprising that more explicit discussion of appropriate methods may be found from the work of Barlow et al. (1999), Razenback and Mairs (1997) and similar literature. Given that the author did not personally carry out these calculations, the methods will not be discussed here. The corrected forces were then normalised by the sail areas into coefficient form, allowing them to be extrapolated to full scale.

As discussed in Section 2.4 there are significant uncertainties involved in scaling such experimental results, since it is impossible to scale all aspects of the design accurately. For these tests, the experimental Reynolds numbers were almost exclusively in the turbulent region ($R_N > 10^5$), and it was considered that the design of the model such as the lacing shown in Fig.38a and the use of wool tufts on the sails for flow visualisation would result in fully turbulent flow over the sails. Since lift and drag coefficients for aerofoils are largely independent of Reynolds number beyond the critical transition value, as show in Fig.17, it was considered acceptable to mismatch the experimental and full scale Reynolds number. Theoretical justification for this decision is given in Appendix A.4.2.

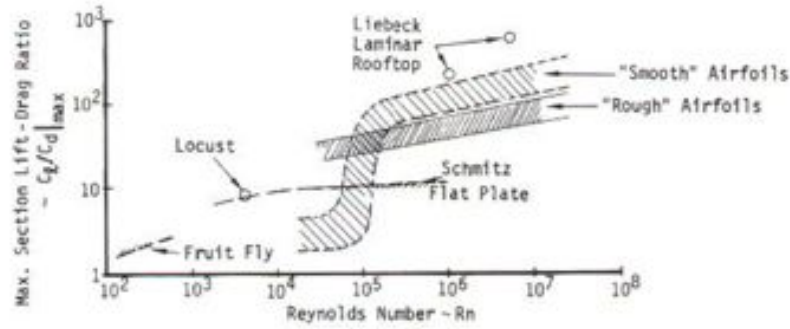


Figure 17: Plot showing the effect of turbulent transition on the Lift/Drag coefficient ratio of a range of aerofoils, grouped into 'rough' and 'smooth' categories. Taken from McMasters and Henderson (1979)

Forces for the full scale rig were therefore calculated for wind speeds such that

$$R_{N(\text{experiment})} = \frac{R_{N(\text{FullScale})}}{10}$$

This factor produced results that correspond to a range of wind conditions which span the likely operating envelope of the vessel, in the range $1.5 \rightarrow 10.5 \text{ms}^{-1}$ or F1 \rightarrow F6 on the Beaufort wind scale.

The results are plotted in various forms, grouped according to the point of sail and angle of heel, in Appendix A.4.5. These results are exclusive of the lift and drag forces due to the hull and rigging, though inclusive of all effects of the wishbone booms. From these plots it was possible to identify the optimum sailing attitudes for this rig, and quantify the associated drive and heel forces. It should be noted that in some cases there are considerable offsets in the data between repeats, caused by latent stresses within the testing rig. The accuracy of the collected data is shown by the fact that the majority of repeats show very close correlation.

Based on the curves in Appendix A.4.5, the optimum sheeting angles for given apparent wind angles at all wind speeds were assessed as shown in Table 2. In some cases, the optimum angle changes with varying wind speed, and for a more precise assessment the reader is advised to consult Appendix A.4.5.

The maximum predicted drive force from these experiments was $6543N$, in a 20knt apparent wind at 120° . This is expected, as a board reach is the fastest point of sail for almost any wind powered vessel. The maximum predicted heel force was $8076N$, in a 21knt apparent wind at 50° . This is surprising, since the maximum heeling force would be expected to occur in the close hauled condition, and a high heeling moment in this case suggests the main was over sheeted. However Fig.18, taken during testing of this configuration at 5.5ms^{-1} (17.5 knts) suggests this is not the case, since the tufts showing flow over the sail do not indicate stall. Rather, it is likely that there was insufficient twist in the main sail in this case compared to the optimum condition.

Table 2: Matrix of optimum sailing angles in degrees. The character * designates those angles where alternative sheeting angles were not tested. Heel angles were given where the optimum was found to be different

| Apparent Wind Angle (AWA) | Heel Angle | Foresail Angle (A_F) | Mainsail Angle (A_M) |
|---------------------------|------------|--------------------------|--------------------------|
| 20 | - | 12.5 | 0 |
| 30 | - | 25 | 5 |
| 40 | 0 | 25 | 10 |
| | 10 | 25 | 15 |
| 50 | 0 | 25 | 10 |
| | 10 | 25 | 15 |
| 60 | - | 35 | 30 |
| 70 | - | 40 | 45 |
| 80 | - | 40 | 55 |
| 90 | - | (data corrupted) | |
| 100 | - | 50 | 55 |
| 110* | - | 45 | 50 |
| 120 | - | 55 | 45 |
| 130* | - | 60 | 50 |



Figure 18: Author's photograph of the model during testing, at equivalent wind speeds of 17.5 knts and an apparent wind angle of 50° , with the black wool tufts on the sail clearly showing largely attached flow. White tufts on the trailing edge of the mainsail can faintly be seen, indicating fully attached flow up to the level of the third batten. No measurements were taken when photographing the model, due to the disturbance of the airflow with the presence of people in the test section

In order to better evaluate the results of the experiments, and to identify any issues in the design of the rig, observations were made and noted regularly during the experiment, and photographs were taken regularly throughout. During these observations a number of limitations to the rig were noticed.

- A serious concern and limitation to the experiment was contact between the leeward wishbone boom and the aft leeward mast. During the experiments, this caused significant deformation to the main sail at sheeting angles in the region of 55° , and at larger angles the deformation threatened to cause significant damage to the sail, in addition to inducing a highly non-optimum sail shape. This is shown in Fig.19. The limiting angle of 55° is a serious concern, not only for sailing efficiency but also from a safety consideration. A reduced sheeting angle increases the likelihood of an ‘accidental gybe’ during downwind sailing, where a small change in wind angle changes the pressure distribution on the mainsail dramatically. This can cause the sail to flick violently across to the other side of the vessel, risking significant damage to rigging and crew. On a vessel the size of *Boleh*, such an accident has a high likelihood of resulting in serious injury or death to any crew member in the wrong place. One possibility to remedy this would be to move the aft mast outboard, increasing the sheeting angle at which contact would occur.
- As can be seen from Fig.40, the optimum course to windward is around 50° , with a sheeting angle on the fore-sail of around 25° . However, the quadropole mast arrangement placed severe limitations on the foresail angle, as can be seen from Fig.20. According to Marchaj (1964), the optimum force to windward for most jib/mainsail combinations is with a foresail angle of around 17.5° . However, as can be seen from Fig.20 in *Boleh*’s case, a jib in this position would experience very ‘dirty’ air due to the influence of the masts. In the configuration shown, with the jib at 20° there was actually contact between the mast and sail at high wind speeds, resulting in a marked loss of performance as discussed in Appendix A.4.5.
- The final major problem in the design came from the high degree of twist experienced at high wind speed and large sheeting angles. This reduced the drive force considerably, and led to premature contact between the wishbone booms and the masts at high wind strengths. It also produced a marked increase in relative heel force at high wind speeds, as discussed in Appendix A.4.5. This would be likely to increase motions, reducing crew comfort during downwind sailing. The twist was due to the complexity of introducing an effective ‘kicking strap’ to hold the boom down at these large angles. Although complicated by the small scale of the model, this is also expected to be a problem at full scale due to the use of a wire stay to support the mainsail luff, rather than a rigid

mast. The author's experience of traditional sailing craft suggests that a heavy boom (such as one made from solid wood) may reduce this effect, although this presents further issues regarding safety and stability.



Figure 19: Author's photograph of the model during testing, at equivalent wind speeds of 17.5 knots and an apparent wind angle of 120°. The main and jib are both set to sheeting angles of 60° and the deformation of the mainsail due to contact between the wishbones and the mast can be clearly seen. Note the severe curvature of the battens around the end of the wishbones, and the blurring of the trailing edge. This was caused by rapid movement due to the detached flow over both sides of the deformed sail

Further observations on the construction of the rigging are given in Appendix A.3.4.

In addition to the results in Appendix A.4.5, using the work of Slater (2012) the results have been grouped into a polar velocity diagram which is presented in Fig.40 in Appendix A.4.5. It should however be noted that due to the limitations on this project, this diagram uses a highly crude estimate, and cannot be considered a reliable estimate of *Boleh's* performance, due to a number of factors.

Primarily, the data given by Slater (2012) is not representative of a sailing condition. It corresponds to the vessel in the upright condition with zero leeway, and without added resistance due to waves. Also, due to time constraints it was not possible to produce a full Velocity Prediction Program (VPP) and apparent wind vectors were calculated without iteration. In order to examine the accuracy of the resulting plot Kilroy (1951) was consulted for data relating *Boleh's* speed to a given sailing condition.

For this, an extract was required giving a reasonably constant average speed, wind speed and sailing attitude. In order to give an accurate result, this data should as far as possible refer to an upright condition with a minimal sea state. One extract was found (Page 68) in which *Boleh* was described as recording a 24h average of 7.5

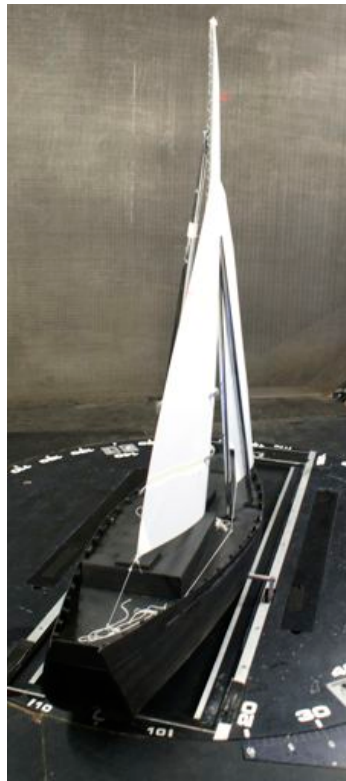


Figure 20: *Author's photograph of the model during testing, at equivalent wind speeds of 17.5 knots and an apparent wind angle of 30° . The angle of the foresail is 20° , and for most sail configurations this would be close to the optimum upwind condition. However it can be seen that at this wind speed the jib is actually in contact with the fore-leeward mast, reducing the effectiveness of the sail*

knots, on a broad reach in winds averaging 12 knots, with some variation. She was also described as being 'nearly upright' and travelling through a 'slight' sea. Unfortunately there was considerable difficulty in obtaining further information without the logbook, and this was the only relevant extract found.

However, this example, though only a rough estimation, correlated well with the corresponding curves in the polar plot. In order to gain a further check of the accuracy of the results, a comparison with theoretical values was also undertaken.

3.3.1 Theoretical investigations

In order to confirm the validity of the results of the wind tunnel experiments, it was necessary to compare the results with other data. Since there was no data available for a similar rig, more generic data provided by van Oossanen (1993) was utilised. This was presented as a VPP for the International Measurement System (IMS) racing rule, due to Poor (1986). A comparison between the sail plan of a typical yacht designed to this rule and *Boleh* is given in Fig.21. Consequently, this data had the advantage of being representative of many modern racing yachts, although there were complexities in relating the VPP data to the experimental data due to the use of different reference axes. Theoretical data was calculated using identical sail areas for

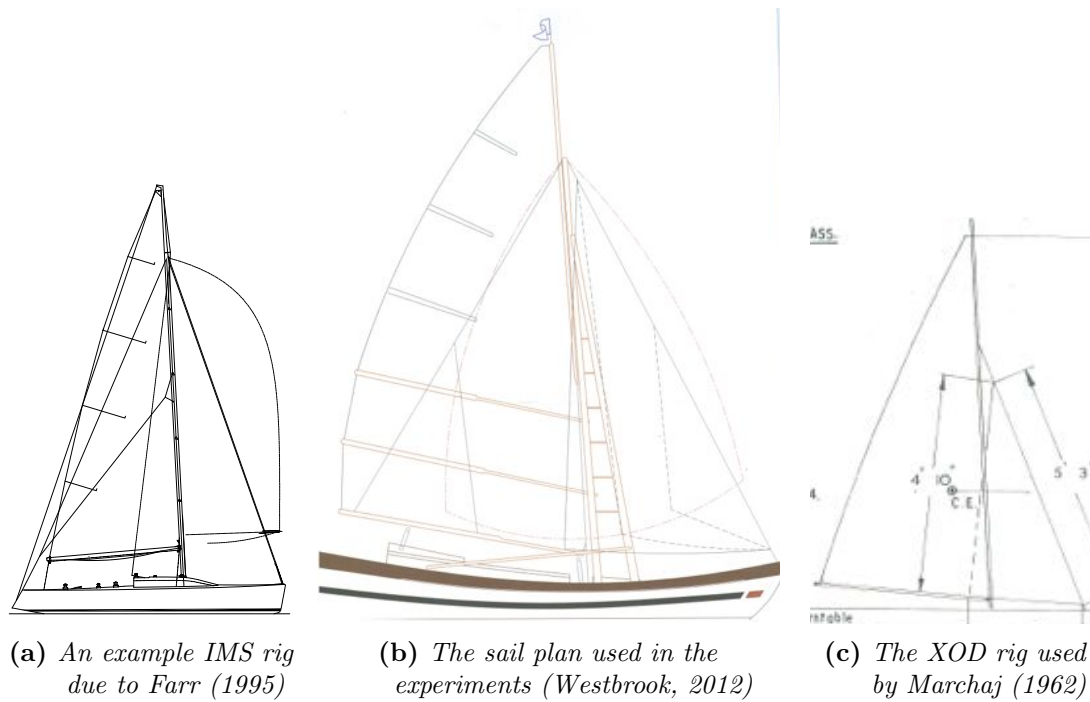


Figure 21: Sail plans used in the data in Fig.41

the Jib and Main, and an overlap coefficient of 0.95, equivalent to that of Boleh's rig. Various comparative plots of the data are given in Appendix A.4.6, but the results can be summarised through analysis of Fig.41 in Appendix A.4.5. A plot of lift versus drag coefficient is used to define an envelope of maximum efficiency as described by Marchaj (1987) and shown in Fig.22.

It can be clearly seen that the results are of a similar magnitude, and follow similar trends. However, clearly the results of Poor (1986) and Marchaj (1962) represent a considerably more efficient sail plan. Particularly in the case of the IMS data, this is expected due to the difference in the sail shapes shown in Fig.21. The higher aspect ratio of the IMS sail plan will give a notably higher lift/drag ratio, and the simpler rigging arrangements will result in much cleaner air over the sails, giving higher lift. However, given the significant difference between the results it is also possible that the sheeting configurations tested in the wind tunnel were not optimum, which would account for further inefficiencies in the experimental results.

3.4 Conclusions of the wind tunnel experiments

From the wind tunnel experiments an extensive amount of data has been successfully collected, and from this it has been possible to realise all the main aims of this phase of the project. The accuracy of the data was enhanced by flow speed corrections for variation in temperature and pressure during testing. Optimum sheeting angles for a wide variety of sailing attitudes have been identified, (shown in Table 2) in most cases from a wide range of tested set ups.

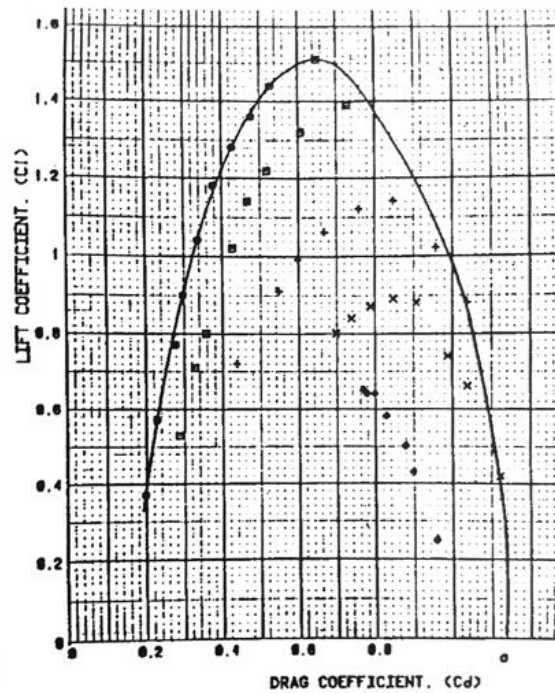


Figure 22: Plot of lift coefficient versus drag coefficient resulting in a 'test envelope', for experimental data from a single sail. Taken from Marchaj (1987)

The data has been validated by comparison with trusted data from two entirely separate sources to suggest reasonable accuracy, considering the limitations posed by the different sail types. This appeared to show that *Boleh's* rig produces significantly more drag, and reduced lift compared to equivalent rigs on modern racing yachts. It is suggested that this is due to a combination of the lower aspect ratio, and significantly more complex architecture of *Boleh's* rigging, although experimental factors may also be involved.

During the experiments a large volume of data on the global loads on the full scale rig was accumulated, far beyond the maximum forces given above. It is hoped this may be of some use during final design of the rigging and layout.

Using the force data it has also been possible to produce a crude estimate of *Boleh's* speed under sail, which appears to correspond well with available voyage data, considering the assumptions used in the estimation. This information suggests that the rig is not especially efficient to windward, with the optimum sailing angle around 50° to the true wind, rather than the $40 \rightarrow 45^\circ$ true of many modern craft. This is to be expected from the high drag of the rigging and the low aspect ratio of the sails.

Furthermore, during the construction and testing of the model significant difficulties were discovered and largely overcome. It is hoped that the documentation of these issues will be of some use to *Boleh's* owners and crew in her ongoing refit, though design and testing of alternative configurations is outside the scope of this project.

4 Numerical investigations

4.1 Aims of the Numerical Investigations

In addition to the physical experiments described above, an investigation using Computational Fluid Dynamics (CFD) was also undertaken. The basic theory of CFD is discussed in Appendix A.1. The aims of this investigation were:

- To investigate the ‘slot-effect’ caused by the interaction between adjacent aerofoils.
- To investigate the wing tip vortices which are the cause of induced drag, and to demonstrate the cause of their production.
- To gain experience of the use of CFD simulations in an investigative context.

A geometry of twin NACA 0010 foils of equal size was generated using the yacht design software *Maxsurf*, and an unstructured mesh for simulation was generated using the Ansys software *ICEM CFD*. Simulations were run using Ansys *CFX 14.0* on a number of different desktop computers owned by the University of Southampton. CPU clock time for each simulation was around 0.002, or 3 minutes.

4.2 Procedure and results of the experiments

The geometry and mesh files were produced as described above, resulting in simulated geometry shown in Fig.23.

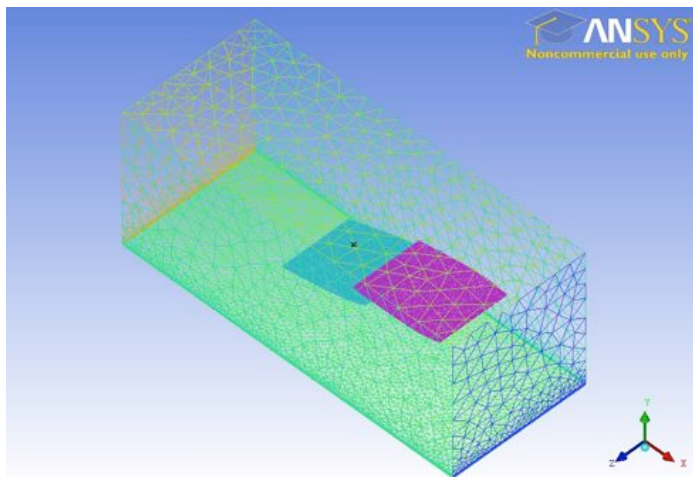


Figure 23: Mesh exteriors of the base case geometry, version 1. Note the higher mesh density along the floor to model flow over this non-slip boundary

The accuracy of results in a simulation are clearly dependent on the size of the elements analysed, however as discussed in Appendix A.1 there is a large penalty in

required computation for increasing the number of elements in a simulation. Therefore the density of this initial mesh was varied, and simulations run for each variation to identify the minimum elements required for an accurate answer. Global forces produced in each case were plotted against the number of mesh elements to produce the mesh dependency analysis in Fig.87 in Appendix A.5. From this an element count of 350000 was selected as optimum.

The geometry of the base case consisted of 2 NACA 0010 foils with a chord (henceforth referred to as C) of 1m. The foils had a span of $0.75C$, and were positioned forward of the centre of a control volume with dimensions $3.75Cx1.5Cx1.5C$. The foils overlapped by $0.15C$, with a spacing between the foil surfaces of $0.06C$. The upper foil had an angle of 5° about the transverse axis, the lower foil had an angle of 15° . The position of the foils was varied systematically to investigate the factors influencing static pressures on the surfaces of the foils and in the slot between them. The positions are given in Table 3. Using an inflow velocity of $5ms^{-1}$ the Reynolds number was set to $R_N = 3.25 \times 10^5$ to match the turbulent regime seen in flow over sails.

Table 3: *Systematic variations in position of the lower foil*

| Configuration | Vertical position (relative to base, %C, +ve up) | Horizontal position (relative to base, %C, +ve fwd) |
|---------------|--|--|
| 1 | 0 | 0 |
| 2 | 1 | 10 |
| 3 | -1 | 10 |
| 4 | -2 | 10 |

An additional control geometry, consisting of a single lower foil was also produced.

Prism meshing was used on all surfaces, with $y^+ = 0.01053$ units and a prism height ration of 1.2. However, since this was not a simulation of any physical phenomenon, the value of y^+ was considered inconsequential in this case.

In this condition measurements were then taken for the base case of transverse flow velocities across the span over the top surface of the lower foil at $0.25C$ from the leading edge. A plot of the results is shown in Fig.88 in Appendix A.5.

Plots of the transverse velocity in vertical cross-sections at various positions across the span are shown in Appendix A.5. These provide an excellent explanation of the sharp changes in transverse velocity shown in Fig.88. At midspan, as the Fig.104 shows, there are no transverse velocities other than local fluctuations. The almost linear increase in transverse velocity with span shown in Fig.88 is a global trend, with the flow much more marked around the lower foil due to the greater angle of attack.

Of particular interest was the sharp change in velocity around the wing tips. By comparing Fig.88 with Fig.106 and the rest, it can be seen that the transverse velocity at the wing tip is actually minimal, the majority of flow being vertical as can be seen from the streamlines. The wing tip vortex can then be seen to produce strong transverse velocities at 120% span, before returning to zero in the ambient flow. In short, the line sampled in Fig.88 passes through the low speed centre of the vortex at full span ($\pm 0.375m$), then through the lower half of the vortex, where the flow is outwards from the centre, before entering ambient flow.

The geometrical variation revealed further information about the properties of the wing tip vortex. It can be seen from Fig.103 in Appendix A.5 that the strength of the vortex appears to increase with increasing foil separation distance. This is indicated by the greater radius of the streamline curves, which have the same origin in each case. The reason for this appears to be that the presence of the second foil impedes the vortex flow, in two ways.

- The physical presence of the foil acts as a barrier, much as some jet aircraft have wing tip fins.
- The outward flow from beneath the upper foil impedes the inward flow on the upper surface of the lower foil.

This latter point can be seen by close attention to the streamlines passing through the slot between foils, especially in Fig.102c. The flow is fully reversed from outwards to inwards, with the magnitude of the accelerations increasing with decreasing foil separation.

In the systematic investigation of pressure distribution, the rather surprising result was found that the pressure in the slot decreased with separation, rather than increasing due to blockage as is known to occur in sails (see Section 2.3.5). Pressure distributions along the three streamlines shown in Fig.94 were measured in each of the configurations and plotted as shown in Fig.89. The position of the streamlines was varied to replicate their relative positions to the foils as closely as possible in each case.

Unfortunately the difficulty of accurately positioning the streamlines has introduced some error to the measurements, so that the peak values, which are highly localised, may not be accurately plotted. However, it is clear to see that a very sharp peak low pressure is produced in the slot between foils, which appears to become stronger with decreasing separation. It was expected that this would result in separated flow even at this turbulent Reynolds number, but this did not occur. Comparison with Fig.87e shows that the presence of the upper foil has little effect on the low pressure peak at the leading edge of the lower foil, except in the case of configuration 2, where the separation is just 5% of chord length.

There is some noise in the results for the high pressure peaks due to the highly localised nature of the pressure reasons. However, the pressures over the upper surface of the lower foil, shown by the upper and central streamlines, are virtually identical. This shows that away from the surface the pressure varies little with height.

4.3 Conclusions of the numerical investigations

The cause of wing tip vortices was successfully shown using CFD simulations of interacting foils. From systematic variation of the foil separation it was speculated that placing an aerofoil upstream of another with very limited separation in the plane of thickness may result in a slight reduction in the strength of the wing tip vortex from the downwind foil.

The simulations suggested a reduction in pressure in the slot between aerofoils, which was magnified by separation distances of around 5% chord length. This is contrary to current theory concerning the slot effect between interacting sails, but a similar effect is known to occur between more bluff bodies placed in proximity, for example catamaran hulls. It is therefore speculated that this reduction in pressure is due to the thickness of the aerofoils, as opposed to sails which have negligible thickness. An alternative explanation would be to question the accuracy of the simulation due for example to the difficulty in meshing small features accurately. However great care was taken to ensure the coherence of the mesh in each configuration. Details of the mesh within the slot showing its coherence are provided in Appendix A.5.

A great deal of time was required to prepare these simulations, and a great deal of experience was gained from the process. It was hoped that this experience could be utilised in producing CFD simulations of the sails in the wind tunnel, to provide corroborative data particularly in analysing the effect of the wishbone booms on flow over the sails. However, due to time constraints on the project and the difficulty in persuading a mesh to converge over geometry with such a low relative thickness, this section of the project was abandoned. Mesh geometries for the sails showing the difficulties encountered are shown in Appendix A.5.1.

5 Conclusions

The investigation has been carried out into the efficiency and practicalities of the sailing rig designed for the Junk Yacht *Boleh*, using a detailed scale model of the yacht rig tested in the University of Southampton's 7x5 wind tunnel. From these tests it has been possible to identify the optimum sailing attitudes for the jib and mainsail combination, and to estimate the full scale global loads imparted on the rig when sailing. The forces generated by the sails have been extracted from the experimental data and reduced to coefficient form for comparison with available data on alternative rigs. This comparison gave reasonable validity to the experimental data, and showed the rig to produce comparatively high drag and low lift with respect to the sails of a modern racing yacht. This result has been analysed and justified by comparison between the form and architecture of the sailing rigs.

The practicalities of *Boleh's* rig, with respect to its efficacy and the practicality of its use has been discussed. Some issues in the design and construction of the rig have been identified for consideration by the *Boleh* Trust. These include the sheeting angles possible for the mainsail due to the wishbone battens, and the regulation of twist in the mainsail at large sheeting angles. Further considerations regarding the limitations placed on jib sheeting angle by the mast arrangement are also noted, along with notes on considerations for construction. Within the limited scope of the investigation some alternative design considerations are proposed.

Using the global loads on the rig and some simplifying assumptions, a preliminary estimate of the vessel speeds to be expected in a given sailing condition has been produced. Given the limited data available on the sailing performance of this vessel, a good correlation was found to the experience of *Boleh's* original crew.

An additional investigation into wing tip vortices and the slot effect has been performed using CFD analysis. Interesting observations were made concerning the relative similarity of interactions between sails and those between more typical aerofoils, which may merit further study.

A great deal of data has been collected during this project which it is hoped will be of use to the Trust during *Boleh's* restoration and subsequent sailing career. This data has been collected and presented in the most accurate manner feasible, but is subject to the limitations of the project in terms of time available and the author's experience.

Therefore, there is limited confidence in how 'optimum' the recommended sheeting angles may be, due to the limited number of configurations tested. Further testing utilising broader investigation of a smaller range of initial conditions may prove more profitable in terms of optimising the sail configurations.

In conclusion, it may be said that the practicality and efficiency of *Boleh's* unique rig is perhaps not what was hoped for by Cmdr. Kilroy when he designed the vessel. Although perfectly useable in the cruising context for which she was designed, any limited advantages of the set up appear from this research to be outweighed by significant issues with parasitic drag and practicality.

6 Further work

Though this report represents a satisfactory conclusion to this project, additional work to extend the project could be carried out as proposed below;

- As discussed above, further testing to identify optimum sailing attitudes more systematically than in the current work may be of value, as would testing in the downwind condition using a spinnaker. This work could also be extended through the use of more appropriate towing tank data to produce a VPP, to predict more accurately the speed of the vessel when sailing.
- Comparisons of sailing efficiency against a broader range of existing sailing rigs could be carried out, for example, a comparison with the data discussed in the work of Marchaj (1987).
- Further work on the CFD investigation could be conducted to investigate the effects of variation in Reynolds number and/or the thickness and symmetry of the aerofoils.

7 Bibliography

References

- Ansys. *Ansys CFX-Solve Theory Guide*, 2006. Guide to CFD theory provided for users of Ansys Inc's CFX-Solver Program. Accessed at <http://product.caenet.cn/Uploadfiles/12872437250986625020081129090050986.pdf> 05/04/12.
- Ansys. *Ansys CFX-Solve Theory Guide*, 2009. Guide to the use of Ansys Inc's CFX-Solver Program, with an Introduction to CFD Theory. Accessed at <http://orange.engr.ucdavis.edu/Documentation12.0/120/CFX/xintr.pdf> 05/04/12.
- J.B. Barlow, W.H. Rae Jr., and A. Pope. *Low-Speed Wind Tunnel Testing*. John Wiley & Sons, 3rd edition, 1999. ISBN 0471 55774 9.
- J. Booth. *Construction of a Heeling Apparatus for Model Wind Tunnel Testing and Comparing Upright Data for Optimum Sheeting Angles with Heeled Data*, 2007. 3rd Year Individual Project testing 1 Meter Class yachts using a specially created heeling apparatus.
- I.M.C. Campbell. Optimisation of a sailing rig using wind tunnel data. In *13th Annual Chesapeake Sailing Yacht Symposium*, volume 1, page 49, 1997.
- A.R. Claughton and I.M.C. Campbell. Wind tunnel testing of sailing yacht rigs. In *13th International Symposium on Yacht Design and Construction*, volume 1, page 89, 1994.
- A.R. Claughton, J.F. Wellicome, and R.A. Sheno. *Sailing Yacht Design: Theory*. Henry Ling Ltd, 2nd edition, 2006. ISBN 085432 8297.
- Farr. Sailplan of ims 43 'flash gordon' produced by farr design ltd. Accessed at <http://www.farrdesign.com/329.htm> 14/04/13, 1995.
- F. Fossati. *Aero-Hydrodynamics, and the Performance of Sailing Yachts*. Adlard Coles Nautical, 1st edition, 2009. ISBN 978 1 4081 1338 7. Originally published as *Teoria dello yacht a vela*, 2007, by Politecnico di Milano.
- A. Gentry. Another look at the slot effect. *Sail Magazine*, July 1973.
- I. Howlett. Considerations relating to the performance of large sailing vessels. In *Proceedings of the Symposium on 'Performance Prediction of Small Craft'*, November 1974.
- H.F. Kay. *The Science of Yachts, Wind and Water*. Whitefriars Press Ltd, 1st edition, 1971. ISBN 0 85429 114 8.

- Cmdr R.A. Kilroy. *Boleh*. Hodder and Stoughton, London, 1st edition, 1951. Account of *Boleh's* design and construction in Singapore and her subsequent voyage to Salcombe, Devon in the early '50's. Written by her designer, owner and skipper.
- L. Larsson. Lectures on "sailing yacht design". Delivered in a series of 6 public lectures at Southampton Solent University on behalf of ISYD Ltd, Spring 2013, 2013. Based on his books 'Principles of Yacht Design' and 'Ship Resistance and Flow'.
- C.A. Marchaj. Wind tunnel tests on a 1/3rd scale model of an x-one design's sails. *University of Southampton Advisory Committee for Yacht Research*, Report 11, October 1962.
- C.A. Marchaj. *Sailing Theory and Practice*. Dodd, Mead and Co., 1st edition, 1964. ISBN N/A, (2nd ed. 0396084281).
- C.A. Marchaj. The comparison of potential driving force of various rig types used for fishing vessels. In *8th Annual Chesapeake Sailing Yacht Symposium*, volume 1, page 51, 1987.
- McMasters and Henderson. low speed single element aerofoil synthesis. *Technical Soaring, Journal of the OSTIV*, 4, Volume 2, 1979. Taken as referenced by the Doctorate Thesis of John McArthur, University of Southern California. Accessed at <http://www.scf.usc.edu/~jmcarthu/qual.pdf> 21/11/12.
- P. van Oossanen. Predicting the speed of sailing yachts. In *Transactions*, volume 101, page 337, 1993.
- C.L. Poor. A description of the new international rating system. A publication of the United States Yacht Racing Union (USYRU), 1986.
- P. Rattanasiri. *Optimisation of a fleet of AUVs to minimise energy dissipation: Transfer Report*, 2012. Transfer Report of the PHD Thesis of Ms. Rattanasiri, investigating the energy losses in a fleet of UAVs through CFD simulations. Report obtained from Ms. Rattanasiri in her work as a research assistant at the University of Southampton.
- R. Razenback and C. Mairs. Experimental determination of sail performance and blockage corrections. In *13th Annual Chesapeake Sailing Yacht Symposium*, volume 1, page 245, 1997.
- M.J.A. Slater. *An Investigation into the Hydrodynamics of the Junk Yacht Boleh*, 2012. 3rd Year Research Project produced in parallel to the current work.
- S. Slight. *Complete Sailing Manual*. Dorling Kindersley, 1999. ISBN 075130784 X.

J.F. Wellicome. Lecture notes on “high performance craft”. Delivered to Undergraduate Ship Science Students at the University of Southampton, Autumn 2012, 2012. With Additions by Prof. G. E. Hearn and Dr. J. Blake.

J.F. Wendt, J.D. Anderson, G. Gegerz, and E. Dick. *Computational Fluid Mechanics: an Introduction*. Springer-Verlag, 1st edition, 1992. ISBN 3-540-53460.

G. Westbrook, 2012. Communication with Graham Westbrook, of Westbrook Marine Ltd, consultant Naval Architect to the *Boleh* Trust.

A Appendices

A.1 Computational fluid dynamics

In order to allow improved understanding of Section 4, a short explanation of the theory behind CFD is presented below.

A.1.1 Introduction

It was stated in Section 2.4 that many fluids problems in the real world are analytically unsolvable. However the expense of physical experiments in both money and time mean it is desirable for many problems to find an alternative method of solution, and in the past few decades great advances in the field of Computational Fluid Dynamics (CFD) have been made. The field of CFD is fast evolving, and so complex as to be beyond the scope of any single volume work. However, an introduction to the theory as it pertains to this project is presented below.

A.1.2 Basic theory

The overarching method behind CFD is that, rather than analytically solving the PDEs over the entire problem, a computer is used to solve the PDEs of each small sections within the problem. This allows approximate calculations of the required variables such as forces and velocities, without generating an equation to describe the entire problem which is likely to be unsolvable. Put another way, Wendt et al. (1992) describe CFD as “the art of replacing the governing partial differential equations of fluid flow with *numbers*, and advancing these numbers in space and/or time to obtain a final numerical description of the complete flow field of interest.” The dominant form of CFD presently in use for steady flow is the Reynolds Averaged Navier Stokes (RANS) method. Unsteady flow, where there is a high degree of turbulence present, is beyond the scope of this work.

A.1.3 RANS CFD

All CFD is achieved through numerical solution of three fundamental equations of physics, the continuity of mass and energy, and Newton’s second law. (Wendt et al., 1992) However the transfer of mass, energy and other variables is best described by the PDEs known as the Navier-Stokes equations. (Ansys, 2009) The program simulation program used in this work was Ansys CFX-Solver 14.0 which discretises the equations through the finite volume technique Ansys (2009). Wendt et al. (1992) describes the finite volume technique as a method in which the fundamental physical principles

of the problem are applied to a “reasonably large, finite region of the flow.” The governing equations of the flow are obtained indirectly from the resulting integrals in their conservative form. For further information on this complex mathematics, it is advisable to consult specialist literature.

There are however practical limits on the application of this theory. Turbulence, discussed in Section 2.2.2, consists of large fluctuations in velocity and pressure within often infinitesimal regions in space and time. Since full accurate application of the finite volume technique requires volumes within which there is little variation, according to Ansys (2006) “Direct Numerical Simulation (DNS) of these flows [for practical Reynolds numbers] would require computing power which is many orders of magnitude higher than available in the foreseeable future.”

Instead, the RANS method uses ‘Turbulence Models’ to statistically predict the behaviour of particles within control volumes of an acceptable size. The Navier Stokes equations are effectively modified to include separate quantities accounting for the average and fluctuating components of the flow, resulting in the RANS equations. Ansys (2006) This produces reasonably accurate simulations of the mean flow including the ‘random’ element of the turbulent fluctuations, without resorting to computing the movement of every infinitesimal particle in the flow. Nonetheless, the resulting PDEs must be solved iteratively for every element, and managing the computational cost of a problem is still a primary concern.

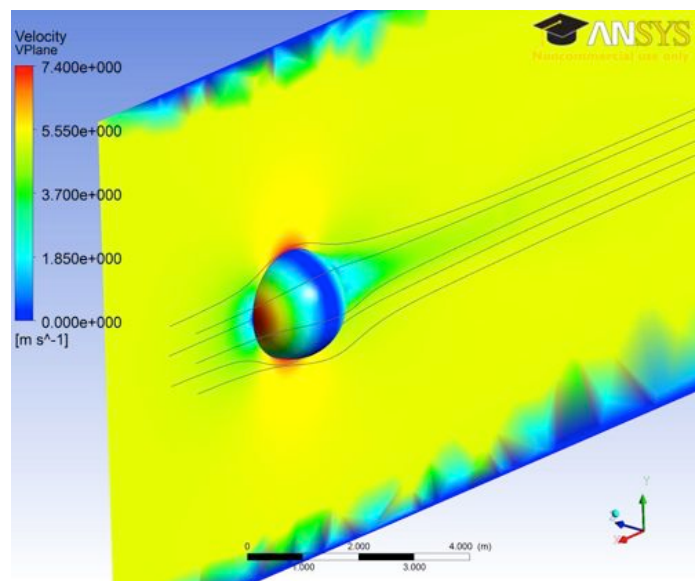


Figure 24: Visualisation of flow over a sphere produced by the author using a CFD simulation. Colours on the plane indicate the variation of velocity, colours on the sphere indicate the variations in pressure.

A.1.4 Turbulence models

Additional stresses exist in turbulent regimes, due to the fluctuations in the flow. Since the turbulence is averaged, these stresses are unknown, and must be approximated using a turbulence model to allow a solution to the system of equations, called ‘closure’. Ansys (2006) There are numerous different averaged turbulence models available in Ansys CFX-Solver, suitable for different applications, but the models considered for this project are given here, adapted from a list due to Rattanasiri (2012);

- The Spalart-Allmaras (SP-A) model is a relatively simple one-equation model that solves a transport equation for a viscosity-like variable. The SP-A model has shown to give reasonably good predictions for wall-bounded flows, and boundary layers subjected to adverse pressure gradients. (Karim et al.)
- The $k - \epsilon$ is a two-equation model which the transport equations are solved by the turbulent kinetic energy, k , and the rate of dissipation of turbulent energy, $\epsilon = \nu \frac{\partial u'_i}{\partial x_j} \frac{\partial u'_i}{\partial x_j}$. The eddy viscosity (ν_T) is predicted by $C_\mu \frac{k^2}{\epsilon}$. This model is good for volumes of revolution.
- The $k - \omega$ model is a two-equation model in which the transport equations are solved through the turbulent kinetic energy, $k = \frac{1}{2} \overline{u'_i u'_i}$ and the specific dissipation $\omega = \frac{\epsilon}{k}$. Then the eddy viscosity (ν_T) is predicted by $\nu_T = \frac{k}{\omega}$. This model is widely used to model flow over a blunt body as it provides a good prediction of the forces near wall (Karim et al.)
- The SST model is a two-zone model that combines the $k - \epsilon$ model for solving the inner boundary layer and the $k - \omega$ model for that of the outer boundary layer and flow field away from wall. This model “accounts for the transport of the turbulent shear stress and gives highly accurate predictions of the onset and the amount of flow separation under adverse pressure gradients.” (Ansys, 2006)

A.2 Time plan

A gant chart was produced at the initial report stage of the project in order to enhance organisation and planning of the project. This has been revised and updated in the light of current progress and the evolving nature of the project aims, and the updated interim time plan is presented in Fig.25.

A.3 Experimental model

For the wind tunnel experiment, a sail plan provided by Westbrook (2012) was used to produce a suit of sails at a scale of 5:31. This had been suggested as the most appropriate for the wind tunnel to be used in the experiment. The sail plan used was produced as part of the restoration project. Though not original, the design is heavily based on the original rig, and so is suitable for the project. In addition, the results of the experiments will be directly applicable for the future life of the ship.

To ensure the sails were accurately made and durable, it was decided to have them professionally produced. This was done by Graham Bantock of SailsEtc., a respected manufacturer of sails for radio controlled sailing craft, such as the 1 meter class. These sails were delivered satisfactorily in early October 2012.

In order to gain an accurate impression of the sail forces generated on the actual vessel, it is necessary to test them in a flow regime equivalent to that on the actual ship. Consequently, accurate models of the hull and rigging must also be produced at the same scale, and included in the experimental apparatus. The wind tunnel facilities at University of Southampton include a shallow tray sunk into the floor of the wind tunnel. The model is placed into this, and surrounded with water to ensure the flow conditions match reality. Images of the experimental setup are shown in Appendix A.4.4.

Due to the unusual nature of the model, the high cost of manufacture and the limited facilities for this kind of model available to the university, the author decided to construct the model as part of this project. The hull model was constructed from shaped horizontal sections of larch and pine, based on the lines plan given by Kilroy (1951). (See Fig. 27.) This construction method combined relative ease of manufacture with low cost and high strength, to withstand loads during the experiment and ensure the model was sufficiently robust for transport.

The spars of the rig model were constructed of steel piping of the correct diameter for each part, in order to ensure a high degree of stiffness. Control lines were made from the strongest cord available, which was pre-stretched to minimise variation during the experiment. The luff of the jib and main sail were reinforced with wire to reduce curvature and flapping, replicating the full scale condition where these areas would

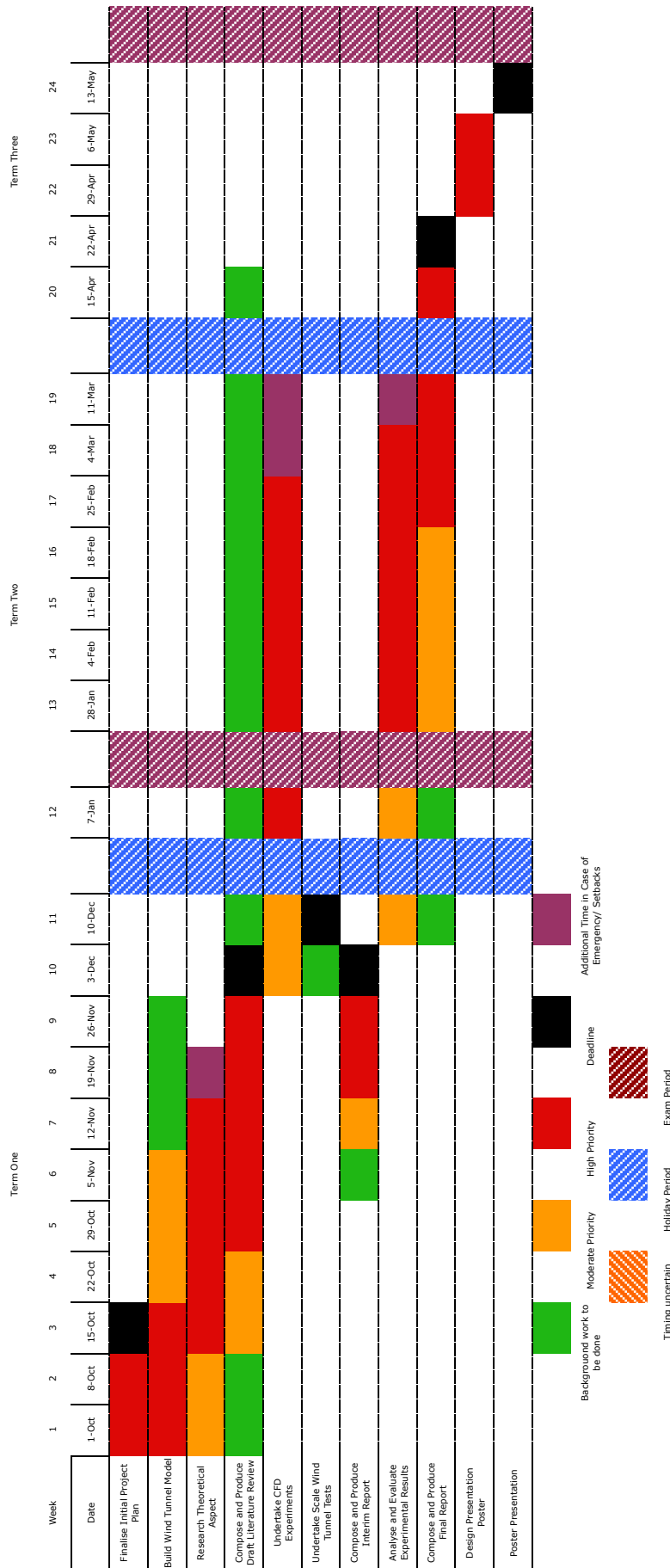


Figure 25: Gantt chart of tasks for this project

be under higher tension than obtainable at model scale. During research prior to construction, it was noted that a number of references were made in papers to the use of electronic winches to adjust the angle of sails. However, these papers uniformly stated their ineffectiveness in anything other than light wind speeds. Given that the sail plan used in this experiment was larger than any in these papers, it was decided to use a purely mechanical ‘cleat’ fixing for all the control lines, with sail angles measured directly from the sails using the specially constructed protractor shown in Fig.38c.

It was intended that the the hull model should be constructed largely during the summer vacation, however unfortunately due to the considerable time required for construction this was not the case. Material was sourced and production began in mid September 2012. Construction of the rigging began at the beginning of November, and the model was completed on the first of December. It is important to note that the time spent on manufacture of the wind tunnel model severely limited the scope of this project.

Images of the model under construction are given in Appendix A.3.4.

A.3.1 Heel angle derivation

The experiments included testing at an angle of heel. Consequently it is desirable to calculate a realistic angle of heel for normal sailing. For this, a program was written in the open source programming language Python, using data from a previous wind tunnel test by Marchaj (1962) and GZ data taken from Slater (2012). The code for the program is given in Appendix A.3.2. The force coefficients for varying heel taken from Marchaj’s work were used to find the forces on *Boleh*’s rig at full scale, and balanced against the GZ data. The results are given graphically in appendix A.3.2, along with a copy of the program script.

Unfortunately, whilst the data used (Marchaj, 1962) was the most appropriate available in terms of craft, there were significant issues. Specifically, there was a slight difference in the Aspect Ratio, which was 3.25 for the *Boleh* rig, and 4 for the rig in the work of Marchaj (1962). The effect of AR is discussed in Section 2.5.

More significantly, the experiments were conducted at a slightly different range of Reynolds numbers to those expected for *Boleh*. As both Reynolds numbers are close to the transition (or sub-critical) region, and the level of turbulence stimulation used by Marchaj (1962) is not stated, this means that there may be some discrepancies in the physics. Discussion and calculations are given in Appendix A.4.1.

Nonetheless, the results showed heel angles between $10^\circ \rightarrow 20^\circ$ to be appropriate in common wind conditions. This result was compatible with a range of other experiments, including those in Marchaj (1962) and Booth (2007). According to Barlow

et al. (1999), “if only one heel angle is to be used it should be in the $20^\circ \rightarrow 30^\circ$ range.” However, due to the large size of the model in comparison with the basin to hold it, it was decided to use a heel angle of 10° , as any greater angle of heel would have required raising the model above its natural waterline to fit. Additionally, the work of Booth (2007) suggests that there is little variation in drive and heel forces in the range of heel angles from $10^\circ \rightarrow 30^\circ$ so it is considered that the results would be similar across this range.

A.3.2 Derivation of heeling moment

Using the Integrated Development Environment IDLE, a program was written in the open source programming language Python to estimate the heel angles at which *Boleh* could be expected to sail in a given wind strength. Due to the unique nature of *Boleh*'s rig, there was insufficient information on any similar craft on which to base the information. Consequently, data from experiments by Marchaj (1962) was used as the closest available match. As noted in Section A.3.1, there were some compatibility issues between the data taken from the work of Marchaj (1962) and *Boleh*. Principally, these were Reynolds number and Aspect Ratio issues.

The resulting plot of heel angle against wind speed is given in Fig.26.

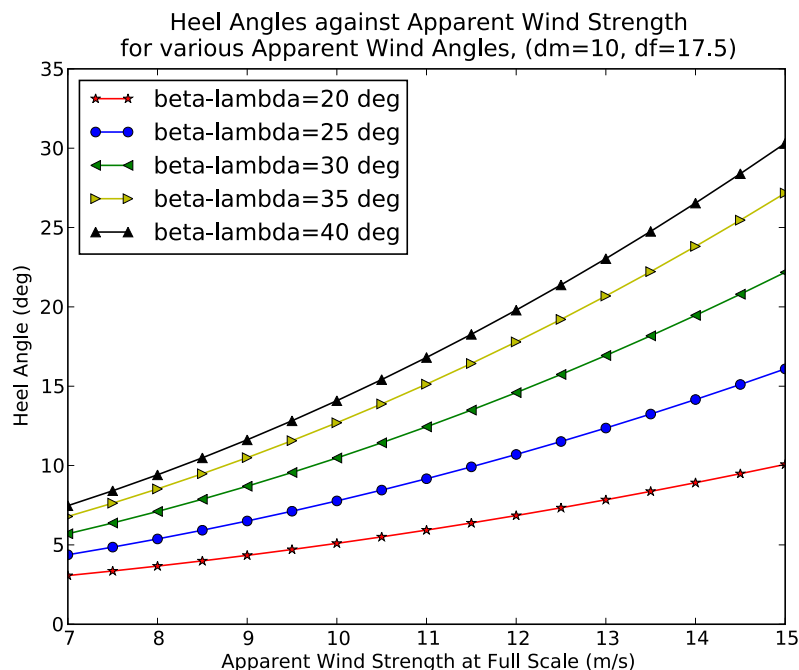


Figure 26: Graph of heel angle against wind speed for various sheeting angles for the yacht Boleh. Produced by the author

The code for the program is given below.

```
from __future__ import division
import math as m
```

```

import scipy as sp
import scipy.optimize
#import array
import matplotlib.pyplot as plt
import pylab

"""This is a program designed to calculate the angle of heel experienced
by the yacht 'Boleh' in a given wind strength due to the heel moment of
the wind in the sails.
Produced by J Happs for 3rd year individual research project 'An Analysis
of the Sailing Efficiency of the Junk Yacht Boleh' Junk Yacht Boleh' Also
for the parrallel research project of M. Slater
Produces results valid for heel angles between 1 and 20 degrees, apparent
wind angles between 20 and 40 degrees, and wind speeds between 5.14 and
9.25 m/s
Version 1.0, 06/11/12
contact jdh2g10@soton.ac.uk
"""

if __name__=='__main__':
    print "I am running on my own"
else: print "My name is %s"%__name__

#GZ curve data
xi = sp.arange(0,181,5)
yi = [0.000,0.085,0.168,0.249,0.327,0.401,0.474,0.545,0.609,0.665,0.713,\\
      0.755,0.794,0.834,0.882,0.942,0.983,0.992,0.966,0.920,0.862,0.796,\\
      0.723,0.644,0.561,0.475,0.389,0.307,0.230,0.159,0.097,0.046,0.01,\\
      -0.006,-0.005,-0.002,0.000]

#Heeling Moment coefficient data, for zero and 20 degrees of heel,
#mainsail sheeted at 10deg from the hull centreline, Foresail at 17.5deg
#Data calculated from experiments on a scale model of an X-One design sail
#rig bt C.A. Marchaj at University of Southampton, 1962. Model tested in
#wind speeds from 5.1 to 9.26m/s. Since the wind tunnel tests were carried
#out at 1/3 full scale, this implies approximation works for full scale
#wind speeds of 15<VA<30m/s, or Beaufort force 2-3
#Additionally, the heel coefficient for an aparrent wind angle of 17.5deg
#at 20deg of heel is interpolated by the author for ease of programming.
#Reference: "Wind Tunnel Tests on a 1/3rd scale model of an X-One Design
#Yacht's Sails" University of Southampton Advisory Committee for Yacht
#Research, Report 11, October 1962
#Further Information can be obtained from the archives of the Wolfson
#Unit for Maritime Technology and Industrial Aerodynamics, University
#of Southampton
zero={17.5:0.359,20:0.502,22.5:0.663,25:0.839,27.5:1.023,30:1.180,\\
      32.5:1.332,35:1.460,37.5:1.545,40:1.635,42.5:1.690}
twenty={17.5:0.226,20:0.416,22.5:0.558,25:0.708,27.5:0.860,30:0.993,\\
       32.5:1.107,35:1.213,37.5:1.310,40:1.383,42.5:1.442}

```

```

#Sail Data
#Calculated for the proposed new Boleh rig by the Author using the
#preliminary sail plan provided by Westbrook Marine Ltd. using a
#computer spreadsheet calculation through the trapezium rule method.
#units of meters.

SA = 102.68          #The total main and jib combined sail area
VCE = 7.09           #Vertical scentre of effort for the combined sailplan
                    #from WL

def fit_line(x=10):
    """function fit_line produces a mathematical, rather than nuemeric,
    curve fitting the GZ curve up to the xth value.
    Produced by jdh2g10 for 3rd Year IP heeling investigation
    07/11/12
    """
    xj,yj=xi[:x],yi[:x]          #limit curve to 'x'th value
    return sp.polyfit(xj,yj,5)

def fit_line_inv(x=16):
    """function fit_line_inv produces a mathematical, rather than
    nuemeric, curve fitting the GZ curve up to the xth value,
    inverted such that heel angle theta is a fn. of GZ
    Produced by jdh2g10 for 3rd Year IP heeling investigation
    15/11/12
    """
    yj,xj=xi[:x],yi[:x]          #limit curve to 'x'th value
    return sp.polyfit(xj,yj,5)

def fit_plot(x1=16):           #fitted to 'x1'th value in the list
    """function takes the function curve fit and produces a set of points
    following that equation. Then plots these points against the GZ curve
    to provide a check of the fit between the two. Also produces a mean
    of the percentage error between the two curves at each point
    (excluding the zero value)
    Produced by Jonathan Happs for 3rd Year Individual Project
    contact jdh2g10@soton.ac.uk
    07/11/12
    """
    g=[]
    h=[]
    z=[]

    a,b,c,d,e,f=fit_line_inv(x1)

    for i in range (x1):
        g.append(5*i)

```



```

Performance Craft Notes. function uses 'linterpolate' and 'hround'
in this program.
Produced by Jonathan Happs for 3rd Year IP
contact jdh2g10@soton.ac.uk
14/11/12
"""

rtheta = m.radians(theta)
M = VA/340                                #Mach No.

q=0.5*1.4*101.325*M**2                    #Dyanamic Pressure in incompressible
#flow.
#Ref. Elements of Gas Dynamics, Liepmann
#and Roshko, p.55
#standard air properties found from
#"An engineering data book", Calvert and
#Farrar

att = hround(bamda)                       #make beta minus lambde compatable
mcoef = linterpolate(theta,0,20,zero[att],twenty[att]) #find heel
#force coeff.

return SA*VCE*q*mcoef*(m.cos(rtheta))**1.3

def GZmom(theta):
    pass

def momdif(bamda,VA):
    #return momconv(bamda,VA,theta)-
    pass

def heelfind(bamda,VA):
    """Function returns the approximate heel angle due to the yacht
    at an apparent wind angle bamda and apparent wind speed VA. VA
    is in meters per second and due to the imput data valid for 5.14
    <VA<9.26 Uses fit_line' in this program to calculate an
    analytical curve approximating the gz to the 16th point on the
    gz curve. Then uses the bisection algorithm to find the equilibrium
    angle of heel. Does so by finding the difference between the
    Righting moment (GZ*displacement) and the sail force heel moment,
    calculated by 'momconv' in this program. Produced by Jonathan Happs
    for 3rd Year Individual Project
    contact jdh2g10@soton.ac.uk
    15/11/12
    """
    delta = 18000                          #displacement value courtesy of M. Slater
    a,b,c,d,e,f=fit_line_inv(16)
    g,h,i,j,k,l=fit_line(16)

    def theta_est(GZ):                    #calculates theta for a given GZ (not used)

```

```

    return a*GZ**5+b*GZ**4+c*GZ**3+d*GZ**2+e*GZ+f

def GZ_est(theta):      #calculates GZ for a given theta
    return g*theta**5+h*theta**4+i*theta**3+j*theta**2+k*theta+l

def mmt_diff(theta):
    return momconv(bamda,VA,theta)-(GZ_est(theta)*delta)

return m.degrees(scipy.optimize.bisect(mmt_diff,0,90))

def plotcurves(a=[7,7.5,8,8.5,9,9.5,10,10.5,11,11.5,12,12.5,13,13.5,\\
                14,14.5,15]):
    """Function Plotting Heel angle against wind strength for various
    apparent wind angles input as a.
    Produced by Jonathan Happs for 3rd Year IP
    contact jdh2g10@soton.ac.uk
    15/11/12
    """

    b=[]
    c=[]
    d=[]
    e=[]
    f=[]

    for i in a:
        b.append(heelfind(20,i))

    for i in a:
        c.append(heelfind(25,i))

    for i in a:
        d.append(heelfind(30,i))

    for i in a:
        e.append(heelfind(35,i))

    for i in a:
        f.append(heelfind(40,i))

    plt.plot(a,b,'r*-',label='beta-lambda=20□deg')
    plt.plot(a,c,'bo-',label='beta-lambda=25□deg')
    plt.plot(a,d,'g<-',label='beta-lambda=30□deg')
    plt.plot(a,e,'y>-',label='beta-lambda=35□deg')
    plt.plot(a,f,'k^-',label='beta-lambda=40□deg')

    pylab.title("""Heel Angles against Apparent Wind Strength \nfor
    various Apparent Wind Angles, (dm=10, df=17.5)""")

```

```

pylab.xlabel('Apparent Wind Strength at Full Scale (m/s)')
pylab.ylabel('Heel Angle (deg)')
pylab.legend(loc=2)

plt.show()

```

Note that this code has been edited to fit the standard \LaTeX format, and consequently may not run correctly. A “\” has been used to indicate where a new line has been introduced to code.

A.3.3 Sail area calculation

Tables [4,5,6,7] show the derivation of the full size sail areas, using the trapezium rule and taken from the sail plan provided by Westbrook (2012). All dimensions are in meters unless otherwise stated.

A.3.4 Images of wind tunnel model construction

The model was produced from the original lines plan produced by Kilroy (1951), which is given in Fig.27.

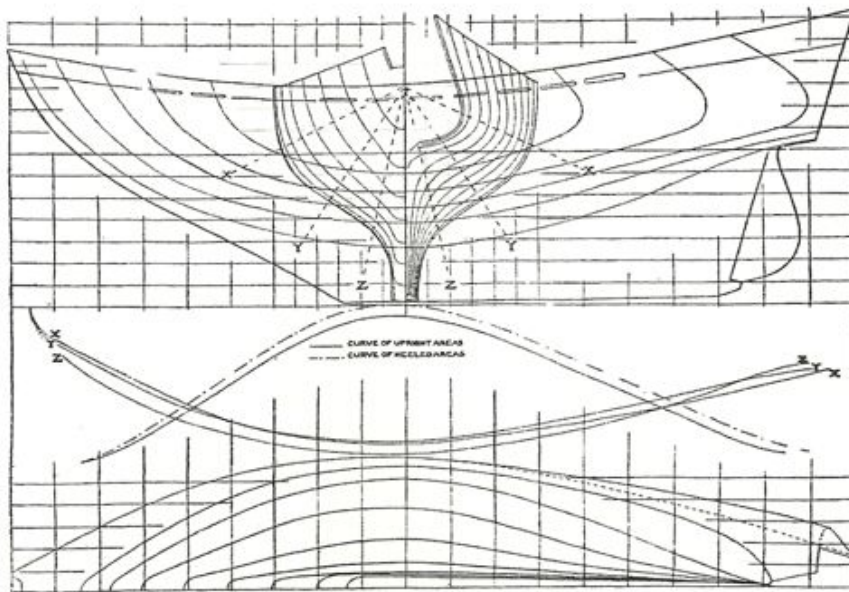


Figure 27: *The original lines plan of Boleh's rig, taken from Kilroy (1951) and copied and scaled for the production of the wind tunnel model*

A series of photographs of the model under construction are shown below, in sequence.

It is worth noting at this point that the 'horizontal section' method used for producing this model is not, in hindsight, the most appropriate. Though the overall strength is good, the high bulk of timber leads to a large time requirement for fairing the hull,

Table 4: Main area derivation. Factor refers to the model-full scale conversion

| h (cm) | w_1 (cm) | w_2 (cm) | $h \times \text{factor}$ | $w_1 \times \text{factor}$ | $w_2 \times \text{factor}$ | area |
|--------|------------|------------|--------------------------|----------------------------|----------------------------|-------|
| 4.00 | 15.40 | 15.40 | 1.92 | 7.39 | 7.39 | 14.19 |
| 4.00 | 15.40 | 14.20 | 1.92 | 7.39 | 6.82 | 13.64 |
| 4.00 | 14.20 | 12.30 | 1.92 | 6.82 | 5.90 | 12.21 |
| 4.00 | 12.30 | 10.40 | 1.92 | 5.90 | 4.99 | 10.46 |
| 4.00 | 10.40 | 8.00 | 1.92 | 4.99 | 3.84 | 8.48 |
| 4.00 | 8.00 | 5.40 | 1.92 | 3.84 | 2.59 | 6.17 |
| 4.00 | 5.40 | 2.50 | 1.92 | 2.59 | 1.20 | 3.64 |
| 2.50 | 2.50 | 0.50 | 1.20 | 1.20 | 0.24 | 0.86 |

Table 5: Jib area derivation

| h (cm) | w_1 (cm) | w_2 (cm) | $h \times \text{factor}$ | $w_1 \times \text{factor}$ | $w_2 \times \text{factor}$ | area |
|--------|------------|------------|--------------------------|----------------------------|----------------------------|-------|
| 4.00 | 12.90 | 10.75 | 1.92 | 6.19 | 5.16 | 10.90 |
| 4.00 | 10.75 | 7.90 | 1.92 | 5.16 | 3.79 | 8.59 |
| 4.00 | 7.90 | 6.30 | 1.92 | 3.79 | 3.02 | 6.54 |
| 4.00 | 6.30 | 4.00 | 1.92 | 3.02 | 1.92 | 4.75 |
| 4.00 | 4.00 | 1.70 | 1.92 | 1.92 | 0.82 | 2.63 |
| 3.10 | 1.70 | 0.00 | 1.49 | 0.82 | 0.00 | 0.61 |

Table 6: Main centroid derivation

| sail edge (cm) | h_1 (cm) | h_2 (cm) | x_{centre} | y_{centre} | x_{mmt} | y_{mmt} |
|----------------|------------|------------|---------------------|---------------------|------------------|------------------|
| 3.80 | 4.40 | 7.00 | -1.87 | 3.22 | -26.57 | 45.64 |
| 3.50 | 8.00 | 11.40 | -1.87 | 5.14 | -25.53 | 70.05 |
| 3.20 | 12.50 | 15.40 | -1.64 | 7.18 | -20.08 | 87.63 |
| 2.80 | 16.80 | 19.30 | -1.38 | 9.14 | -14.44 | 95.65 |
| 2.40 | 21.00 | 23.10 | -1.06 | 11.06 | -8.95 | 93.81 |
| 2.05 | 25.10 | 26.80 | -0.62 | 12.94 | -3.85 | 79.88 |
| 1.80 | 29.40 | 33.55 | -0.08 | 15.59 | -0.31 | 56.75 |
| 1.48 | 33.55 | 34.00 | 0.35 | 16.51 | 0.30 | 14.27 |

Table 7: Jib centroid derivation

| sail edge (cm) | h_1 (cm) | h_2 (cm) | x_{centre} | y_{centre} | x_{mmt} | y_{mmt} |
|----------------|------------|------------|---------------------|---------------------|------------------|------------------|
| 2.60 | 4.55 | 4.53 | 4.09 | 2.66 | 44.53 | 28.97 |
| 2.70 | 8.50 | 8.30 | 3.53 | 4.51 | 30.37 | 38.78 |
| 2.80 | 12.50 | 12.30 | 3.05 | 6.43 | 19.94 | 42.09 |
| 2.90 | 16.50 | 16.30 | 2.63 | 8.35 | 12.47 | 39.64 |
| 3.03 | 20.50 | 20.30 | 2.14 | 10.27 | 5.61 | 26.98 |
| 3.10 | 24.50 | 24.30 | 1.69 | 12.08 | 1.03 | 7.34 |

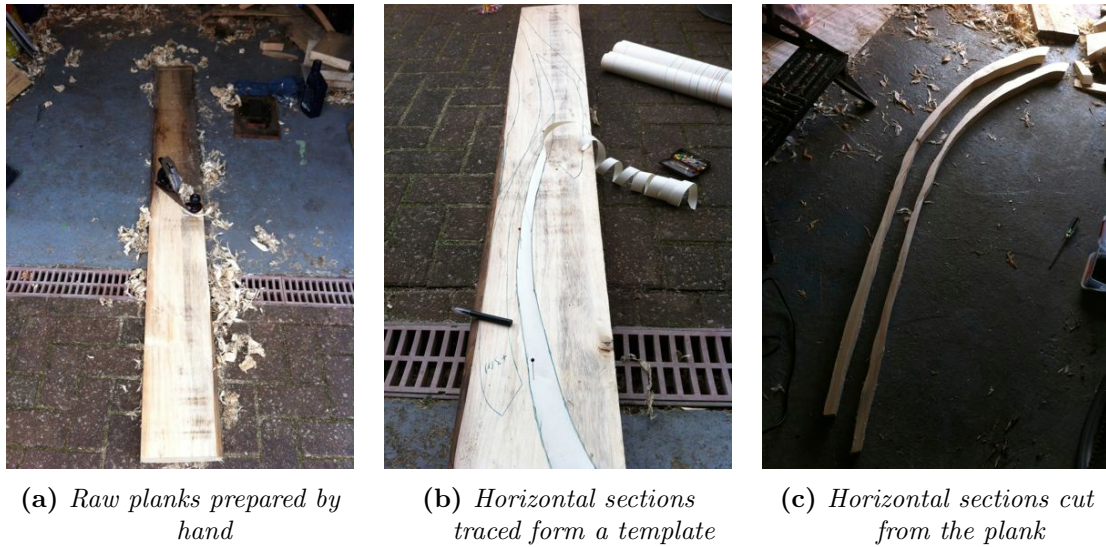


Figure 28: Producing the initial components of the model

and is likely to have lead to increased costs over a plank on frame method. Though the plank on frame method requires greater fore-knowledge for the placement of reinforcements, and is possibly more technically demanding in terms of construction, it is the author's opinion that, when producing models over a meter in length using hand tools, plank on frame is the less time consuming method.

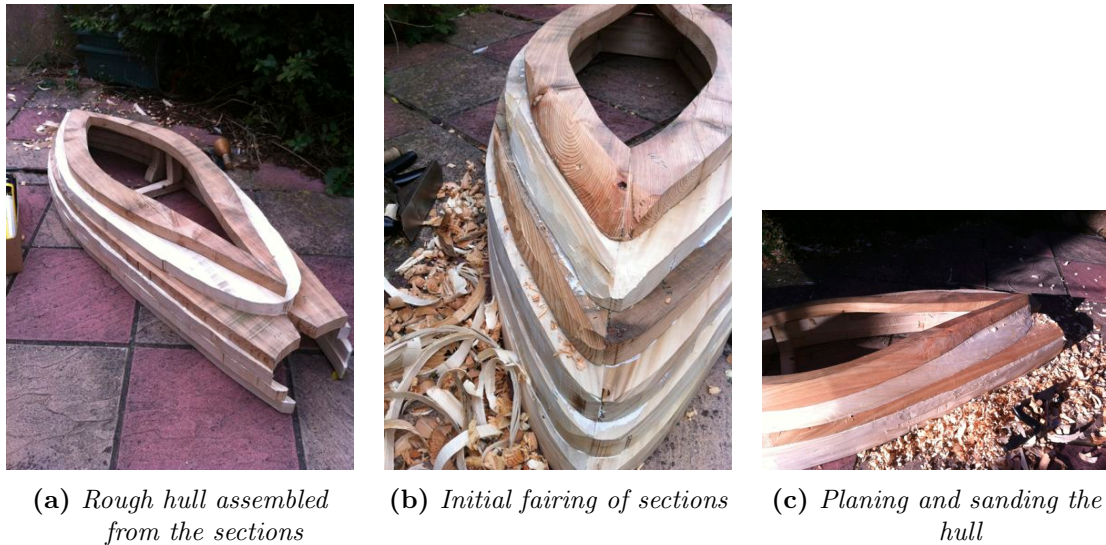


Figure 29: Assembly and fairing of the hull

Fig.31 shows the rig plans produced by Kilroy (1951) for the original rig shown in Fig.14; the rig produced here, designed by Westbrook (2012) as shown in Fig.21b is based on this design.

Fig.32a shows how aluminium reinforcements were stitched to sails to attach the wishbone booms, and the boom ends were stitched into these with linen thread. This is the most delicate section of the rig, and a flexible material such as leather or a synthetic equivalent will be required to hold the wishbone booms in place at full scale. Note the step in the reinforcements shown in Fig.32a such that the main load is



Figure 30: Finishing the hull

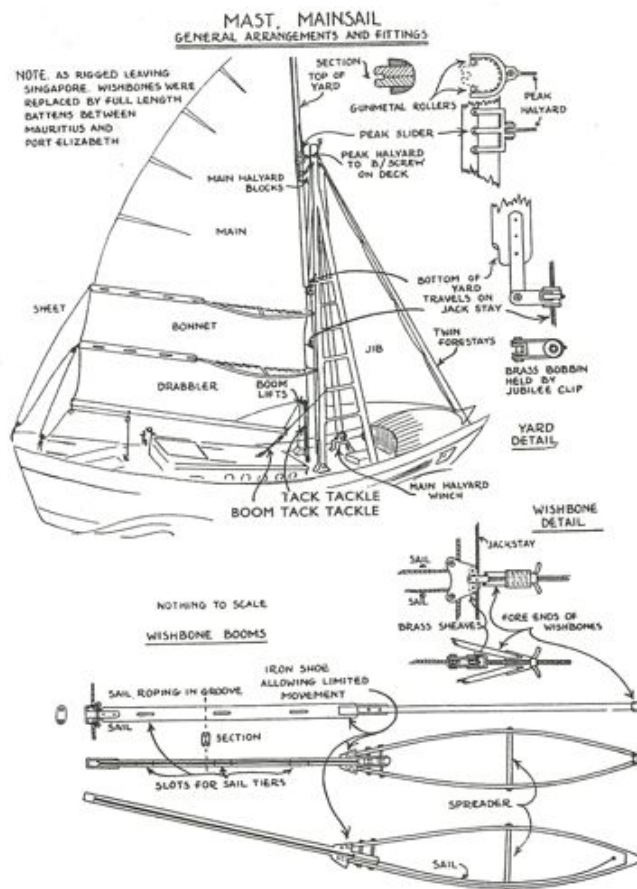


Figure 31: The original design plans of Boleh's rig, taken from Kilroy (1951) and used as a basis for the design and production of the tested rig

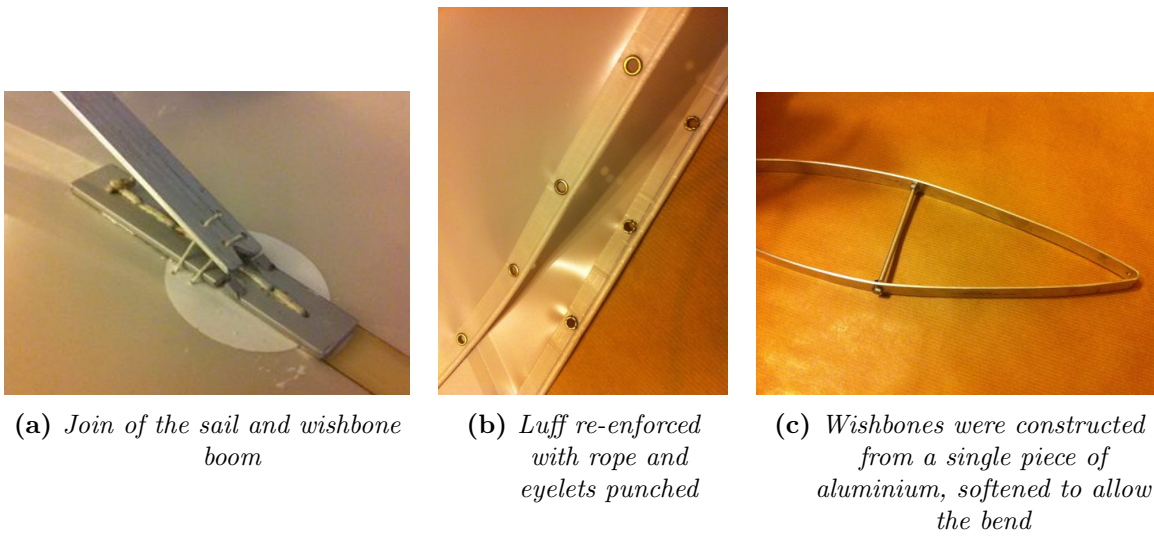


Figure 32: *Sail components*



Figure 33: *The author inspecting the model prior to testing*

transferred directly onto the plate. Note also that the flexible outer batten (orange) begins at the heel of the wishbone, and so is contained between the reinforcement plates on both sides.

In addition to this work, the sails were reinforced with tape along the seams, wool tufts were fitted for flow visualisation, and control lines were produced as shown in Appendix A.4.4.

A.4 Physical experiment planning and data

A.4.1 Calculation of Reynolds numbers for the heel program

The Reynolds number calculations undertaken for the Heeling Angle Program are set out below.

$$\text{Reynolds Number: } R_N = \frac{\rho u d}{\mu}$$

where ρ is the fluid density, u is the relative speed of the flow, d is the reference length and μ is the kinematic viscosity of the fluid.

The Reynolds number (R_N) is a non-dimensional number relating the relative flow velocity of fluid to some reference length of the object in its path. The value of the Reynolds number provides an insight into the flow characteristics that can be expected in a given situation, and allows comparison between geometrically similar situations independent of scale.

For low values of R_N the flow is said to be laminar, and the characteristics of the flow in terms of drag etc. are very dependent on R_N . For high values, above the critical Reynolds number ($\approx R_N > 1 \times 10^5$, dependent on geometry) the flow is said to be turbulent, and the flow characteristics are largely independent of Reynolds number. (Barlow et al., 1999) For medium values of R_N (in the order of 7.5×10^4) the flow is in transition, and may be laminar or turbulent. In the majority of experiments, Reynolds number equivalence across the scale range is impractical to achieve. Consequently, most experiments are conducted in turbulent flow, to simplify scaling. To ensure compatibility of scaling and force coefficients in the sub-critical region, Reynolds number equivalence is required. (Barlow et al., 1999)

The reference length was chosen as the length of the mainsail foot; 1.118m for the XOD and 0.8777 for *Boleh* at model scale.

This is in the mid \rightarrow high transitional region for turbulence effects on aerofoil sections in the case of the XOD experiments, and right across the transitional region for *Boleh*. (McMasters and Henderson, 1979) The wind speeds at which the Reynolds number was calculated for *Boleh* correspond directly to full scale apparent wind strengths of

Table 8: Reynolds numbers at various wind speeds

| <u>XOD</u> | | <u>Boleh (scale)</u> | |
|-----------------------------|--------------------|-----------------------------|--------------------|
| Wind Speed (ms^{-1}) | R_N | Wind Speed (ms^{-1}) | R_N |
| 9.25 | 6.76×10^5 | 6.5 | 3.73×10^5 |
| 6.17 | 4.51×10^5 | 4.5 | 2.58×10^5 |
| 5.14 | 3.76×10^5 | 1.5 | 0.86×10^5 |

0.5 \rightarrow 2 knots.

A.4.2 Justification of mismatched Reynolds numbers in the physical experiments

The principle requirements of scaling are accurate geometric representation of the phenomena under investigation during the test, and correct non-dimensionalisation of the measured results, in order to accurately represent the results at the required scale.

The standard non-dimensionalisation formula used in this experiment reduces a force to coefficient form through the use of the speed, fluid density, and surface area required to produce that force. So defining the relevant fundamental physical dimensions as in Table 9;

Table 9: List of fundamental physical units

| Dimension | Symbol |
|-----------|--------|
| Mass | M |
| Time | T |
| Length | L |

Then the quantities in this case, Force, Area, Density and Speed have respective dimensions MLT^{-2} , L^2 , ML^{-3} and LT^{-1} . Therefore the equation

$$C_F = \frac{F}{\frac{1}{2}\rho AU^2}$$

can be written in terms of the dimensions as

$$1 = \frac{MLT^{-2}}{ML^{-3}L^2L^2T^{-2}}$$

The coefficients were not altered, and the same equation was used both to reduce and expand the coefficients to diminutional form. This part of the scaling process is therefore valid.

A factor of 10 was however applied to the Reynolds number in order to attain results which had relevance to the operating conditions of the yacht. This factor being non-

dimensional, the scaling process will be valid provided the flow regime, and hence the geometry of the problem remain similar between the attained Reynolds number, in the region of 10^5 , and the Reynolds number of the predictions, which are in the region of 10^6 . It can be seen from Fig.17 that this is just beyond the transition range for aerofoils, and consequently it is considered that the coefficients would change little, provided the Reynolds number did not decrease. The turbulence stimulation on the sails discussed in Section 3.3 ensured that the flow over the sails was turbulent in any case.

However, since separation effects etc. are nonetheless strongly dependent on Reynolds number, a review of current practice was undertaken through literature to ascertain the degree to which this was considered acceptable practice. As noted by van Oossanen (1993) “Optimum trim of sails comes from their maximum lift and drag coefficients, dependent on the point of sail. In this condition there is a significant amount of flow separation, which leads to significant inaccuracies in simulation since the full scale Reynolds Number cannot usually be adhered to.”

Though no literature was found quoting directly the factor applied to the Reynolds number, useful information was found from Claughton and Campbell (1994), Razenback and Mairs (1997) and van Oossanen (1993) which clearly showed that some disregard of Reynolds number equivalence in expanding the sail force coefficients is common practice. For example, in discussing standard procedure at the facilities used in this investigation, Claughton and Campbell (1994) notes that “the model Reynolds number will be lower than that at full scale by approximately the scale ratio. The Reynolds number effects on the mast and rigging drag are certainly significant, and it is our practice to measure the lift and drag characteristics of the bare hull and mast and where appropriate make an R_N correction to the drag coefficient in a manner analogous to towing tank data scaling.” Since the aerodynamic forces due to the bare hull and masts were removed from the results of this experiment, it was considered that no corrections were required.

However, clearly “it is, however still desirable to maximise the wind tunnel speed” (Razenback and Mairs, 1997) and it was for this reason that a testing wind speed of 6.5m s^{-1} was used. This was given by the manufacturers of the sails as the maximum wind speed that they could be subjected to, when re-enforced with additional tape, without significant risk of damage.

A.4.3 Testing matrix for the experiments

Since the model is fixed in the wind tunnel, the angle of the wind relative to the model relates to the apparent wind seen in the real case, and must be corrected to calculate the equivalent true wind angle. This must be done iteratively, since the

Table 10: *Matrix of test conditions*

| AWA (deg) | A _F (deg) | A _M (deg) | Repeat 1 | Repeat 2 | Upright | 10° heel |
|-----------|----------------------|----------------------|----------|----------|---------|----------|
| 20 | 12.5 | 5 | ✓ | | ✓ | ✓ |
| | 12.5 | 0 | ✓ | | | ✓ |
| | 20 | 5 | | | ✓ | ✓ |
| | 25 | 5 | ✓ | ✓ | ✓ | |
| 30 | 12.5 | 5 | | | ✓ | |
| | 20 | 5 | | | ✓ | |
| | 25 | 5 | ✓ | ✓ | ✓ | ✓ |
| 40 | 12.5 | 10 | ✓ | | ✓ | |
| | 20 | 10 | | | ✓ | |
| | 25 | 10 | ✓ | | ✓ | ✓ |
| | 25 | 15 | ✓ | | | ✓ |
| 50 | 20 | 10 | | | ✓ | |
| | 25 | 10 | ✓ | | ✓ | |
| | 25 | 15 | ✓ | | ✓ | ✓ |
| 60 | 25 | 20 | | | ✓ | |
| | 35 | 30 | ✓ | ✓ | ✓ | ✓ |
| 70 | 40 | 35 | ✓ | | ✓ | |
| | 40 | 45 | | | ✓ | |
| 80 | 30 | 45 | ✓ | ✓ | ✓ | ✓ |
| | 35 | 50 | | | ✓ | |
| | 40 | 55 | ✓ | ✓ | ✓ | |
| | 40 | 45 | | | ✓ | |
| 90 | 35 | 50 | | | ✓ | |
| 100 | 40 | 45 | ✓ | | ✓ | ✓ |
| | 45 | 45 | | | | ✓ |
| | 45 | 50 | | | ✓ | |
| | 50 | 55 | | | ✓ | |
| 110 | 45 | 50 | | | ✓ | |
| 120 | 55 | 45 | | | ✓ | ✓ |
| | 60 | 60 | ✓ | ✓ | ✓ | |
| | 65 | 55 | | | ✓ | |
| 130 | 60 | 50 | | | ✓ | |

appropriate true wind angle depends on the speed of the yacht, which is dependent in the apparent wind angle and speed. The vector summation which produces the apparent wind speed is shown in Fig.34.

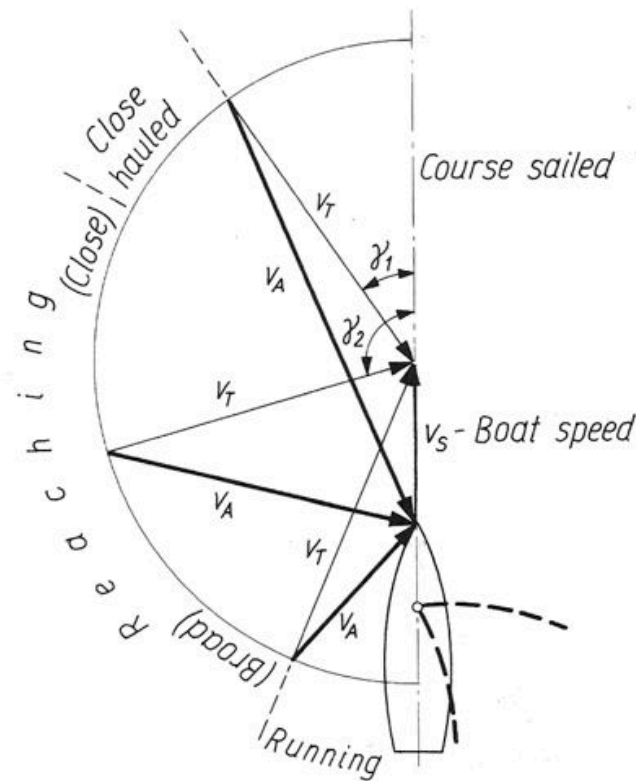


Figure 34: Comparison of true and apparent wind angles for all points of sail, taken from Marchaj (1964)

A.4.4 Notes on use of the equipment and calibration

The 7x5 wind tunnel at the University of Southampton has been used for investigations relating to sailing yachts since the late 1950s. A detailed discussion of the facilities and procedures currently in use are given in a paper by Cloughton and Campbell (1994), but the key consideration for production of the model was the setup of the dynamometers, shown in Fig.35.

Holes can be drilled in the hull in any location, provided the hull is rigid, to take the transverse support, and at several angles to allow measurements at an angle of heel. Due to the size of the model it was necessary to raise it slightly above its natural waterline. The connection between the dynamometers and the hull is shown in Fig.36.

The global experimental set up is shown in Fig.37. Additionally, Fig.38 shows the arrangements for the minor control lines, which were adjusted during initial calibration and then held constant.

Before the experiments the calibration of the equipment was checked to ensure the

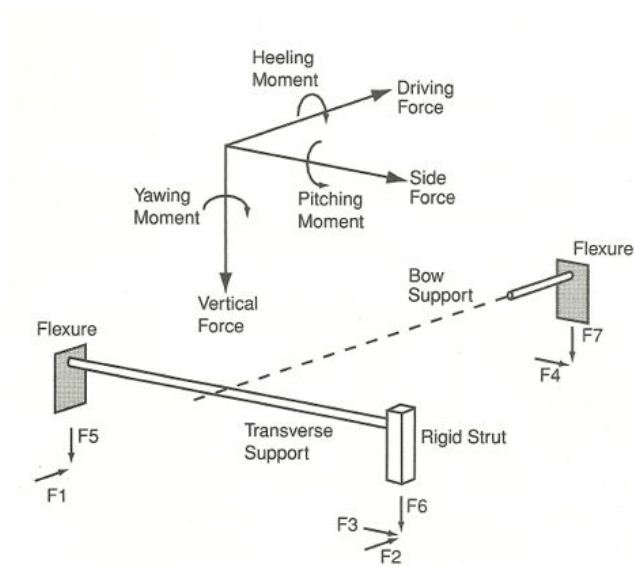


FIGURE 15.22 The Wolfson unit sail model test rig.

Figure 35: Schematic of the dynamometer set up used in the experiments, due to Claughton and Campbell (1994) but taken from Barlow et al. (1999)



(a) Connection between the dynamometers and the transverse bar. Note the extended slot used to raise the model up, and the tape on the bar. Though it was not possible to fix the model on the bar due to the curvature of the hull, it was an interference fit, and the tape was used to mark the position of the model, confirming it did not travel along the bar during the experiment

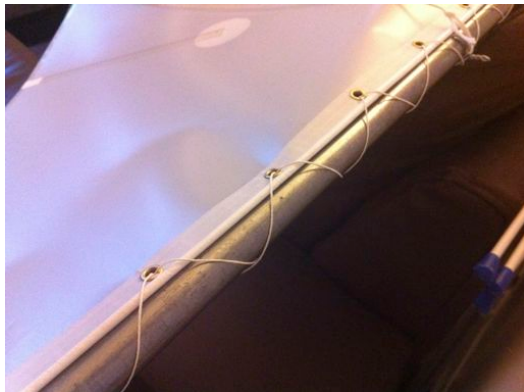


(b) Connection between the bow bar and the flexure. Note the use of an M6 screw thread to enable fine adjustment of the bow bar length

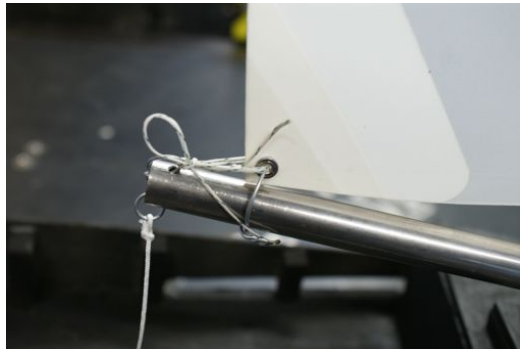
Figure 36: Detail of the connections used between model and dynamometers in the experiment



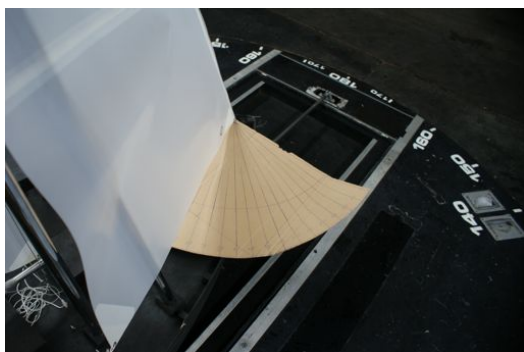
Figure 37: *Experimental setup for the physical experiments, upright condition*



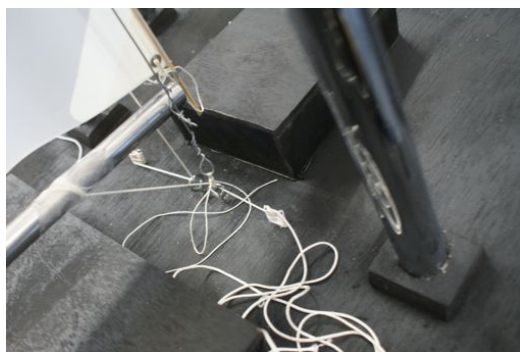
(a) The mainsail was double laced to the gaff, since it was not possible to machine the slot that would normally be used at this scale. This also acted as turbulence stimulation



(b) Outhaul used to control the position of the clew on the boom. Note the wire ring to hold it down to the boom



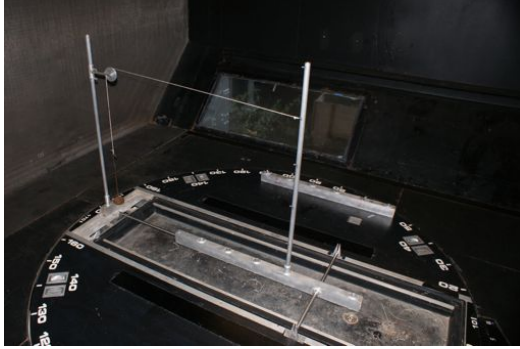
(c) The sheeting angles were measured for every configuration using a large protractor. This eliminated errors due to stretching or slip of the control lines on the cleats



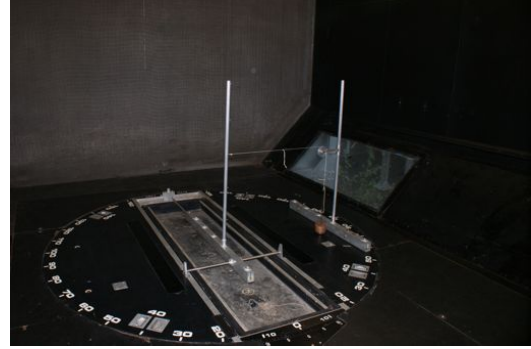
(d) Detail of arrangements around the mainsail tack. Note the wire stay used to support the sail, and the weak kicking strap, which was replaced in later experiments

Figure 38: Control lines and detailed rig modelling used to replicate the character of the real sails as accurately as possible

validity of the experiments. This is done using a system of moment armatures shown in Fig.39. The equipment was found to have an accuracy within 2%, and the Wolfson unit, who own the equipment, have specifically requested that students do not attempt to calibrate the equipment without detailed training. Consequently, no further calibration was carried out.



(a) Calibration of the testing equipment using weights of known value, forward calibration



(b) Calibration of the testing equipment using weights of known value, transverse calibration

Figure 39: Calibration of the experimental equipment

A.4.5 Plots of experimental data

Global plots

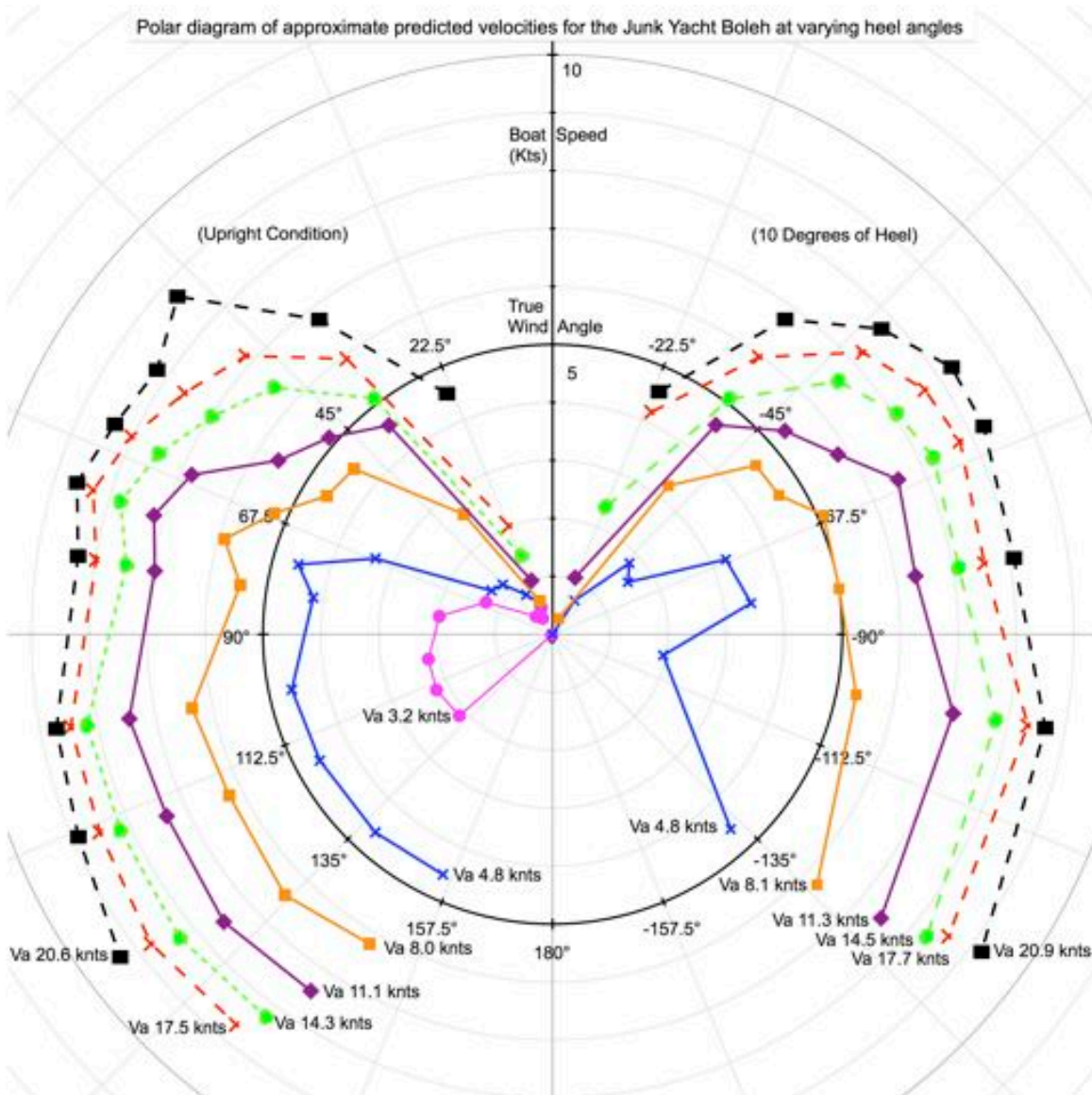


Figure 40: Approximate polar velocity plot for the junk yacht Boleh in upright and heeled conditions. Some anomalous results can be identified, for example $V_a=4.8\text{knts}$, $AWA=100^\circ$ in the heeled condition. These errors are predominantly for the low speed cases due to the resolution and calibration errors in the equipment. It can be surmised from this plot that the best velocity made good to windward is at an apparent wind angle around 50° . Note that measurements at $AWA=130^\circ$ were not taken in the heeled condition, or for full scale wind speeds of 20 knots in the upright condition. Due to the low accuracy of the results, measurements at full scale wind speeds of 3.2knts were not taken in the heeled condition.

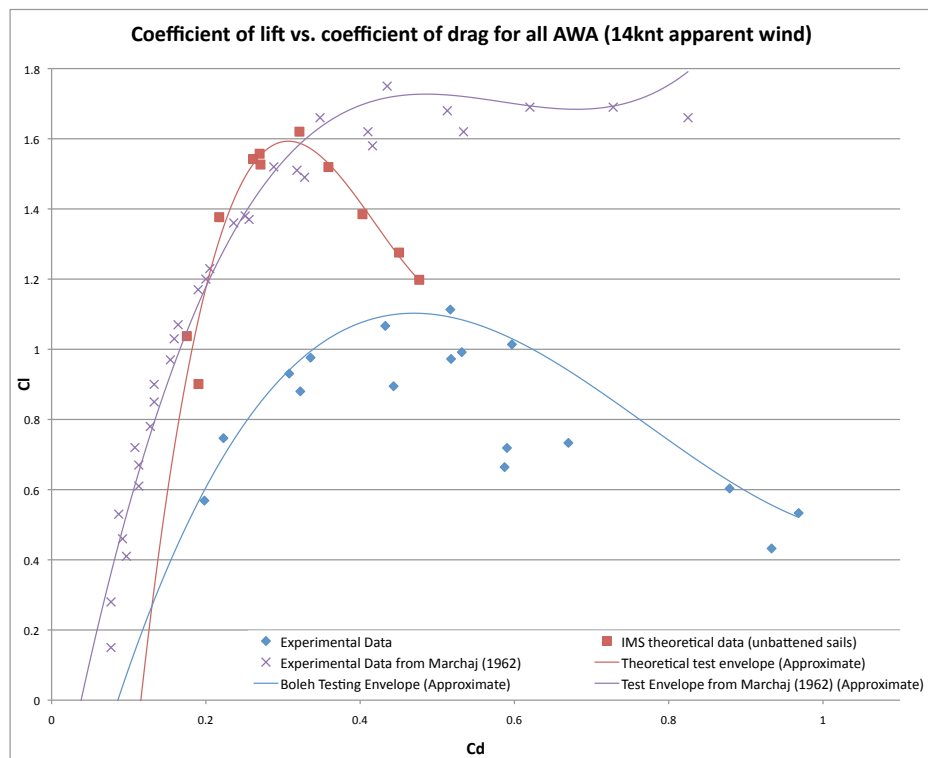


Figure 41: Plot of lift coefficient versus drag coefficient for the experimental and theoretical data, with 'envelopes' of maximum efficiency highlighted as recommended by Marchaj (1987), see Fig.22

Results in the upright condition

It should be noted that some of the repeated show significant comparative offsets, due to latent stresses within the experimental setup as discussed in Section 3.3. The close correlation shown by the remainder of the repeated runs demonstrates the accuracy of the data, however in those cases where erroneous data was produced caution is advised in its interpretation.

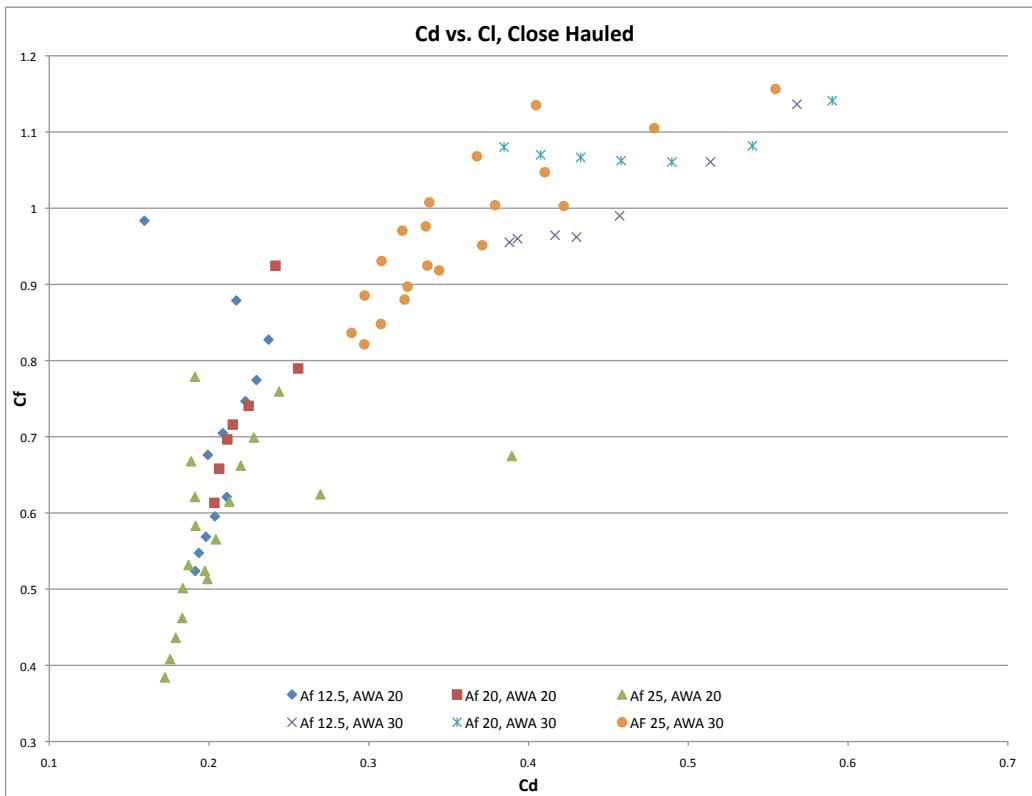


Figure 42: Coefficients of Lift against Coefficient of Drag in the Close Hauled Condition. From examples in literature it would be expected that the case $A_F = 20$ would have the highest lift/drag ratio. However, it can be seen that this is not the case due to the interferon of the masts

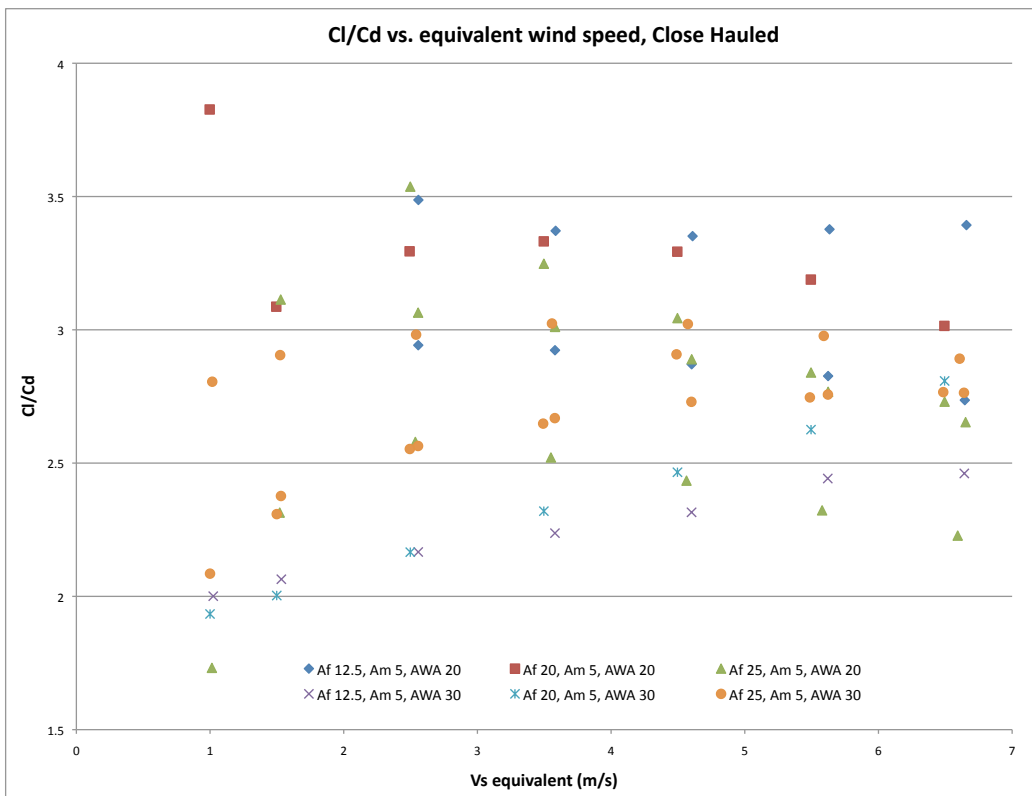


Figure 43: Ratio of Lift and Drag Coefficients against standardised wind speed, in the Close Hauled Condition. Note that there is some discrepancy between repeats for both cases where $A_f=25$

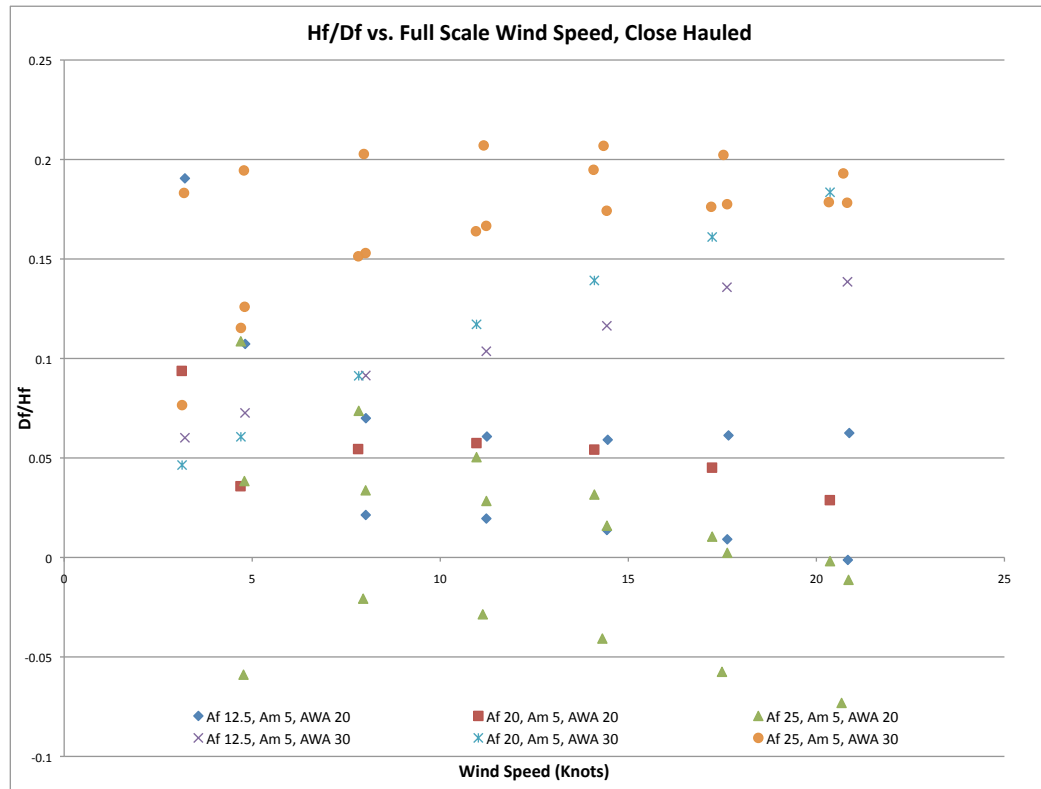


Figure 44: Ratio of full scale Lift and Drag Forces against full scale wind speed in Knots, in the Close Hauled Condition

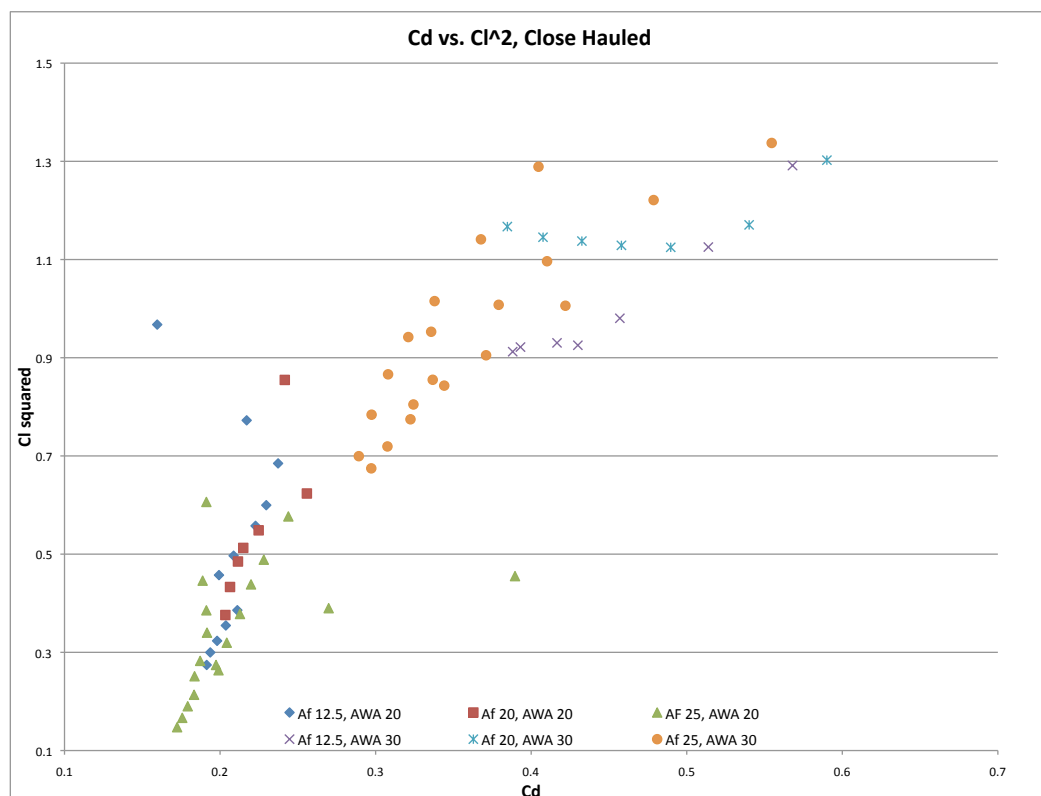


Figure 45: Coefficient of Lift squared against Coefficient of Drag in the Close Hauled Condition

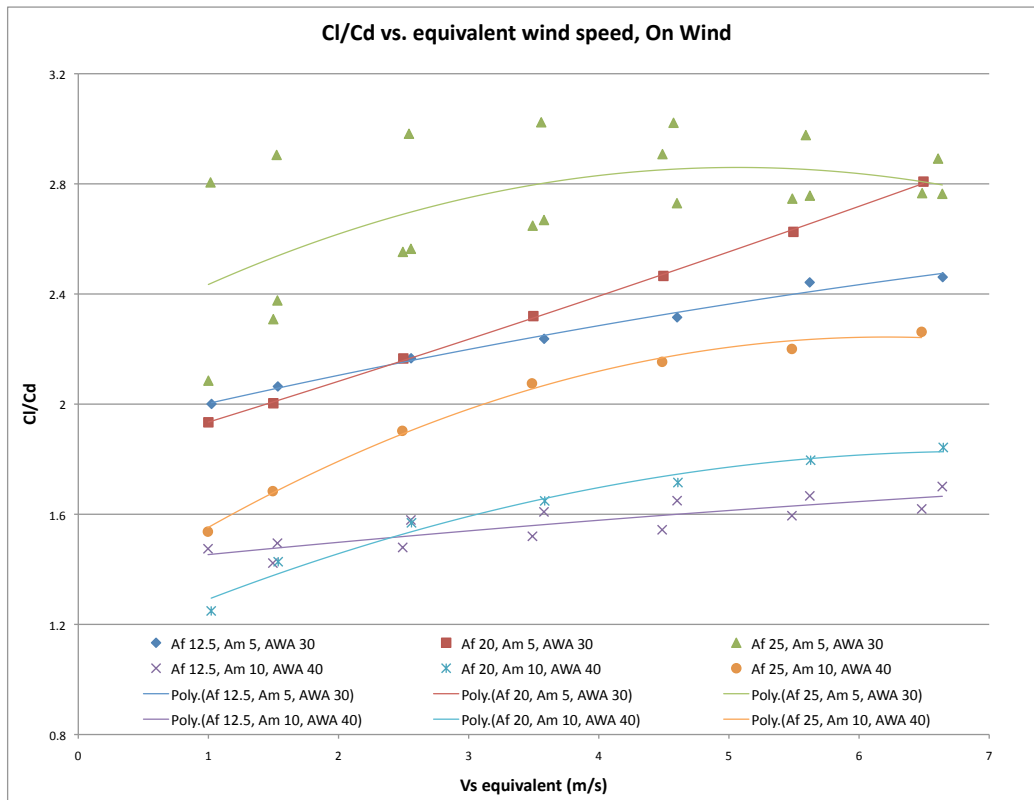


Figure 46: Coefficients of Lift and Drag against standardised wind speed in the On-Wind Condition. Note again the upper erroneous data in series 25,5,30

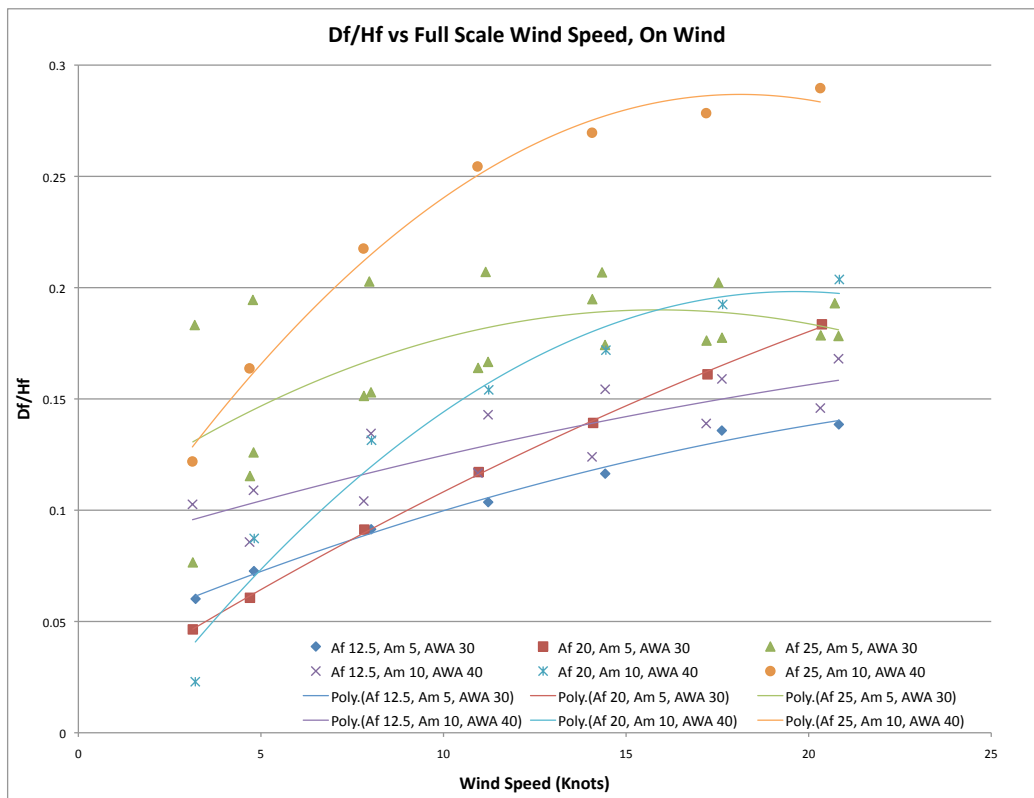


Figure 47: Ratio of Drive and Heel Forces against Full Scale Wind Speed in Knots, in the On-Wind Condition

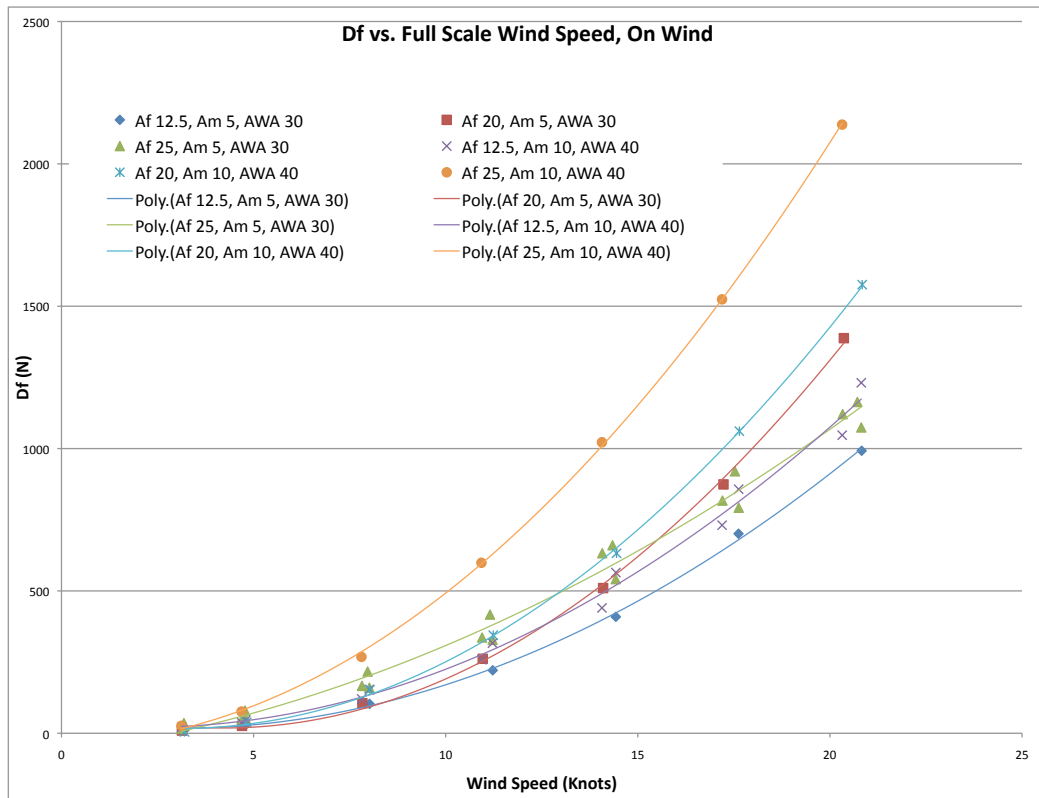


Figure 48: Full scale Drive Force against full scale Wind Speed in Knots, in the On-Wind Condition

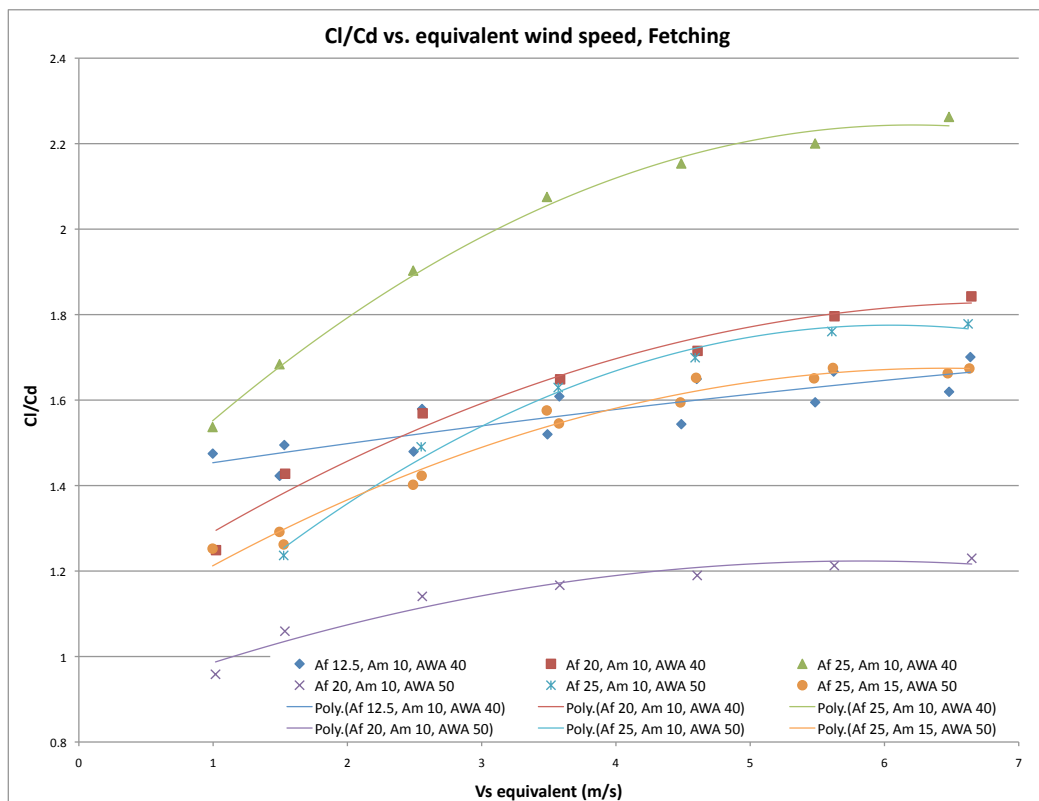


Figure 49: Coefficients of Lift and Drag against Standardised Wind Speed in the Fetching Condition

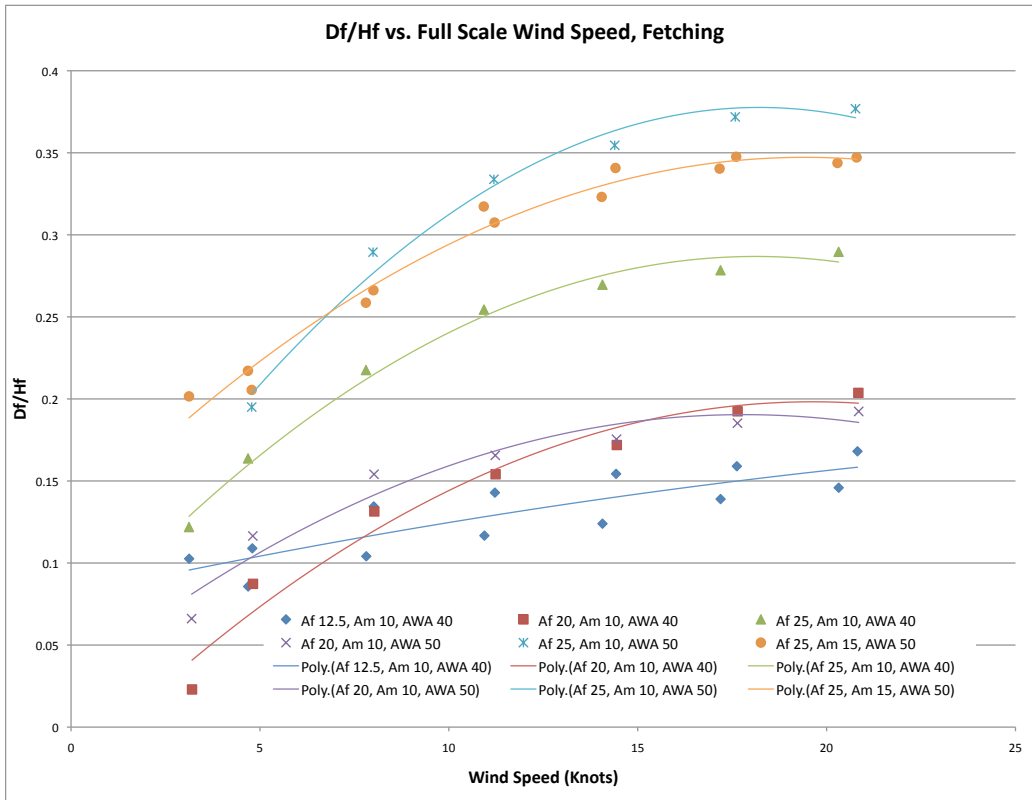


Figure 50: Ratio of Drive and Heel Forces against Full Scale Wind Speed in Knots, in the Fetching Condition. Surprisingly, the drive/heel ratio is shown to be greater in the case of 25,10,50 than for 25,15,50, which produced the highest heel force of the experiment. Consequently, it could be that this data is also suspect. However, this occurs in several cases where the mainsheet angle was increased, and it is possible that it is a feature of this rig for certain sheeting angles, since the drive force remains constant in all those cases.

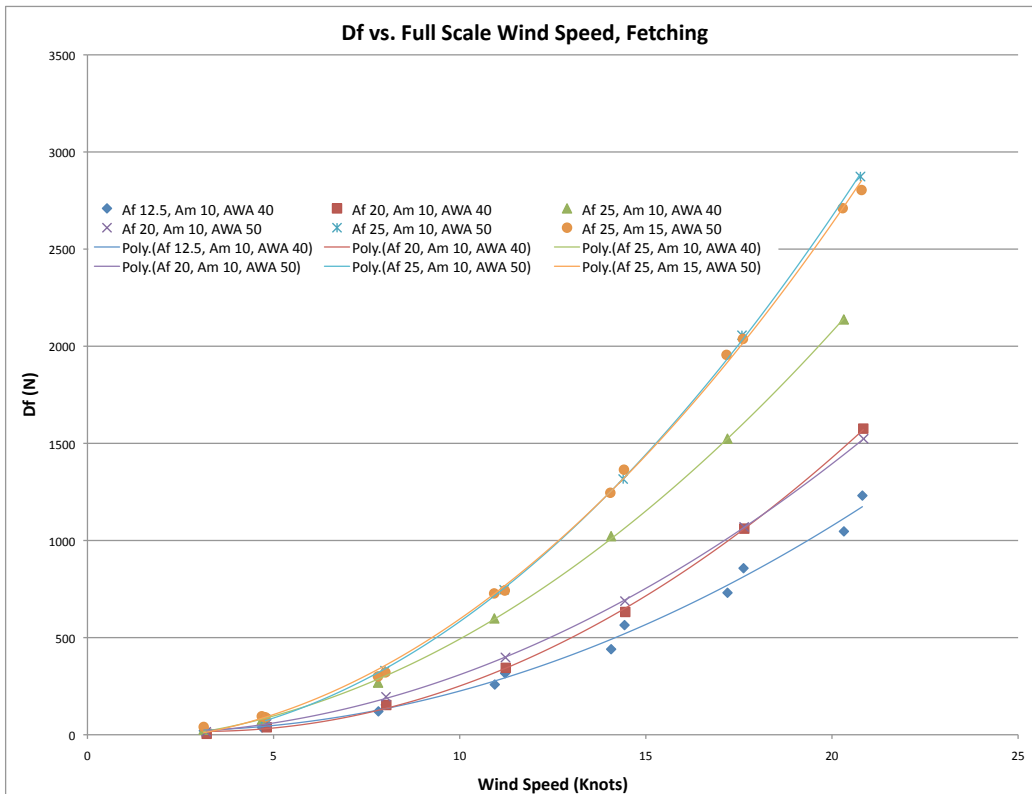


Figure 51: Full scale Drive Force against full scale Wind Speed in Knots, in the Fetching Condition

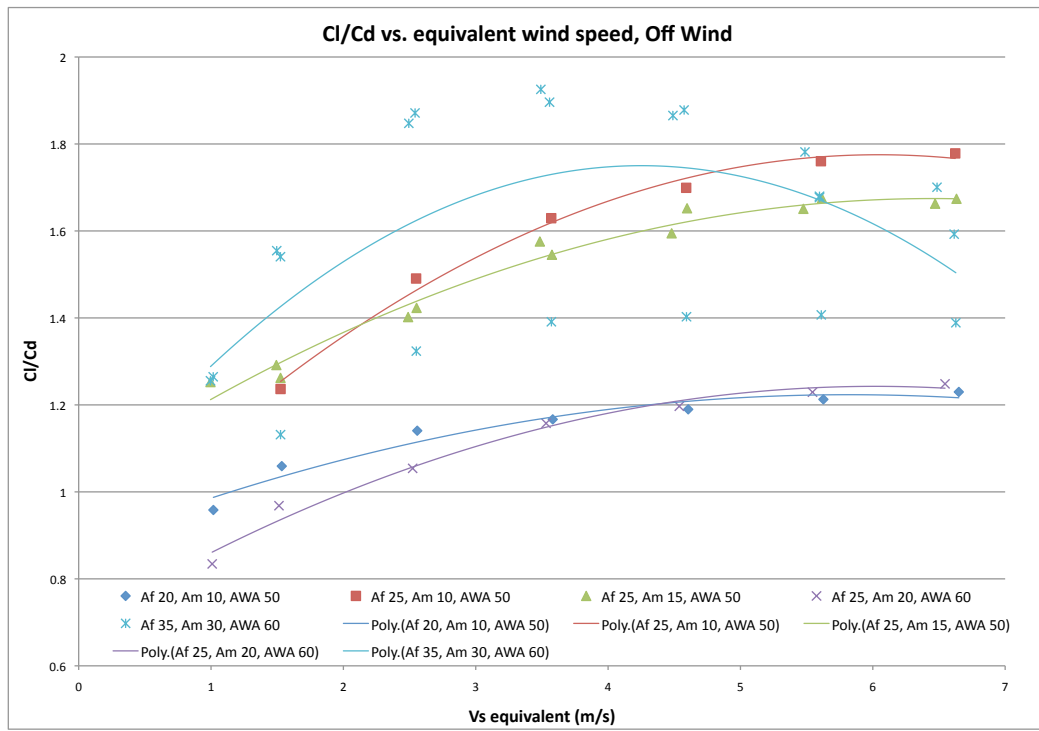


Figure 52: Coefficients of Lift and Drag against Standardised Wind Speed in the Off-Wind Condition. Note the erroneous lower data in the case of 35,30,60

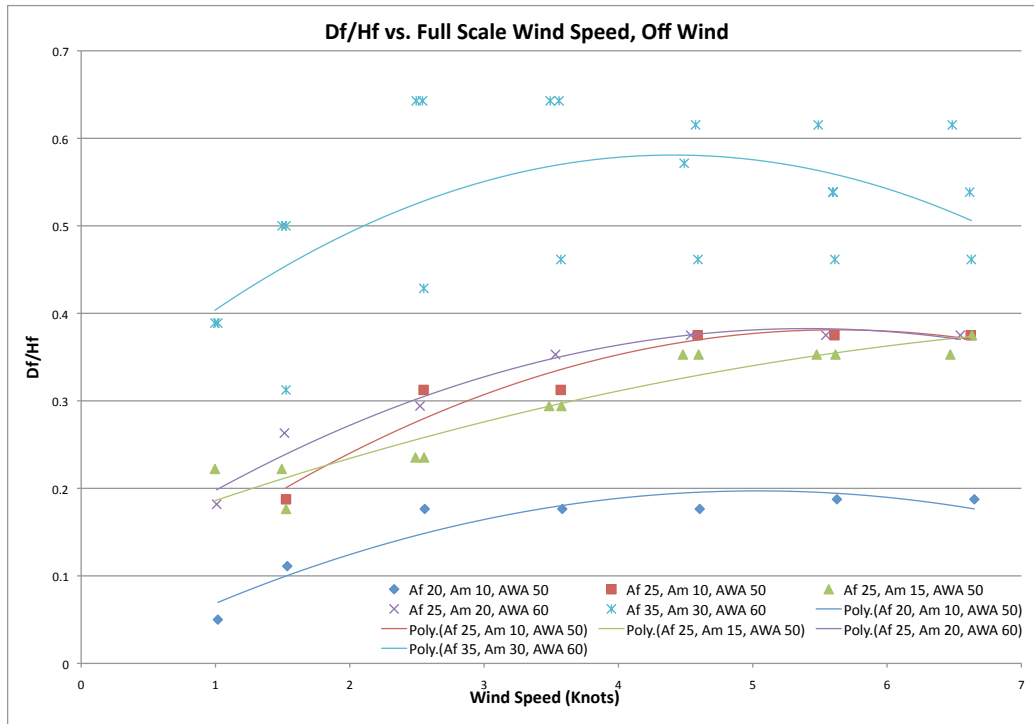


Figure 53: Ratio of Drive and Heel Forces against Full Scale Wind Speed in Knots, in the Off-Wind Condition

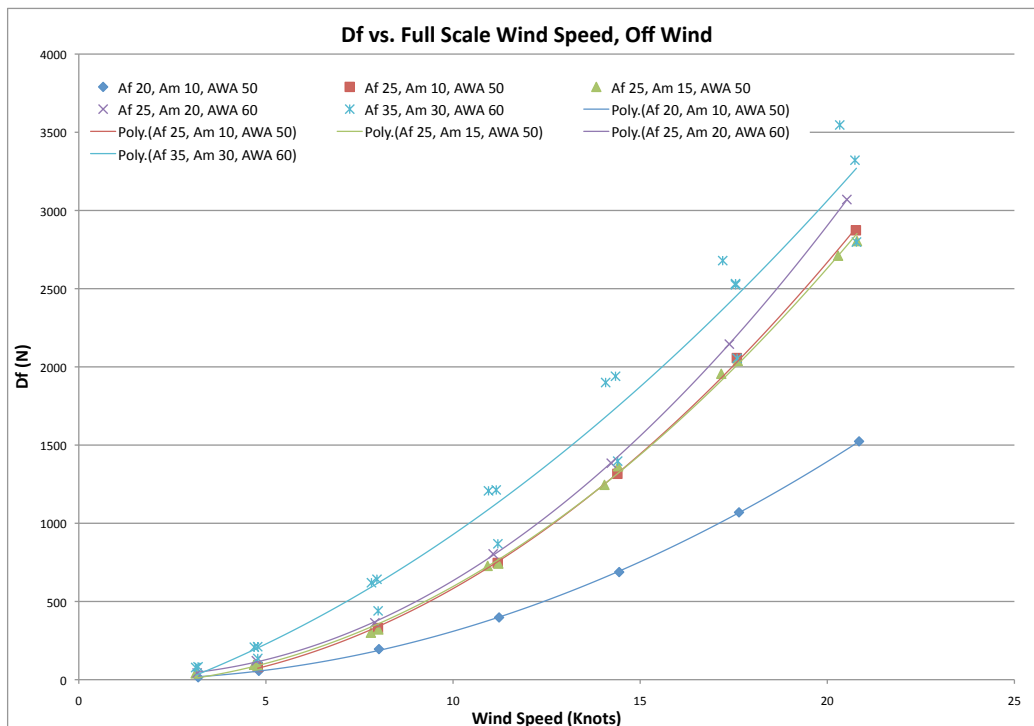


Figure 54: Full scale Drive Force against full scale Wind Speed in Knots, in the Off-Wind Condition

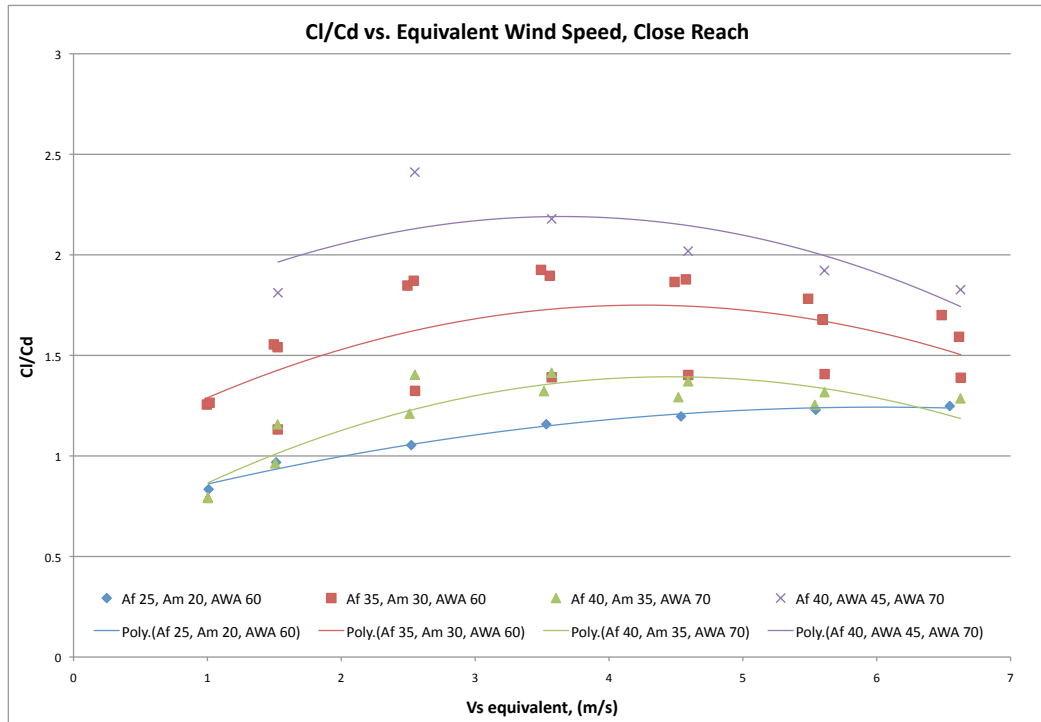


Figure 55: Coefficients of Lift and Drag against Standardised Wind Speed in the Close Reach Condition. Note the erroneous lower data in the case of 35,30,60

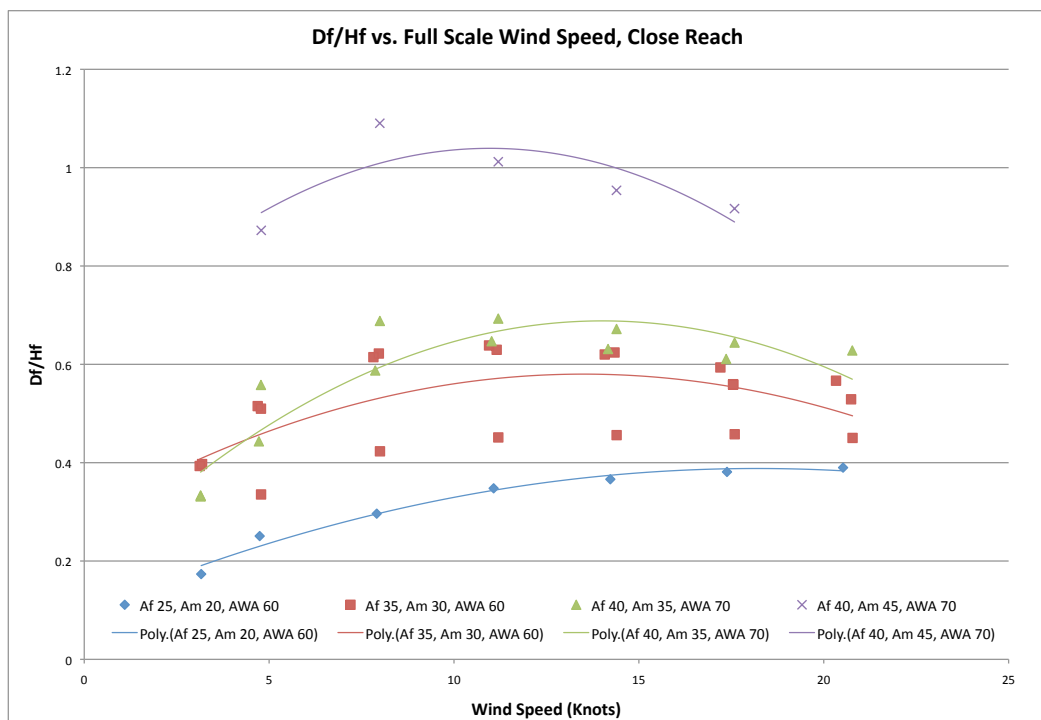


Figure 56: Ratio of Drive and Heel Forces against Full Scale Wind Speed in Knots, in the Close Reach Condition

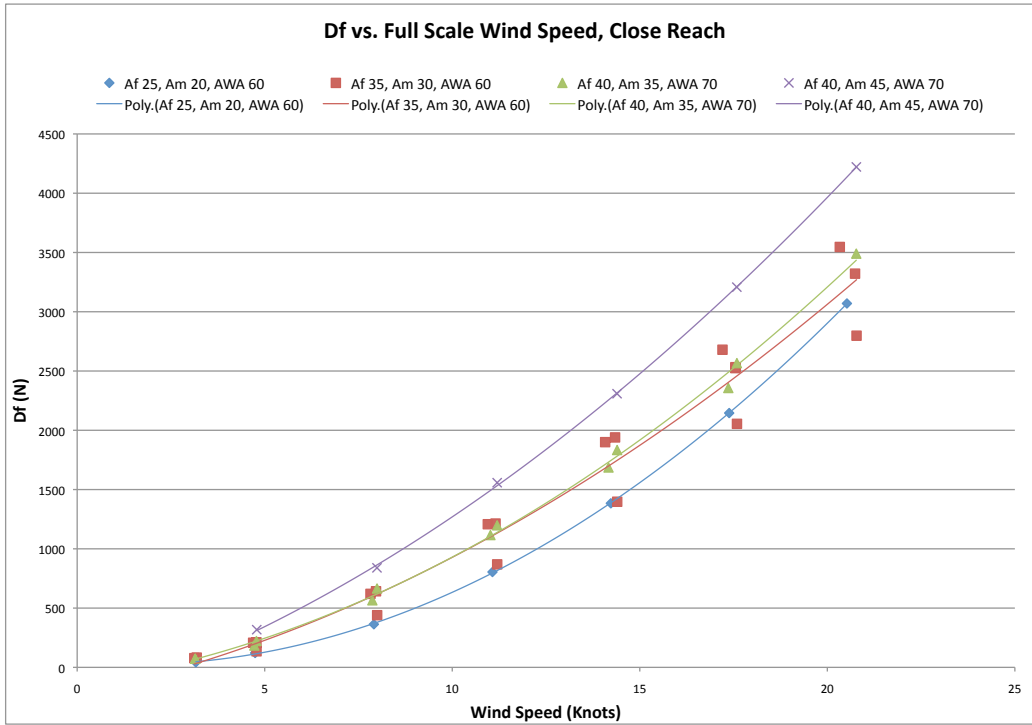


Figure 57: Full scale Drive Force against full scale Wind Speed in Knots, in the Close Reach Condition

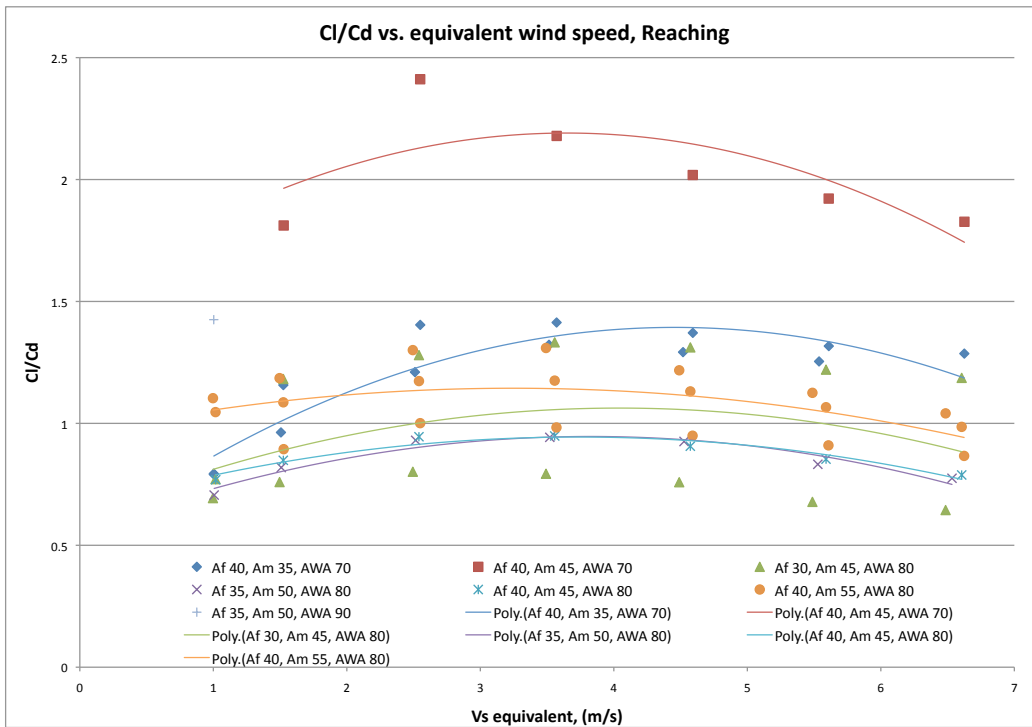


Figure 58: Coefficients of Lift and Drag against Standardised Wind Speed in the Reaching Condition. Note the erroneous upper data in the case of 30,45,80

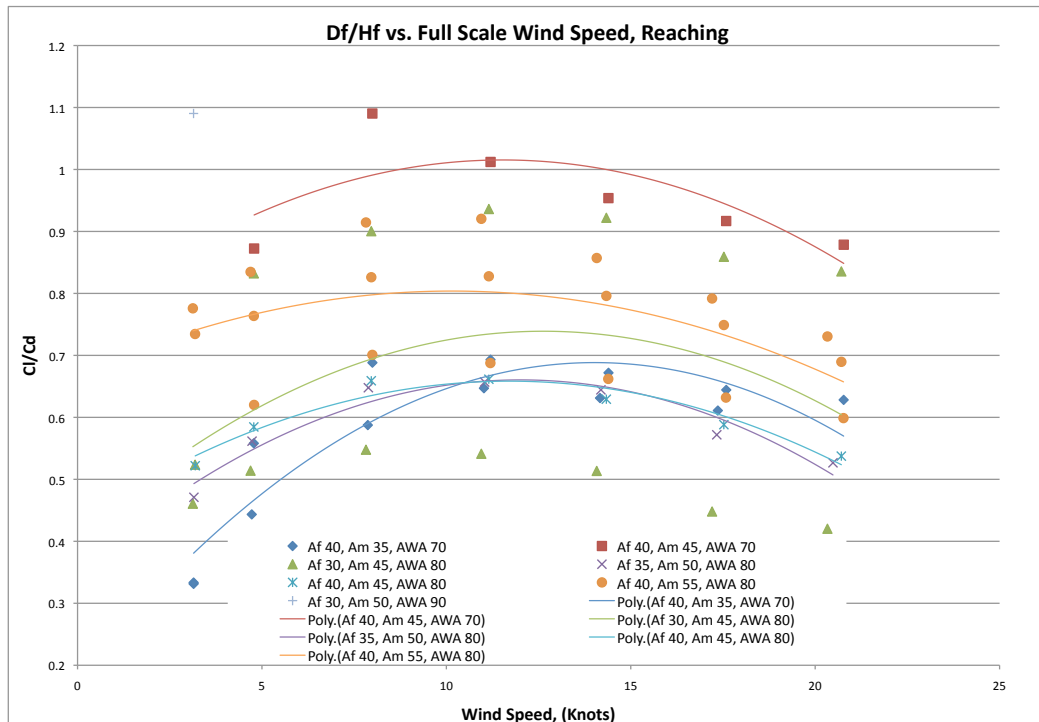


Figure 59: Ratio of Drive and Heel Forces against Full Scale Wind Speed in Knots, in the Reaching Condition

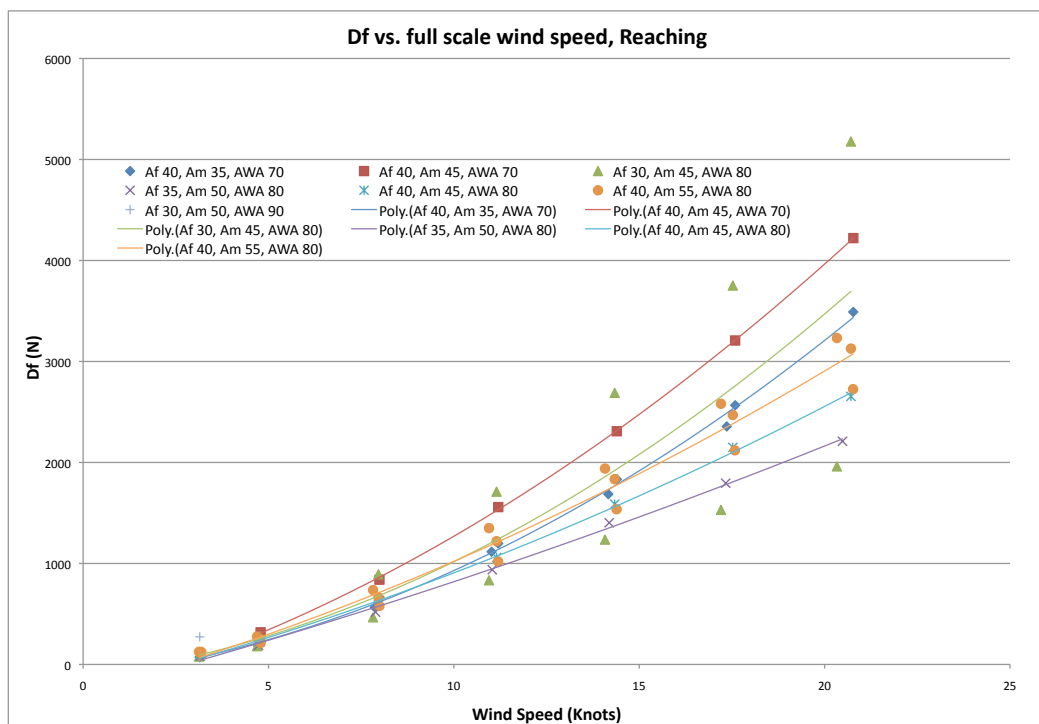


Figure 60: Full scale Drive Force against full scale Wind Speed in Knots, in the Reaching Condition. Note the erroneous upper data in the case of 30,45,80

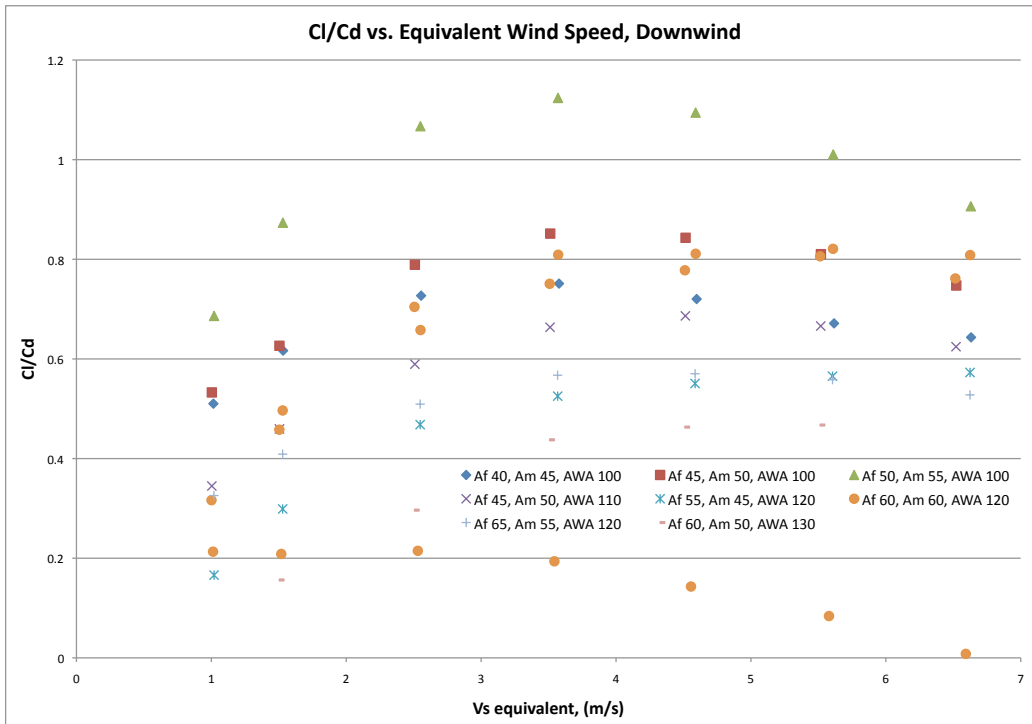


Figure 61: *Coefficients of Lift and Drag against Standardised Wind Speed in the Downwind Condition. Note the erroneous lower data in the case of 60,60,120 which was caused in this case by severe interaction between the wishbone booms and the masts*

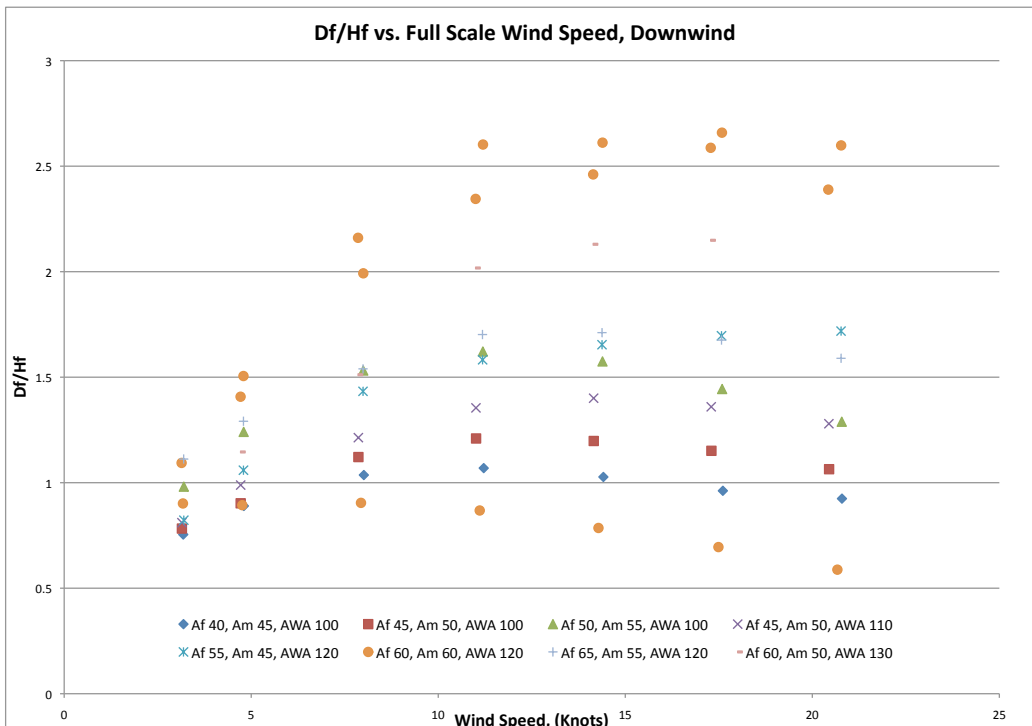


Figure 62: *Ratio of Drive and Heel Forces against Full Scale Wind Speed in Knots, in the Downwind Condition*

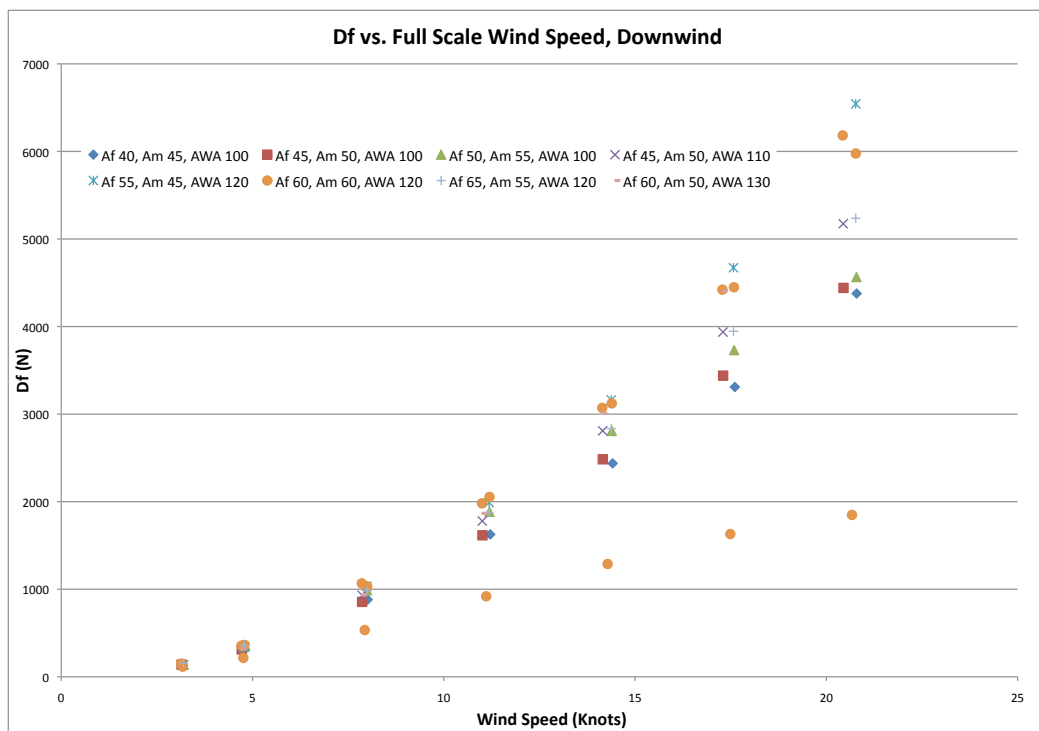


Figure 63: Full scale Drive Force against full scale Wind Speed in Knots, in the Downwind Condition

Results in the heeled condition

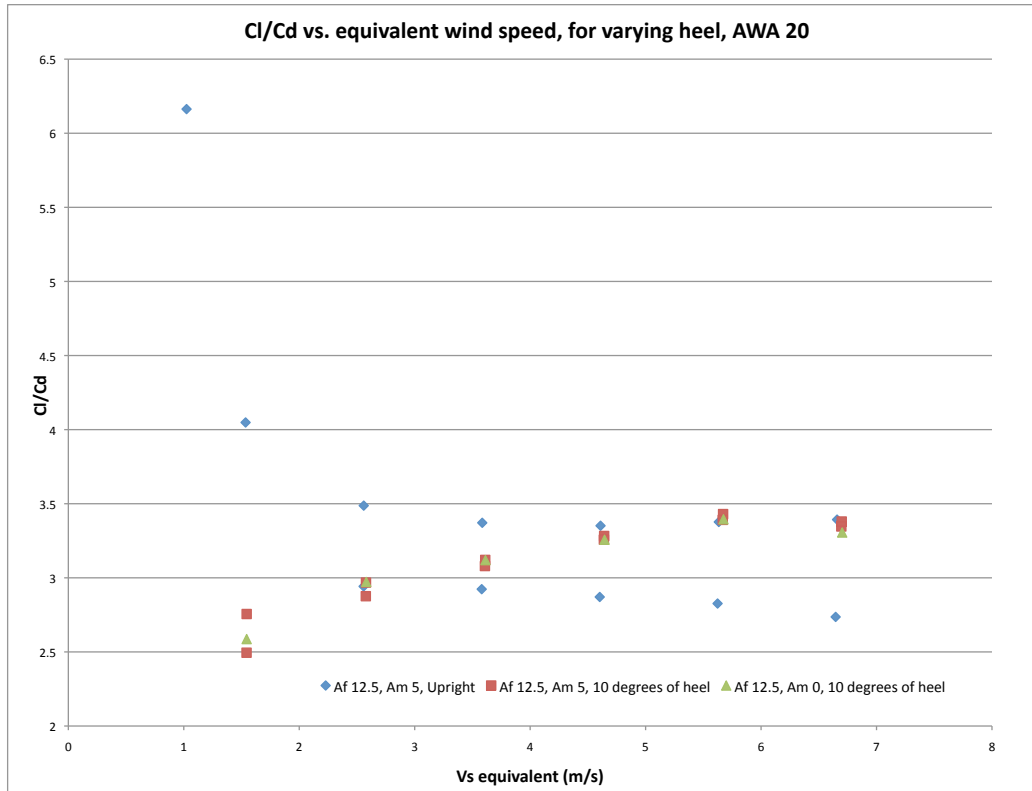


Figure 64: Coefficients of Lift and Drag against Standardised Wind Speed at 10 degrees of heel, with an apparent wind angle of 20 degrees. The error in the upright data is of unknown cause



Figure 65: Ratio of Drive and Heel Forces against Full Scale Wind Speed in Knots at 10 degrees of heel, with an apparent wind angle of 20 degrees

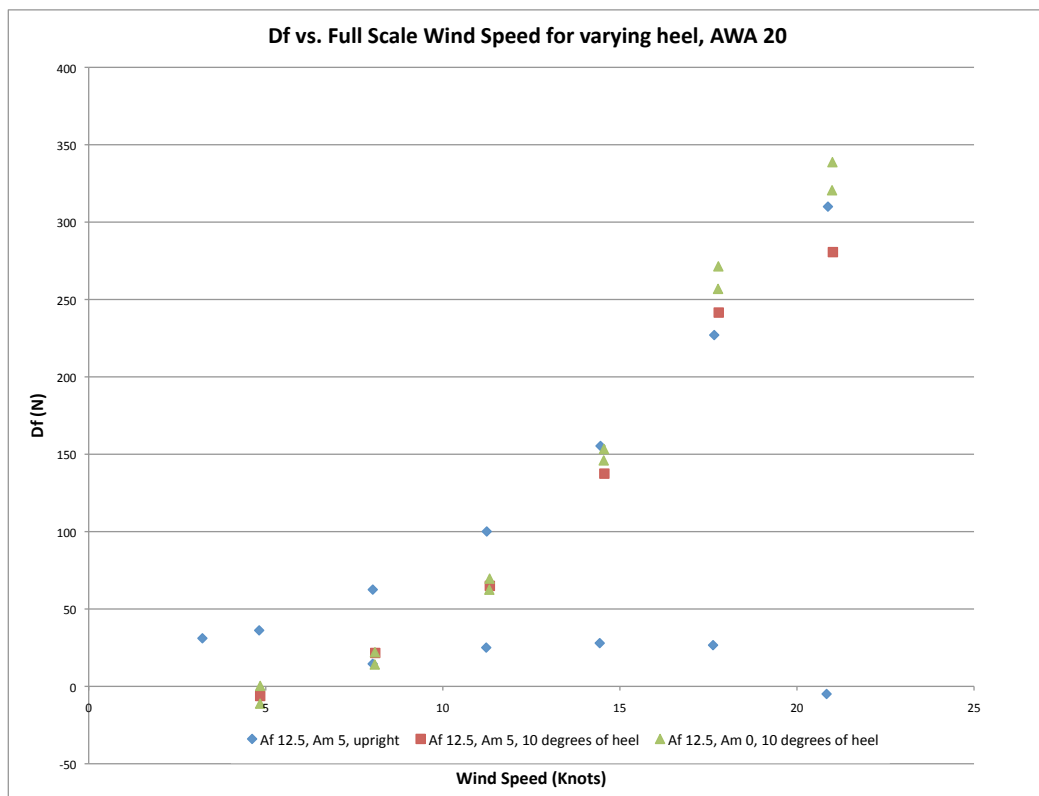


Figure 66: Full scale Drive Force against full scale Wind Speed in Knots at 10 degrees of heel, with an apparent wind angle of 20 degrees

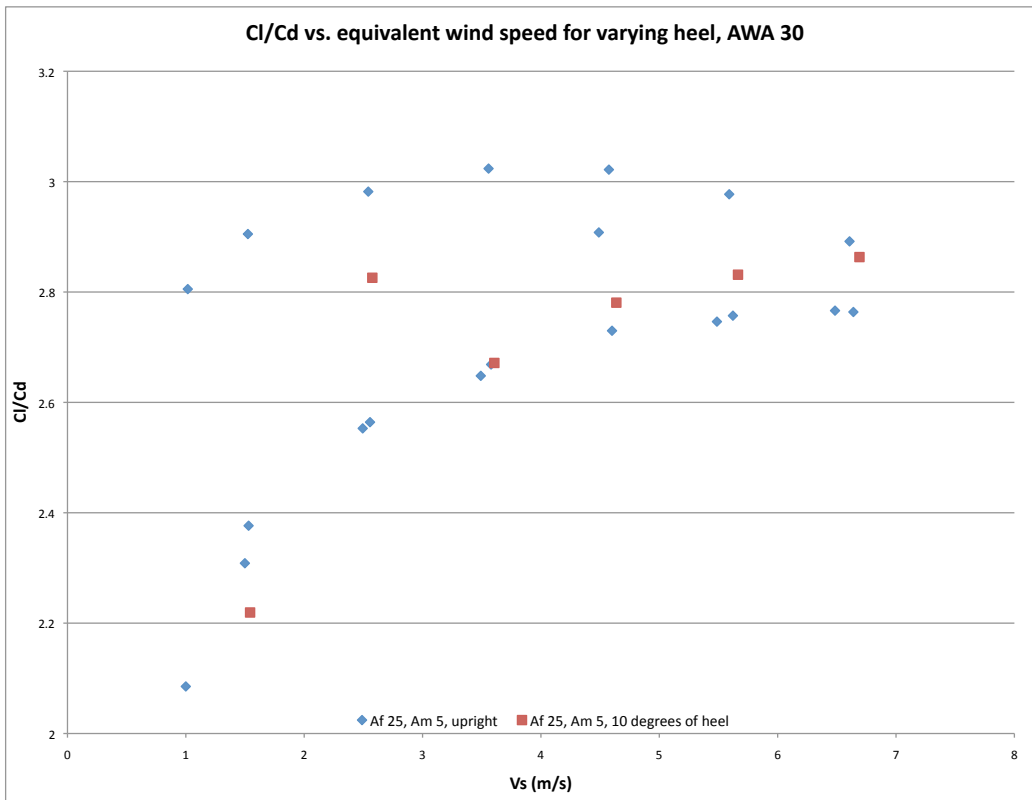


Figure 67: Coefficients of Lift and Drag against Standardised Wind Speed at 10 degrees of heel, with an apparent wind angle of 30 degrees

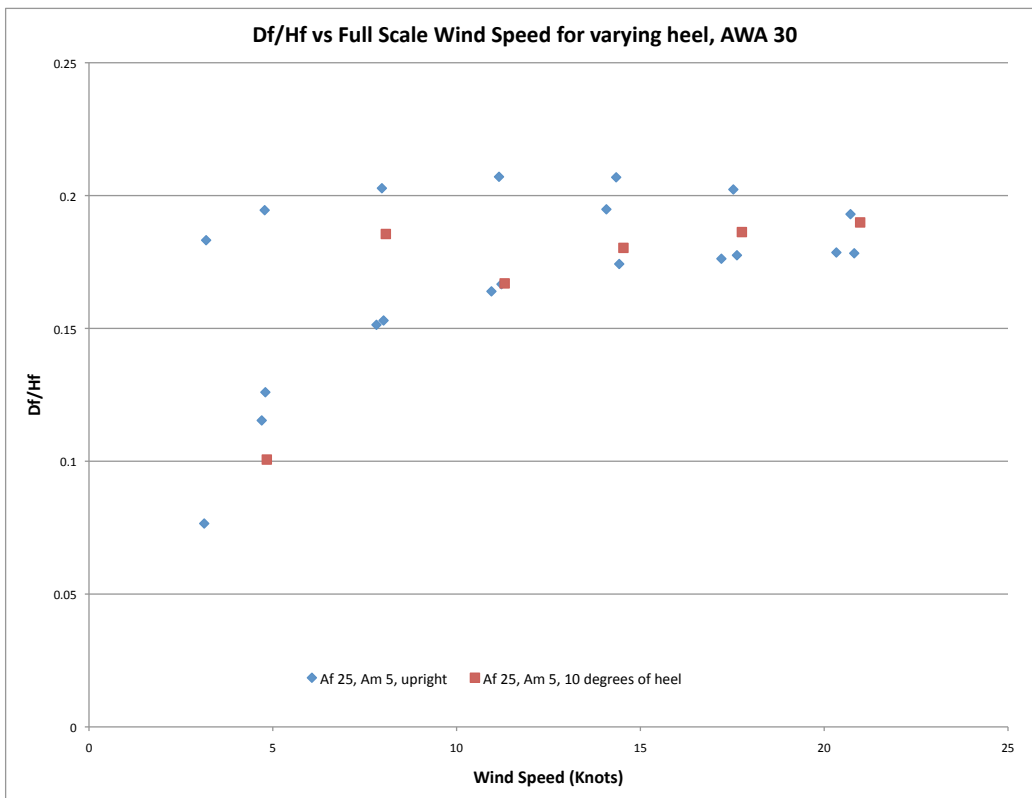


Figure 68: Ratio of Drive and Heel Forces against Full Scale Wind Speed in Knots at 10 degrees of heel, with an apparent wind angle of 30 degrees

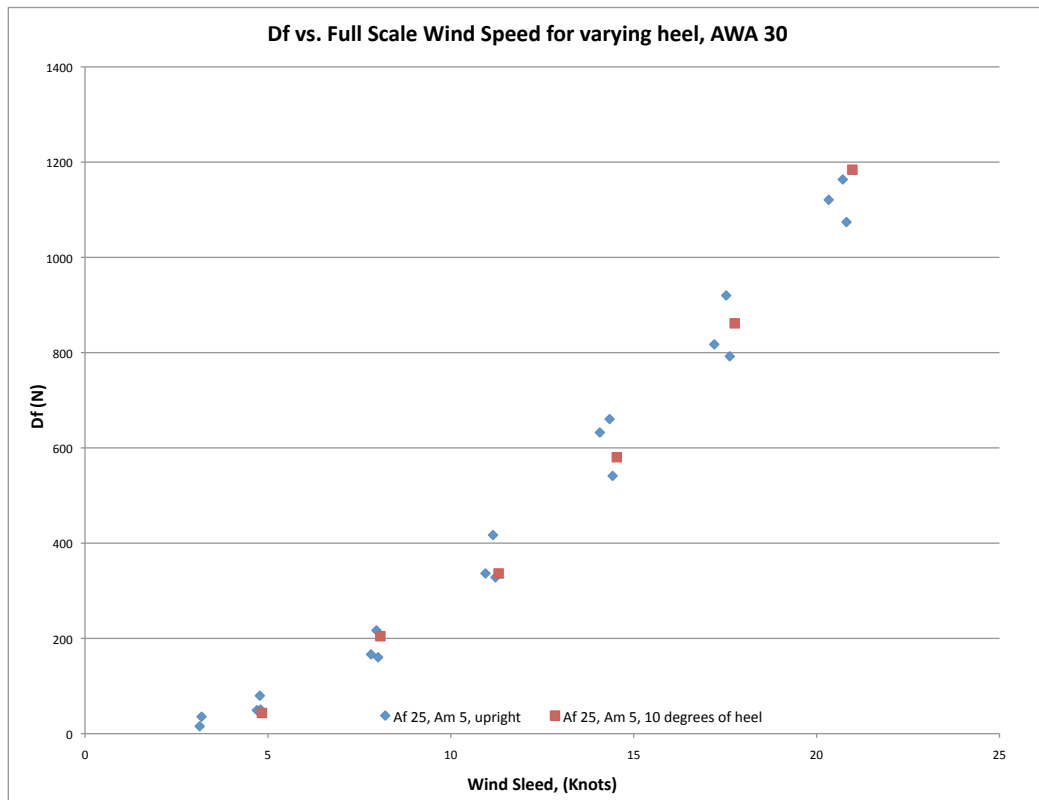


Figure 69: Full scale Drive Force against full scale Wind Speed in Knots at 10 degrees of heel, with an apparent wind angle of 30 degrees

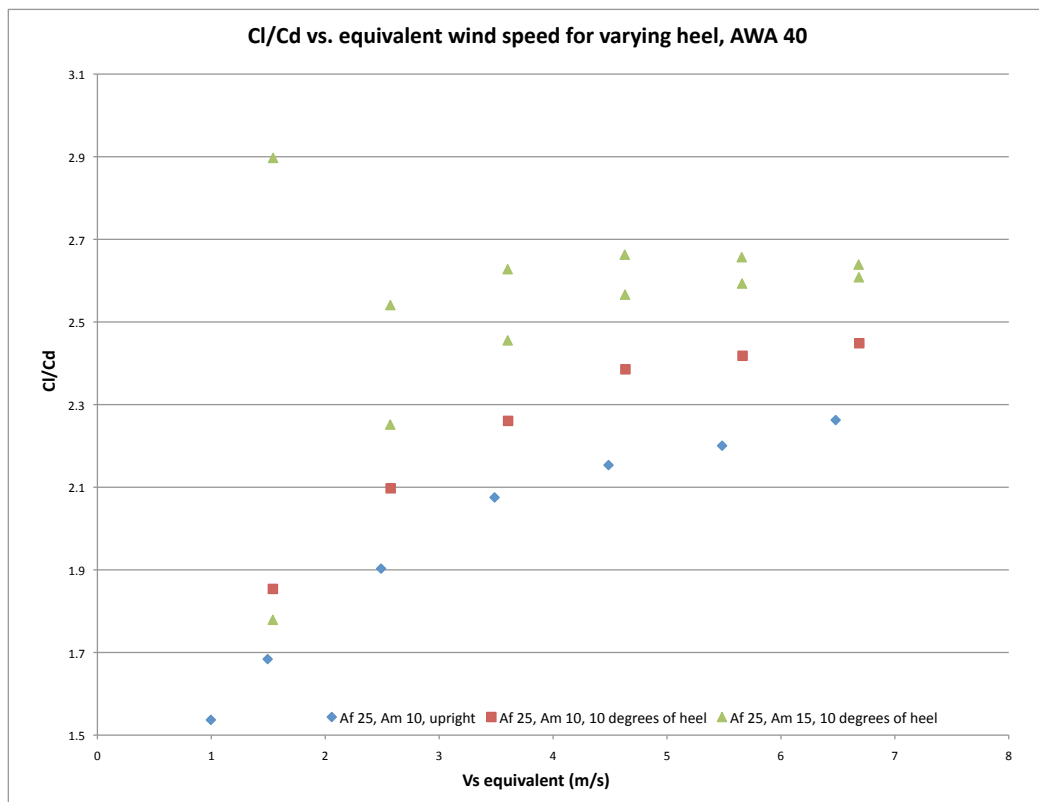


Figure 70: Coefficients of Lift and Drag against Standardised Wind Speed at 10 degrees of heel, with an apparent wind angle of 40 degrees. Note the single anomaly in the case of 25,15,10

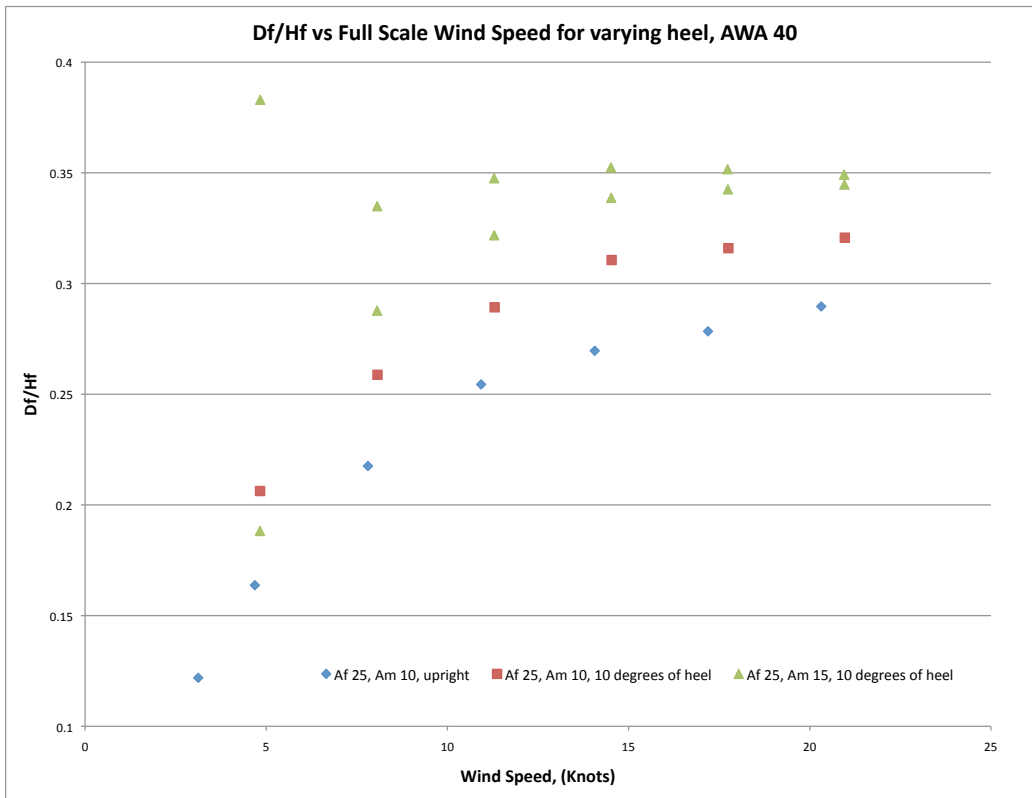


Figure 71: Ratio of Drive and Heel Forces against Full Scale Wind Speed in Knots at 10 degrees of heel, with an apparent wind angle of 40 degrees

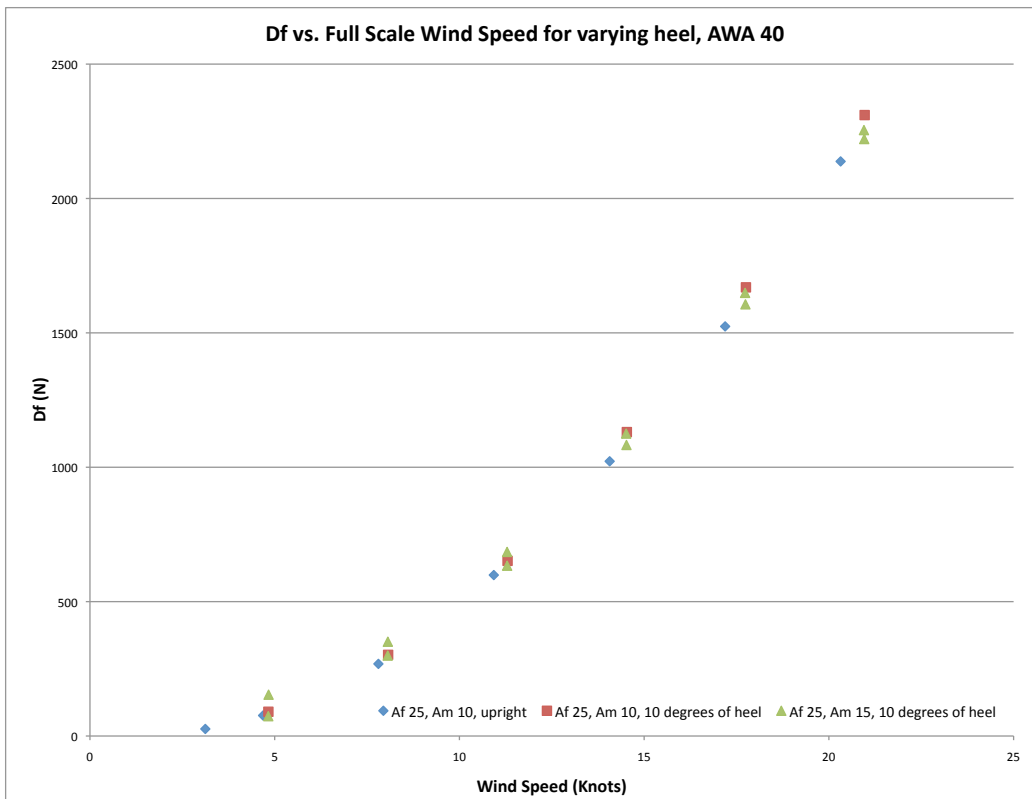


Figure 72: Full scale Drive Force against full scale Wind Speed in Knots at 10 degrees of heel, with an apparent wind angle of 40 degrees. This plot clearly shows how little the effect of small heel angles is on the forces produced by the sails, the reduction in velocity when sailing being due largely to hydrodynamic forces

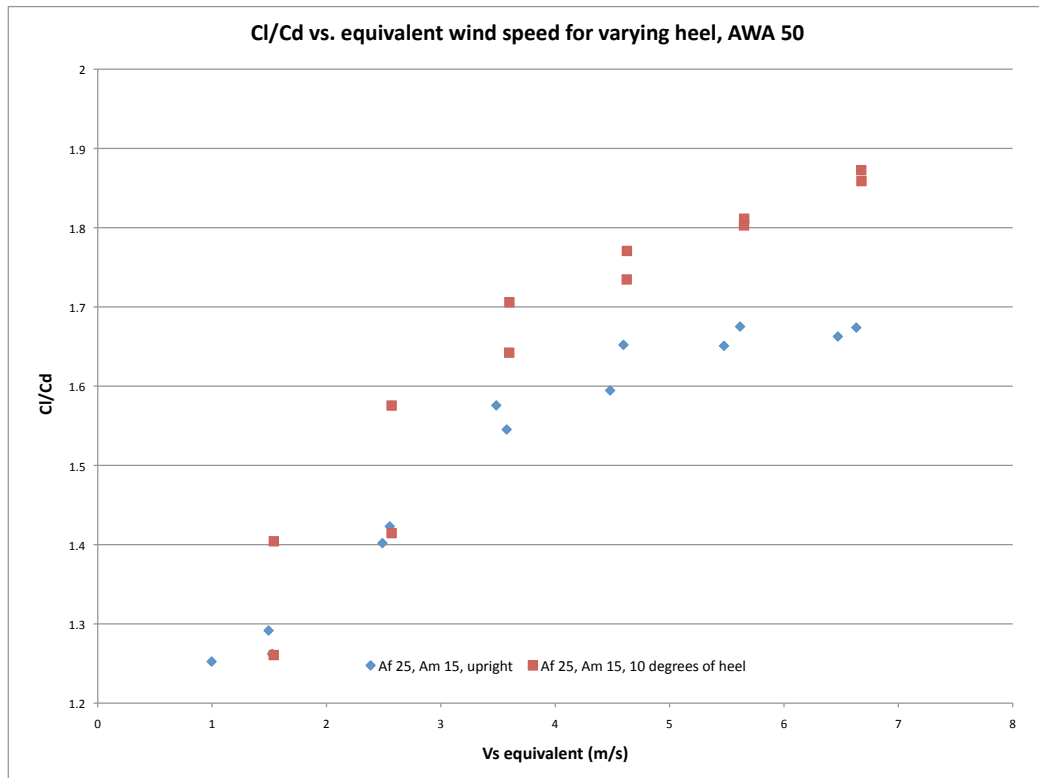


Figure 73: *Coefficients of Lift and Drag against Standardised Wind Speed at 10 degrees of heel, with an apparent wind angle of 50 degrees*

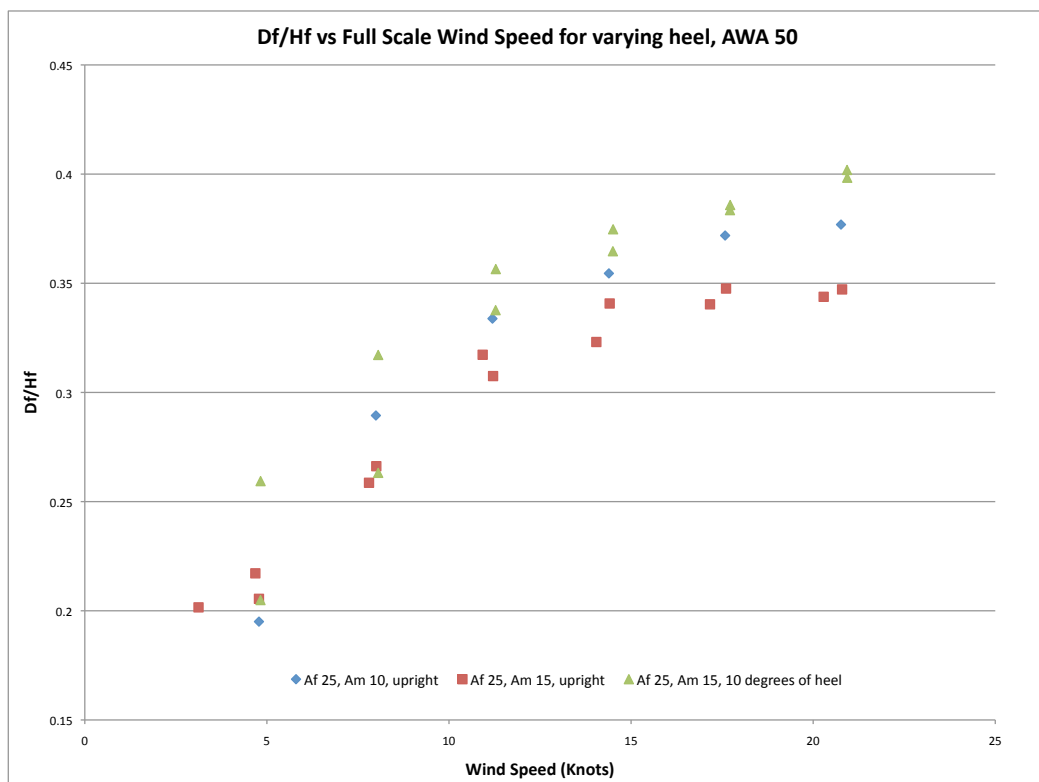


Figure 74: *Ratio of Drive and Heel Forces against Full Scale Wind Speed in Knots at 10 degrees of heel, with an apparent wind angle of 50 degrees*

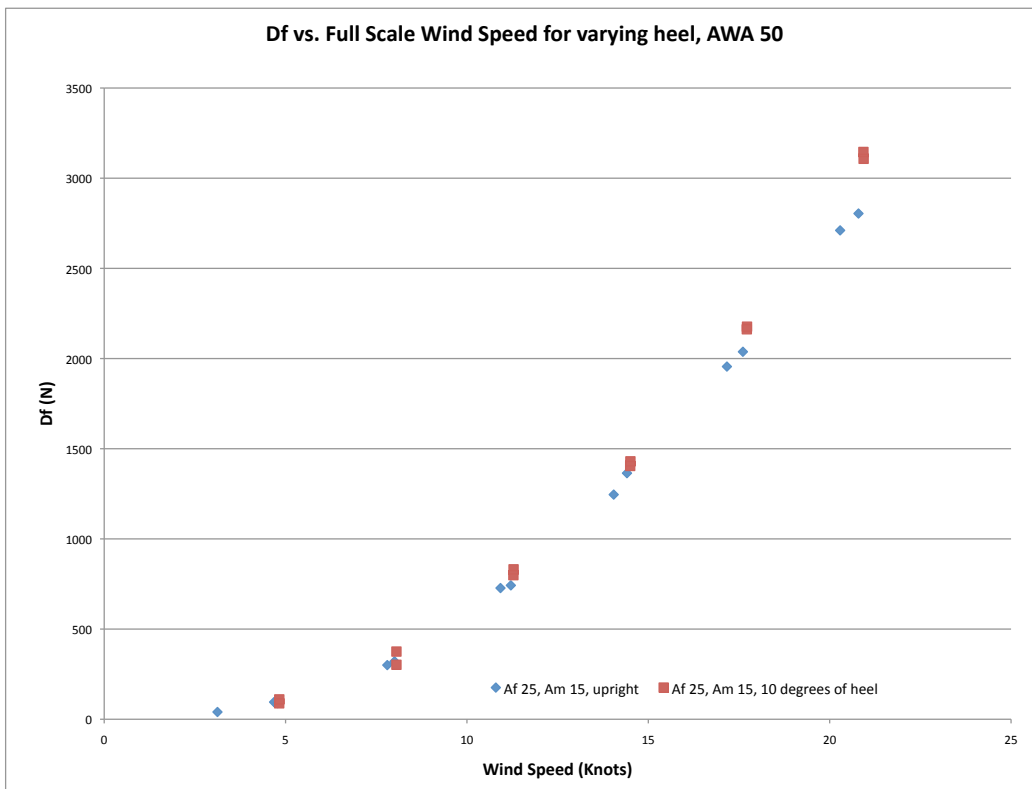


Figure 75: Full scale Drive Force against full scale Wind Speed in Knots at 10 degrees of heel, with an apparent wind angle of 50 degrees

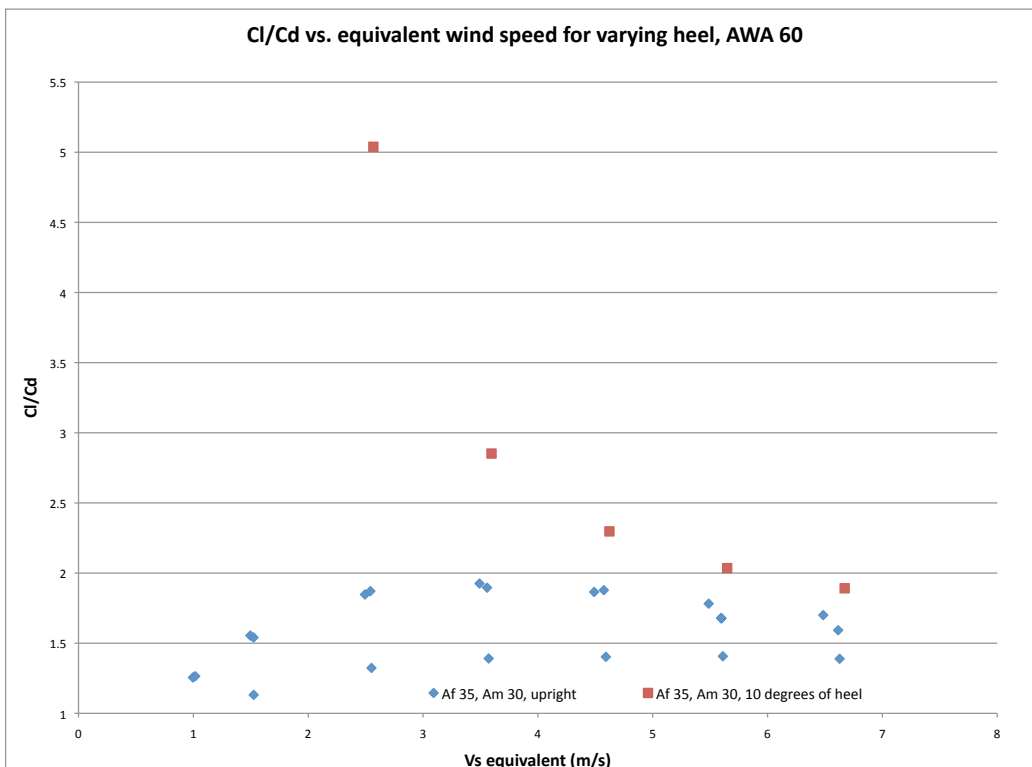


Figure 76: Coefficients of Lift and Drag against Standardised Wind Speed at 10 degrees of heel, with an apparent wind angle of 60 degrees. The results for the heeled data are clearly somewhat erroneous, which it can be seen from the force plots is due to a slight latent stress in the experimental rig

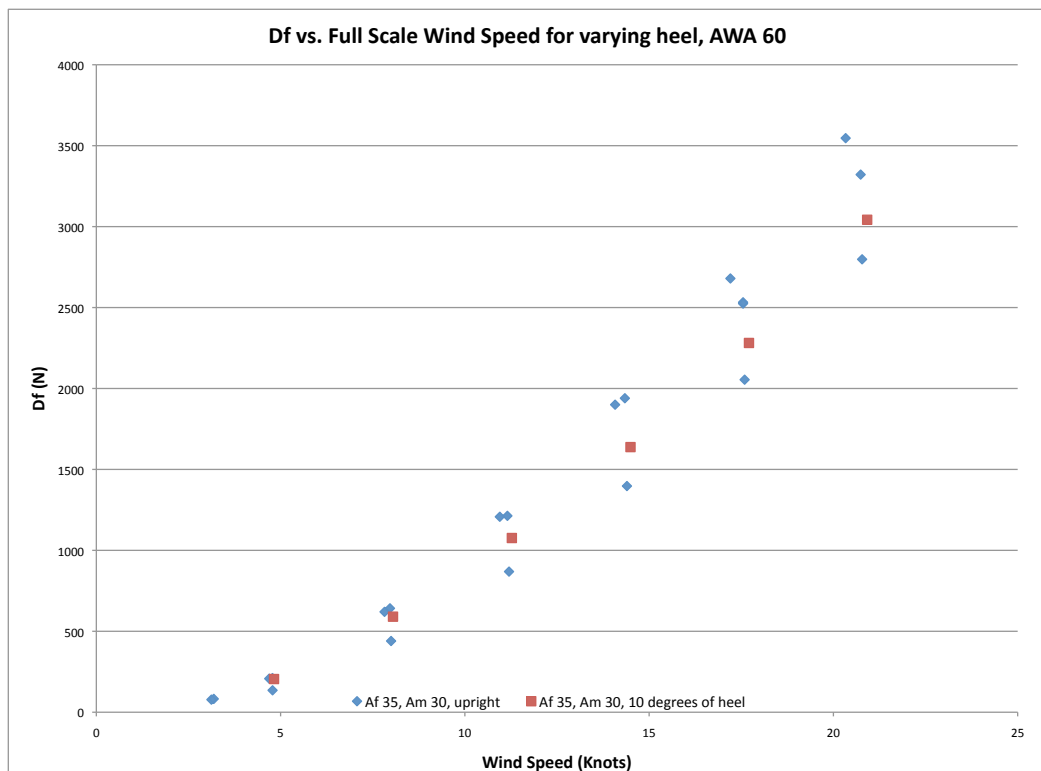


Figure 77: Full scale Drive Force against full scale Wind Speed in Knots at 10 degrees of heel, with an apparent wind angle of 60 degrees

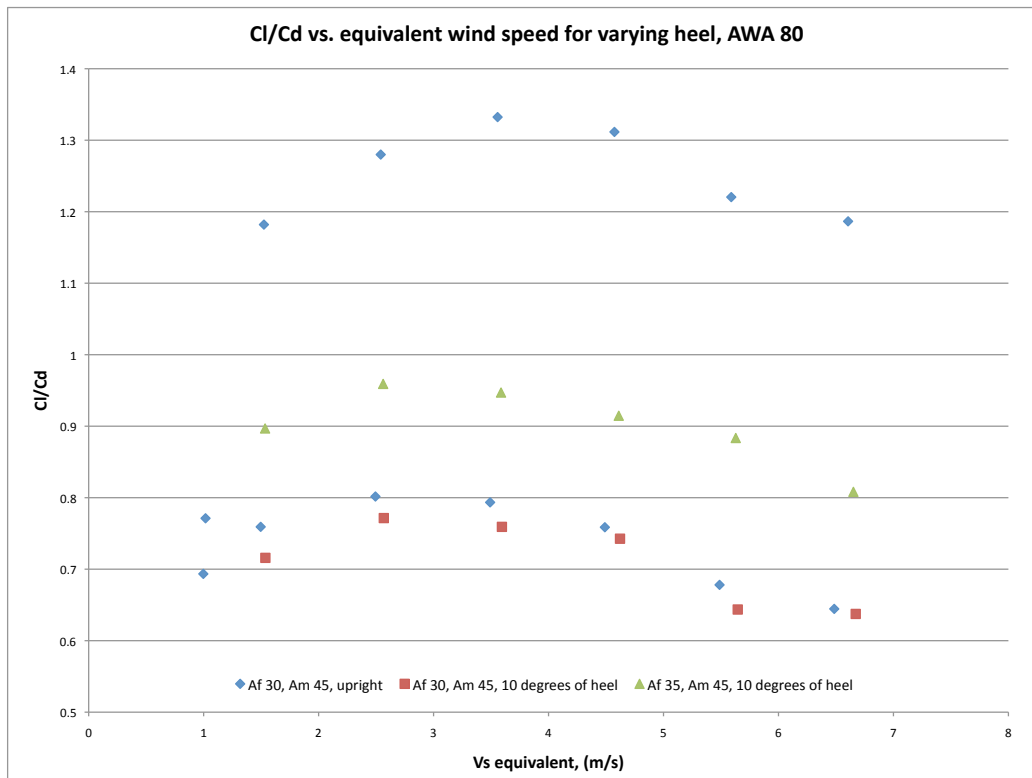


Figure 78: *Coefficients of Lift and Drag against Standardised Wind Speed at 10 degrees of heel, with an apparent wind angle of 80 degrees. Note the erroneous upper data in the upright condition*

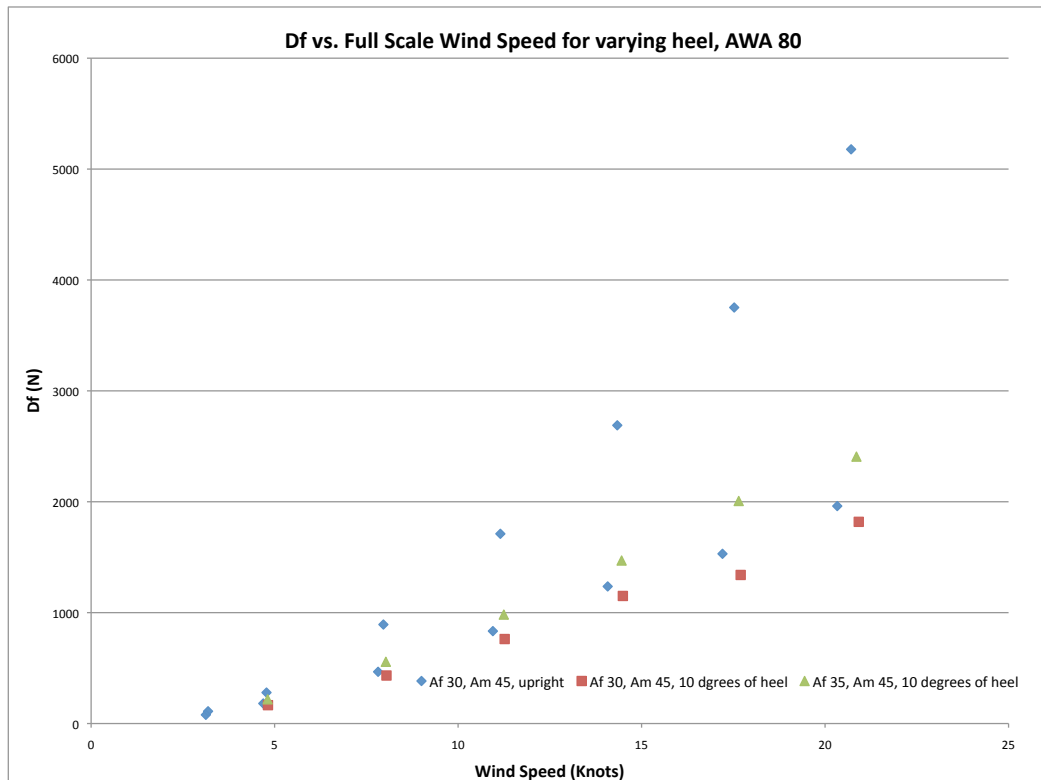


Figure 79: Full scale Drive Force against full scale Wind Speed in Knots at 10 degrees of heel, with an apparent wind angle of 80 degrees

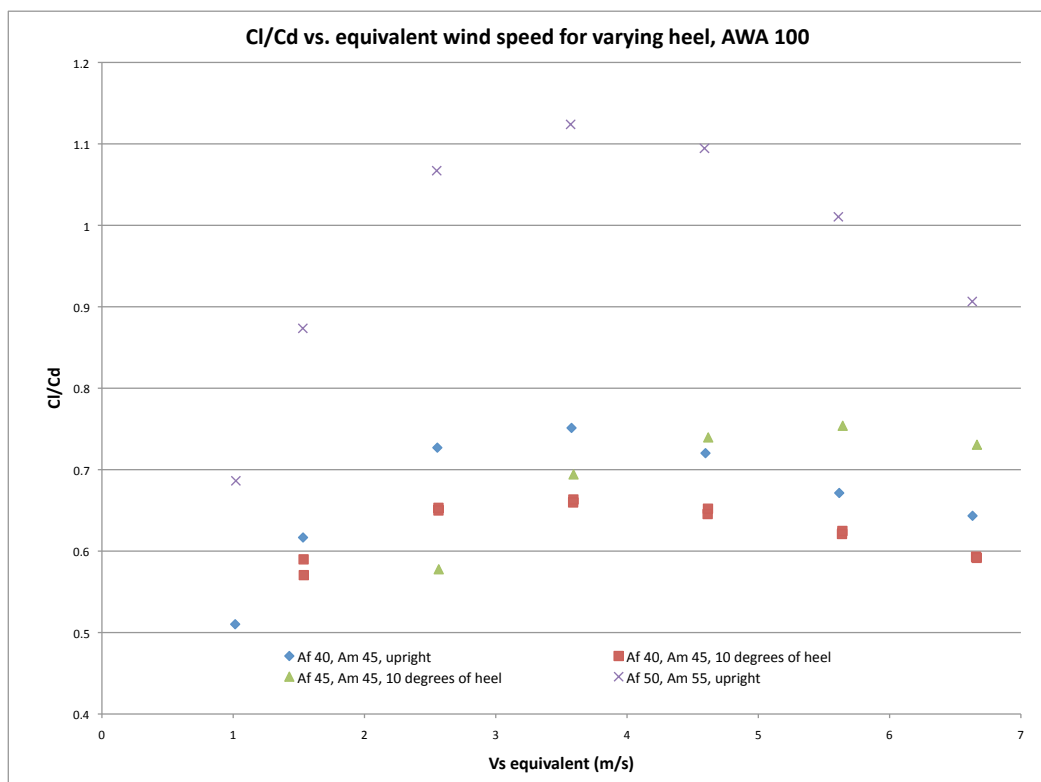


Figure 80: Coefficients of Lift and Drag against Standardised Wind Speed at 10 degrees of heel, with an apparent wind angle of 100 degrees

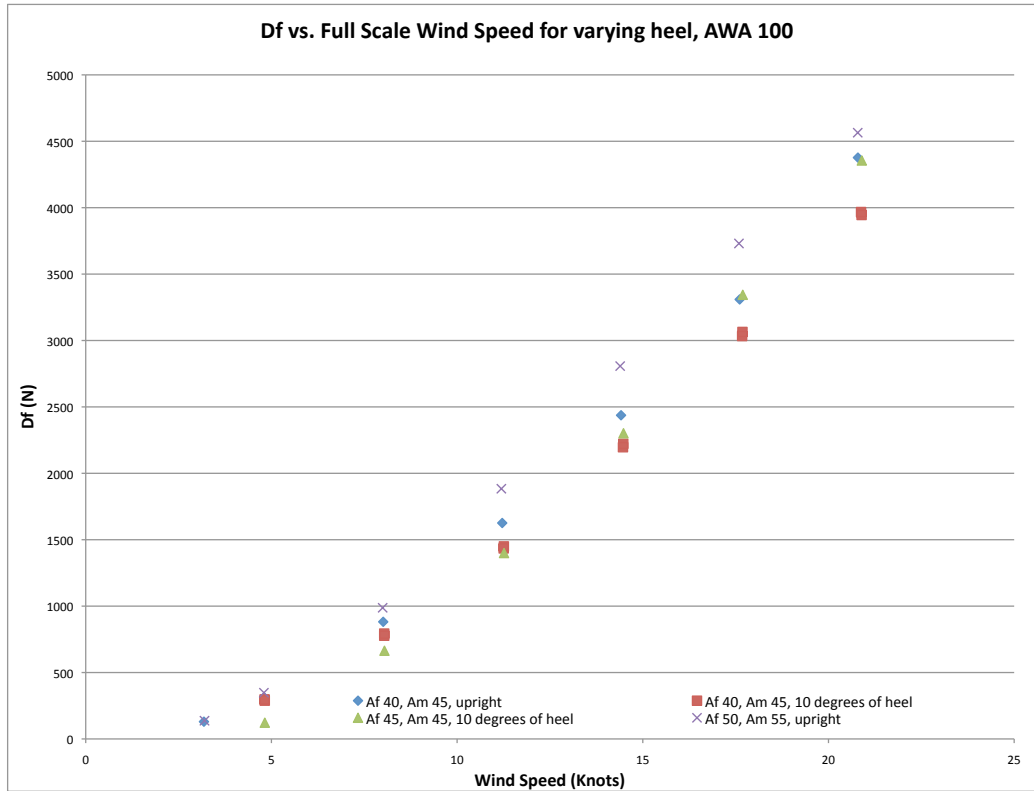


Figure 81: Full scale Drive Force against full scale Wind Speed in Knots at 10 degrees of heel, with an apparent wind angle of 100 degrees

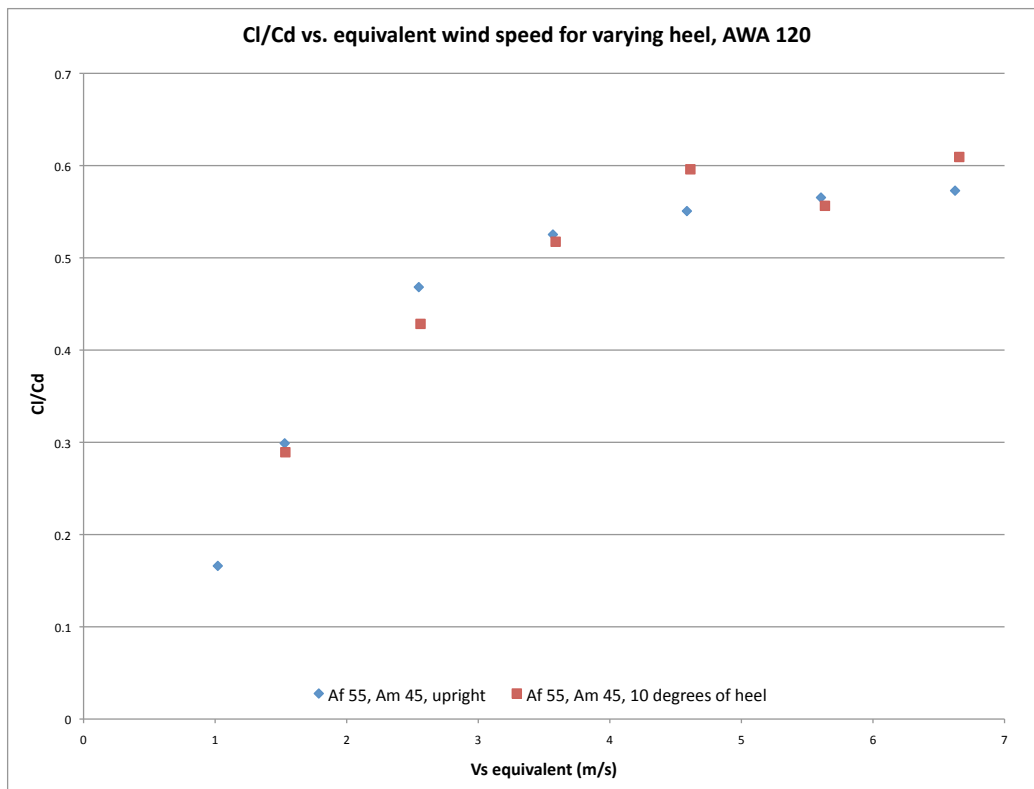


Figure 82: Coefficients of Lift and Drag against Standardised Wind Speed at 10 degrees of heel, with an apparent wind angle of 120 degrees

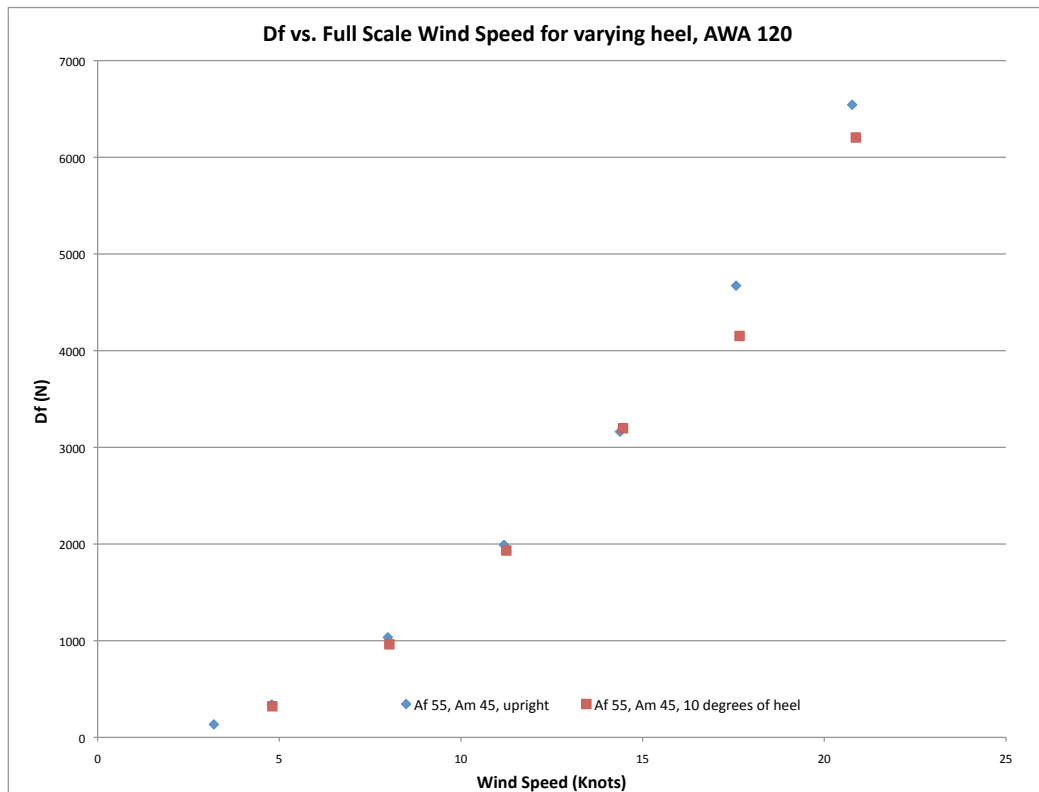


Figure 83: Full scale Drive Force against full scale Wind Speed in Knots at 10 degrees of heel, with an apparent wind angle of 120 degrees

A.4.6 Comparative plots of theoretical and experimental data

These plots show a comparison of *Boleh's* rig to that of a rig of the same sail area designed to the IMS rule. Both cases are exclusive of parasitic drag from the hull and rigging. The theoretical curves have been distorted slightly due to the interpolation required to convert the data to the co-ordinate system used in the experimental data.

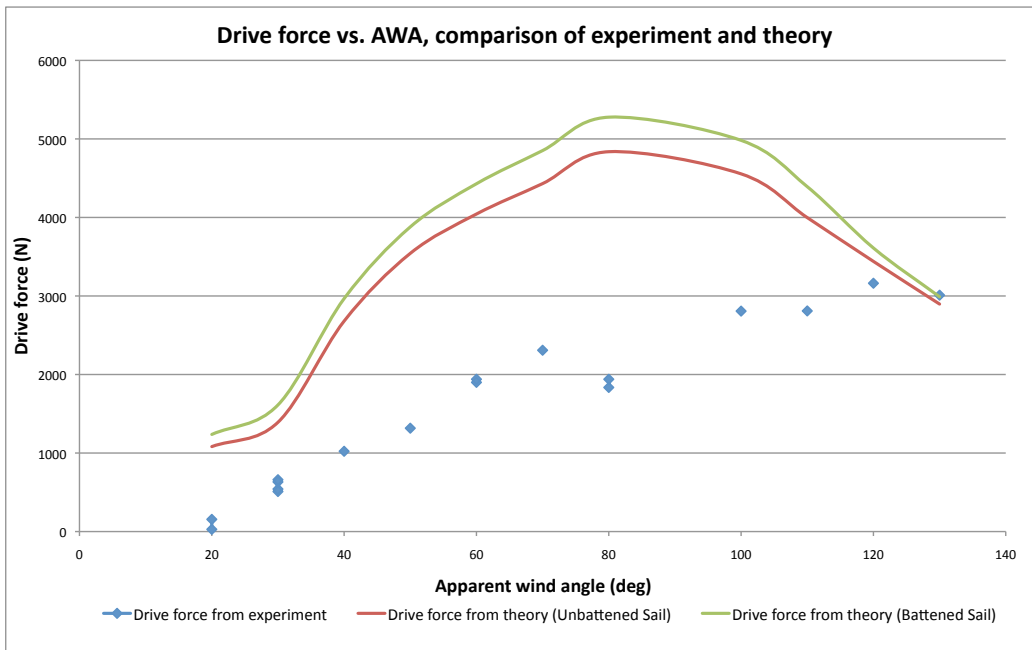


Figure 84: Total drive force against apparent wind angle from experimental data for Boleh and two theoretical data sets for a modern racing yacht taken from Van Oossanen (1993)

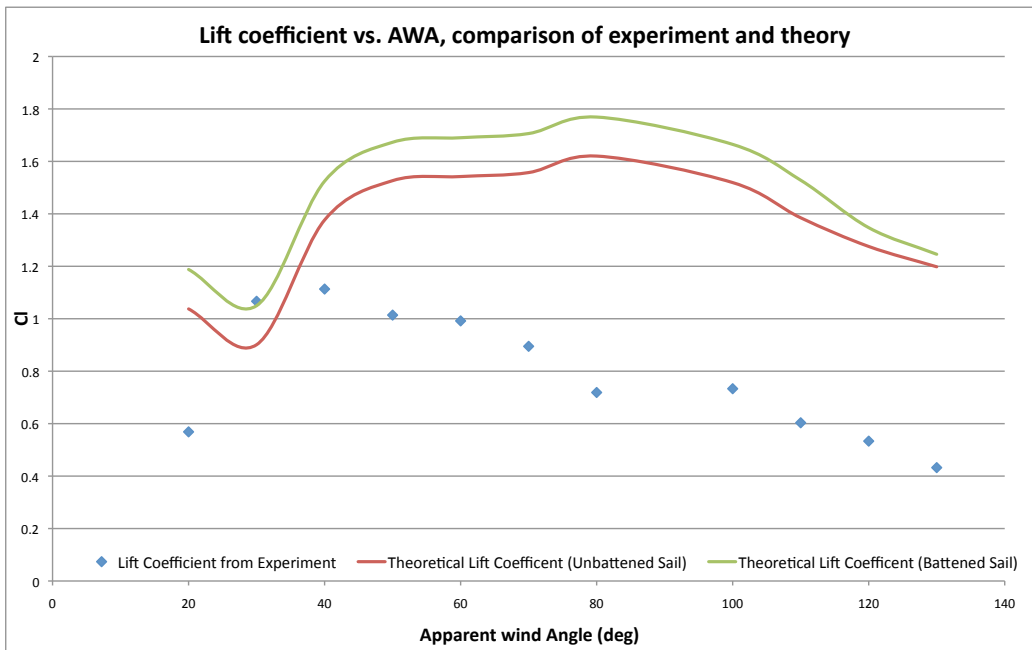


Figure 85: Lift coefficient against apparent wind angle from experimental data for Boleh and two theoretical data sets for a modern racing yacht taken from Van Oossanen (1993)

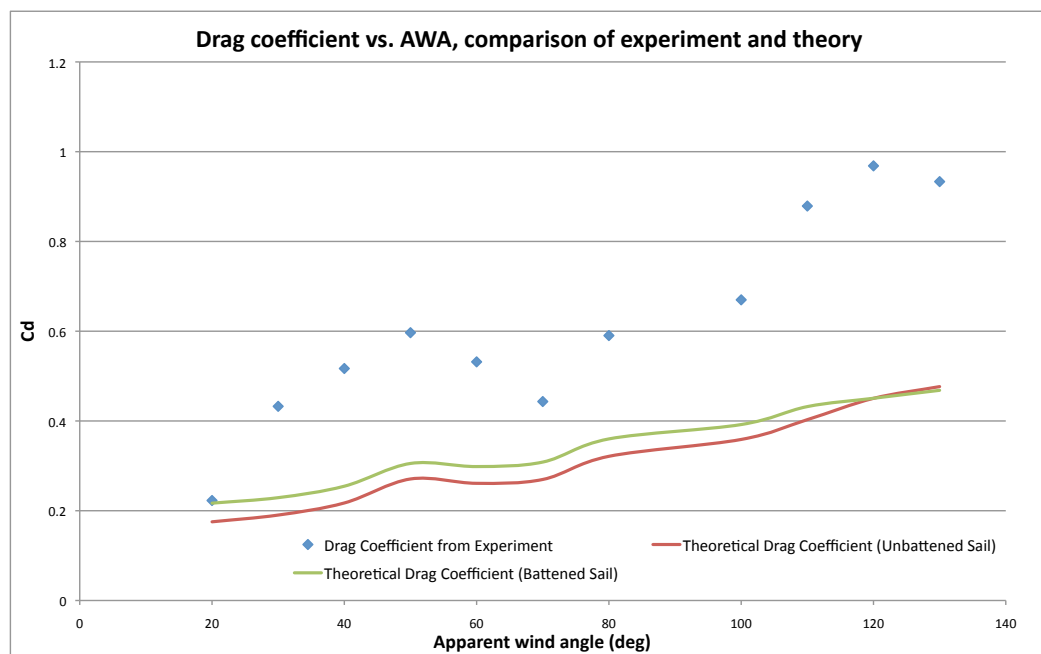


Figure 86: Drag coefficient against apparent wind angle from experimental data for Boleh and two theoretical data sets for a modern racing yacht taken from Van Oossanen (1993) The far greater drag produced by Boleh's rig is due to combination of the additional rigging architecture and the lower aspect ratio of the sails.

A.5 Computational fluid dynamics experiments

Data plots

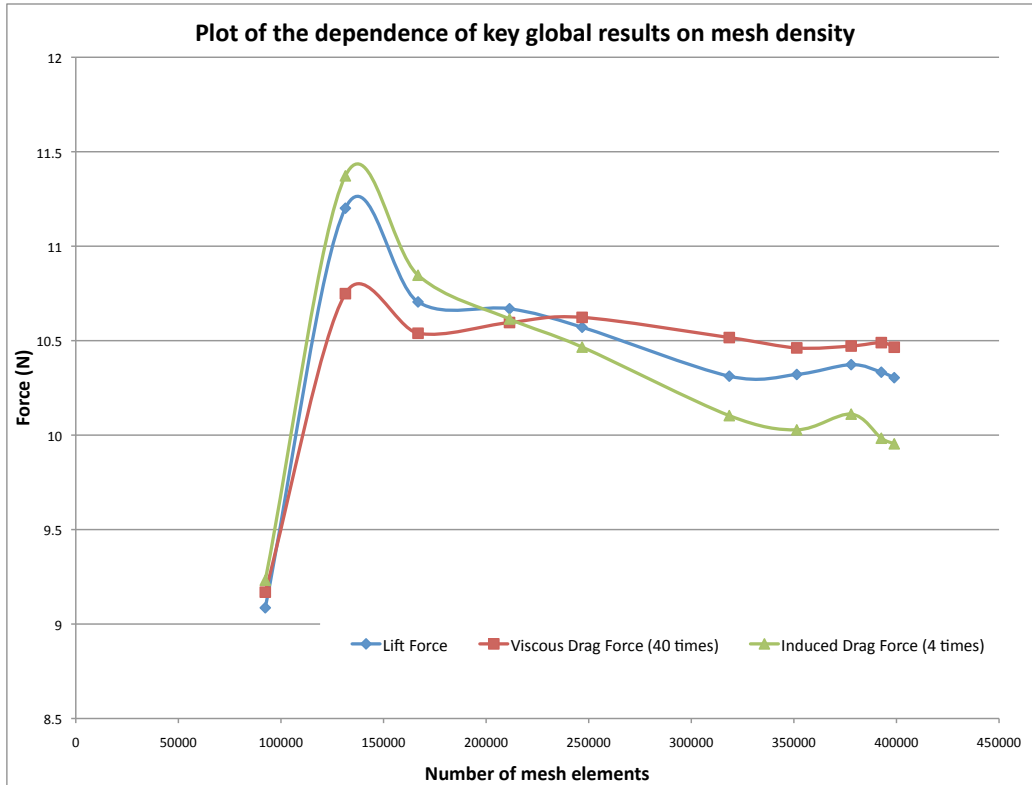


Figure 87: Plot of various global forces against element count for the same geometry. Optimum count found to be 350000, mesh failed to converge for element counts above 410000

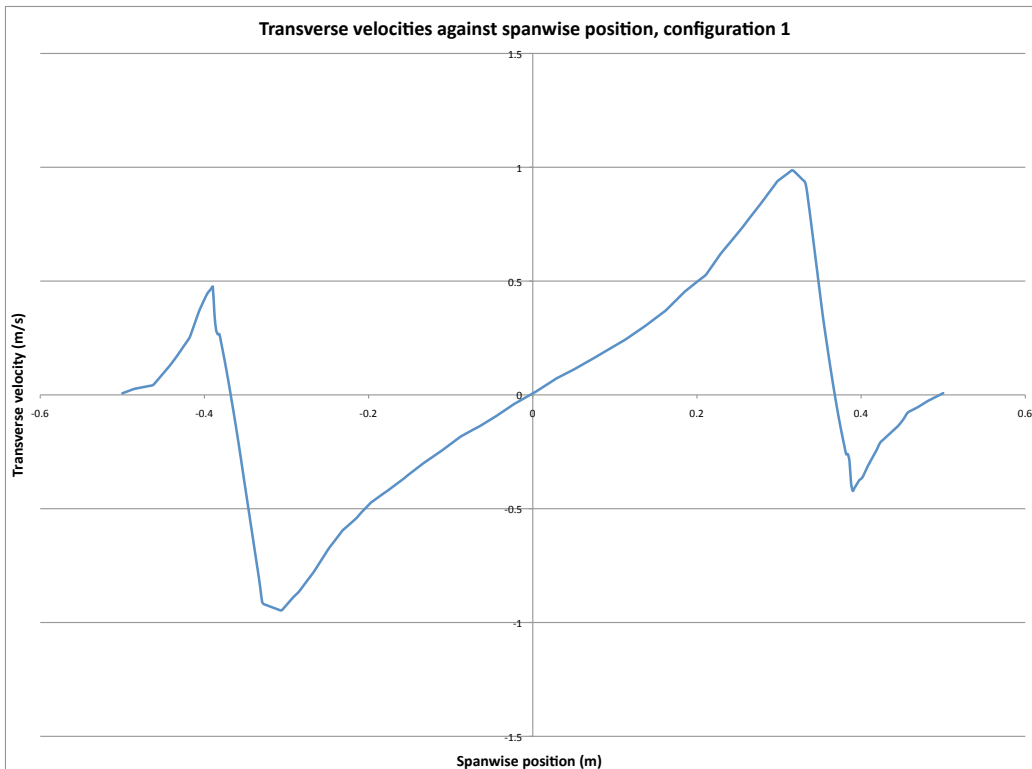
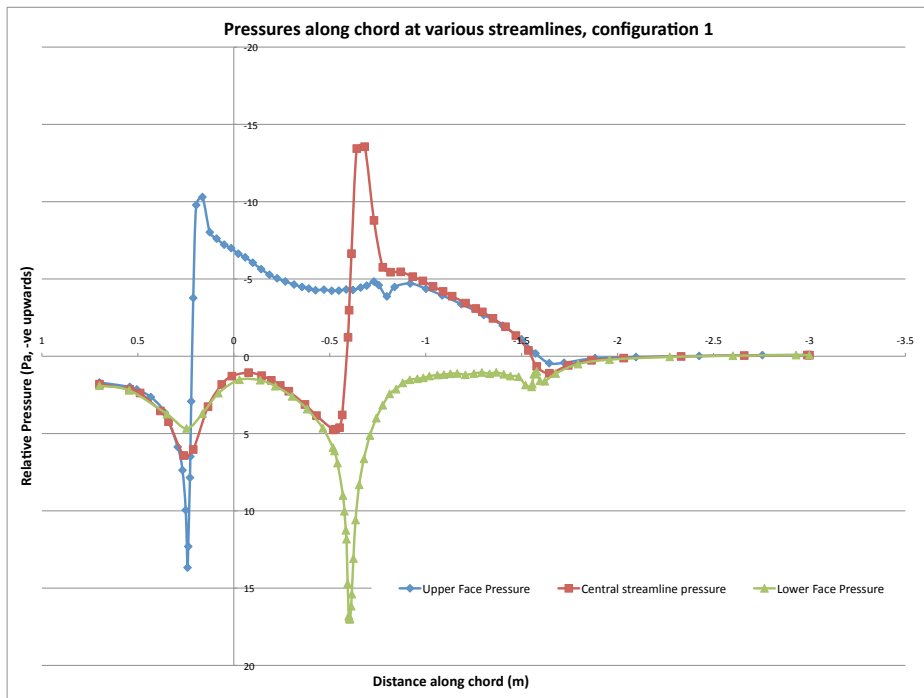
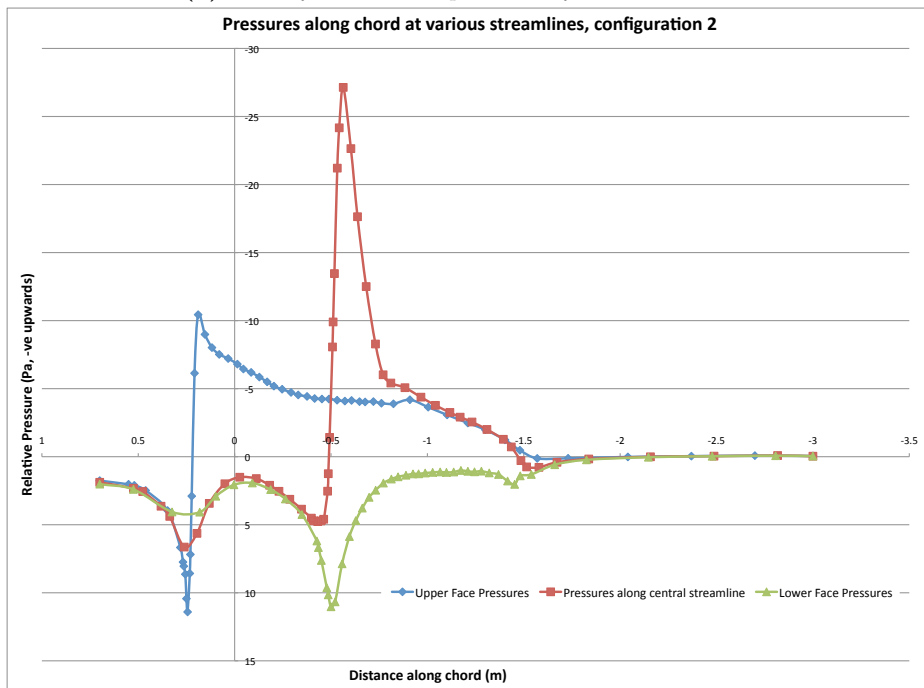


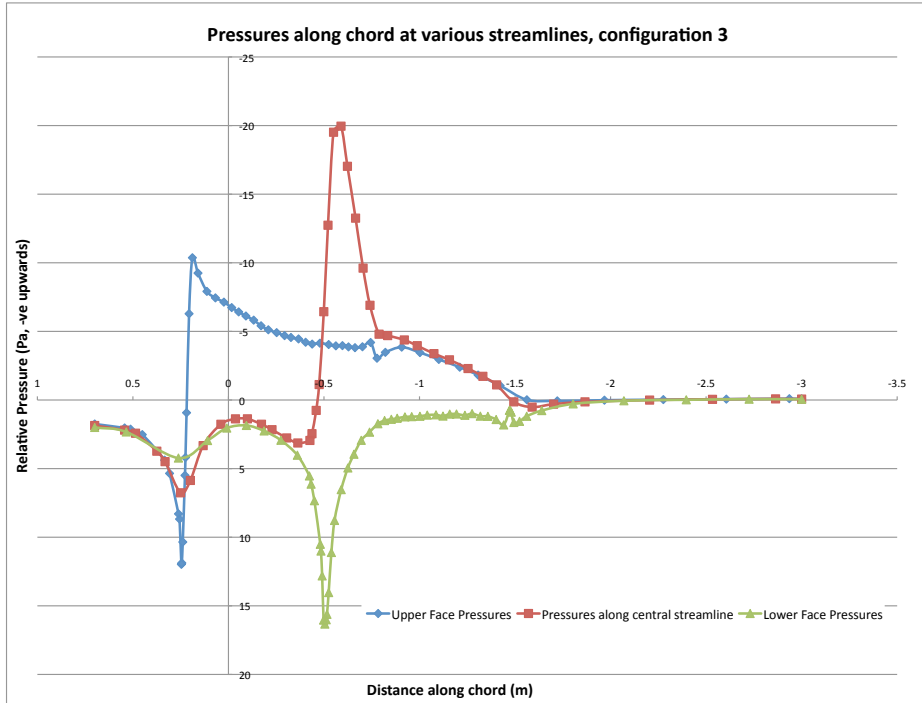
Figure 88: Plot of transverse velocity against span wise position over a foil



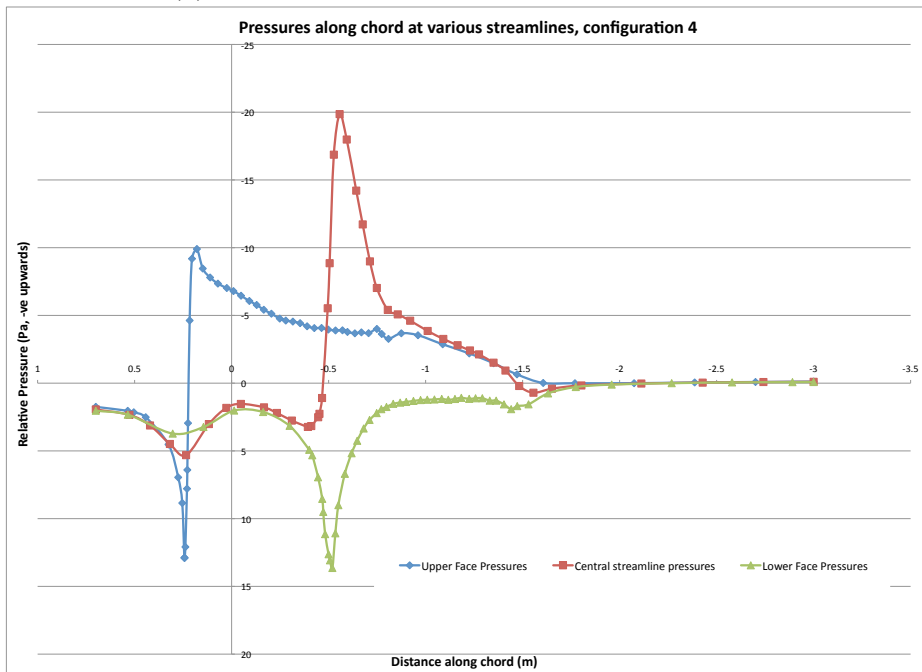
(a) Plot of chord wise pressures for the base case



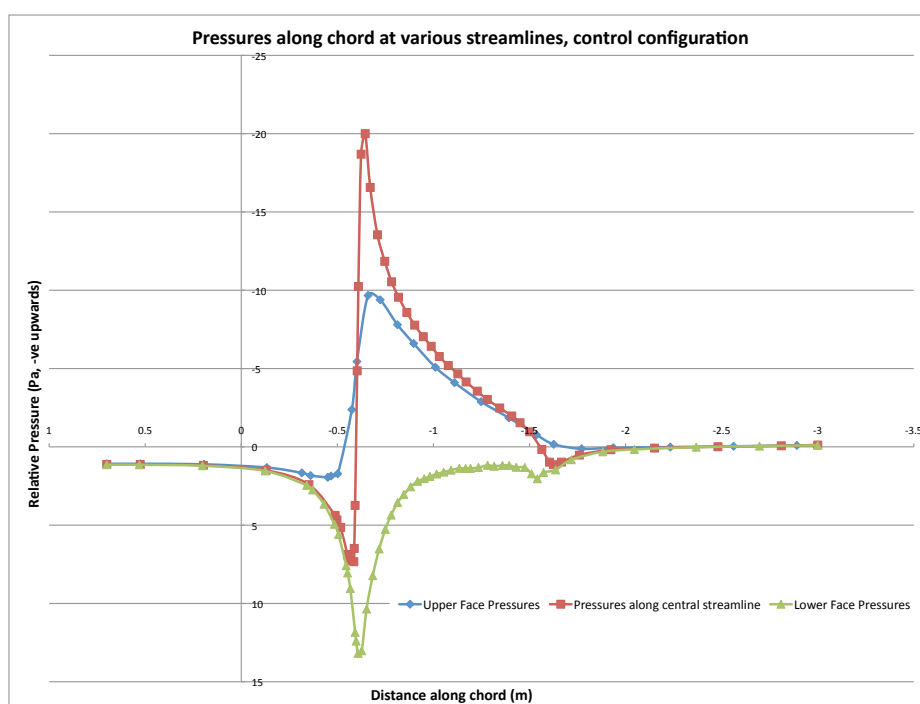
(b) Plot of chord wise pressures for configuration 2



(c) Plot of chord wise pressures for configuration 3



(d) Plot of chord wise pressures for configuration 4



(e) Plot of chord wise pressures for the control configuration

Figure 89: Comparison of pressures along three streamlines for the various configurations

Mesh Geometry

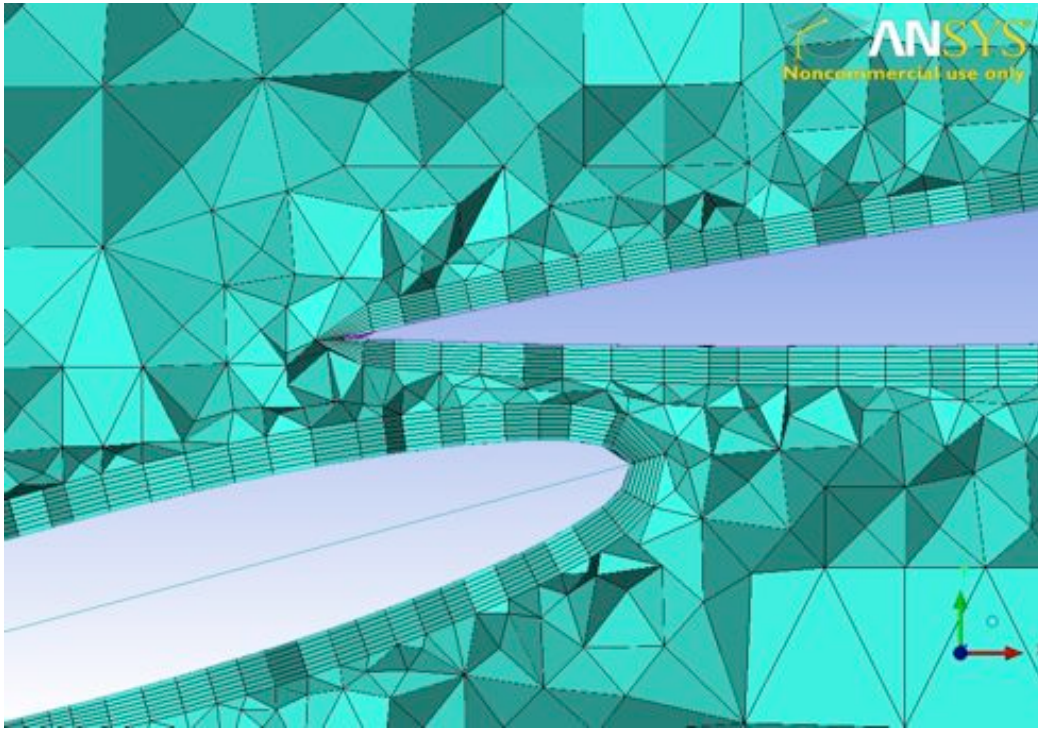


Figure 90: *Detail of meshing in the slot between foils, base case*

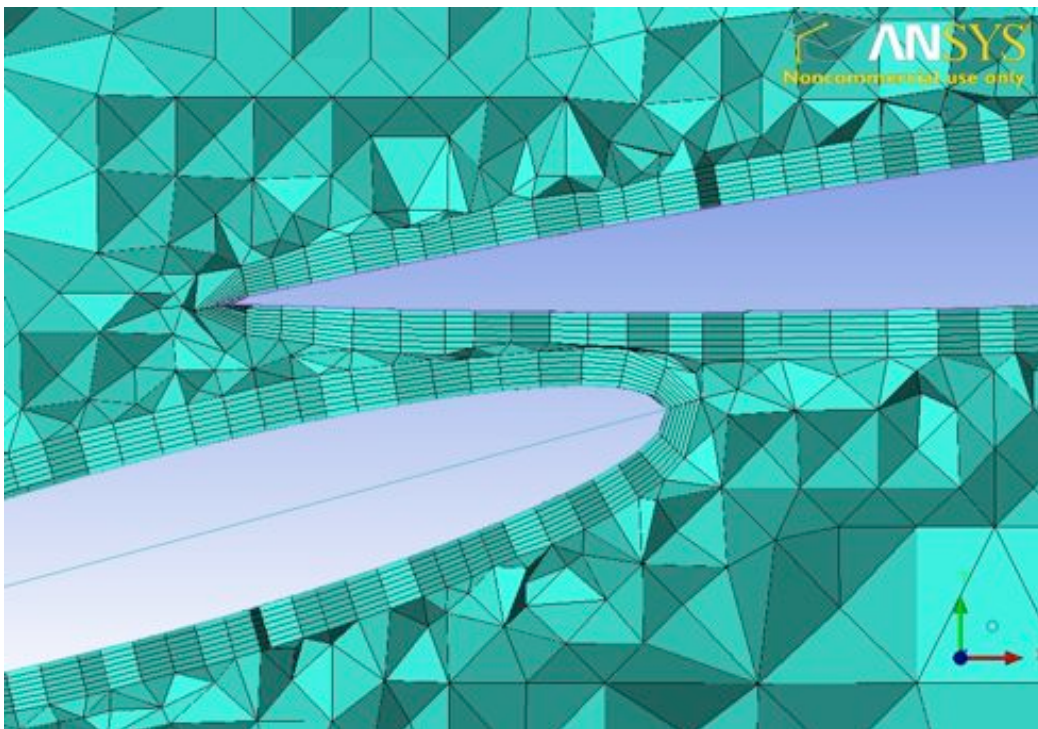


Figure 91: *Detail of meshing in the slot between foils, configuration 2*

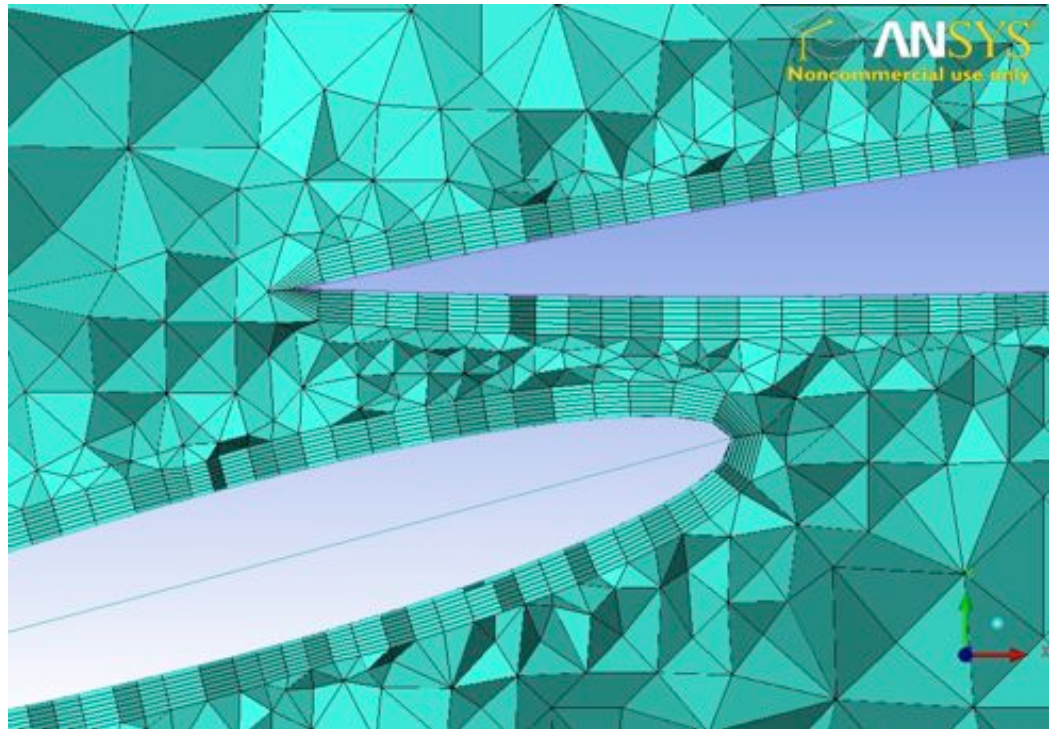


Figure 92: *Detail of meshing in the slot between foils, configuration 4*

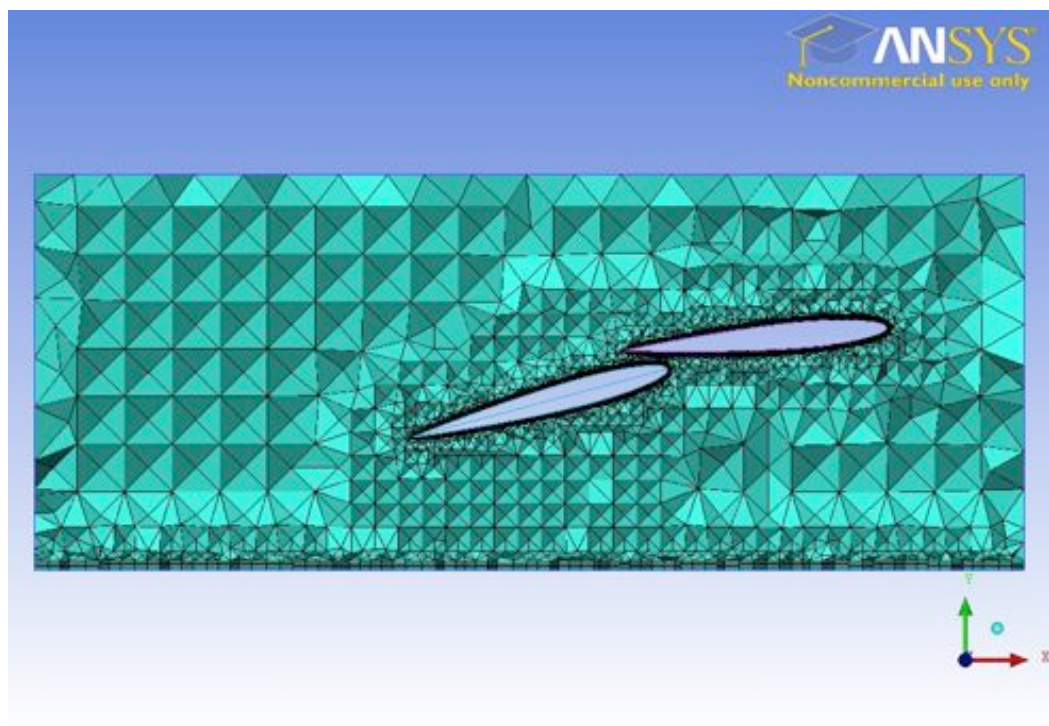


Figure 93: *Cross section of the moderate-fine mesh, 350000 elements. Note heightened density and prism layers around foils*

Pressure distribution

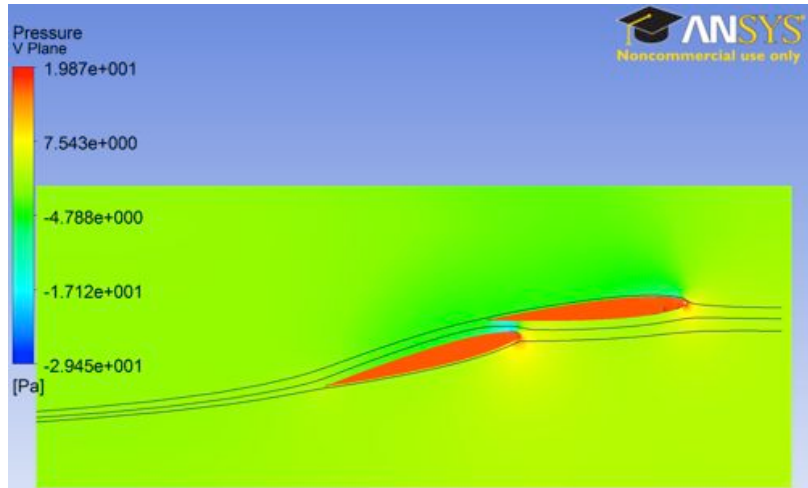


Figure 94: Cross section of pressures at mid span, configuration 1

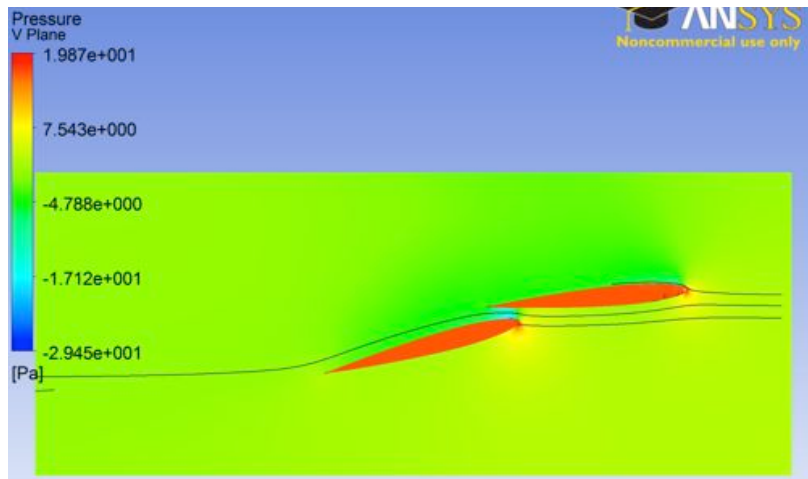


Figure 95: Cross section of pressures at half span, configuration 1

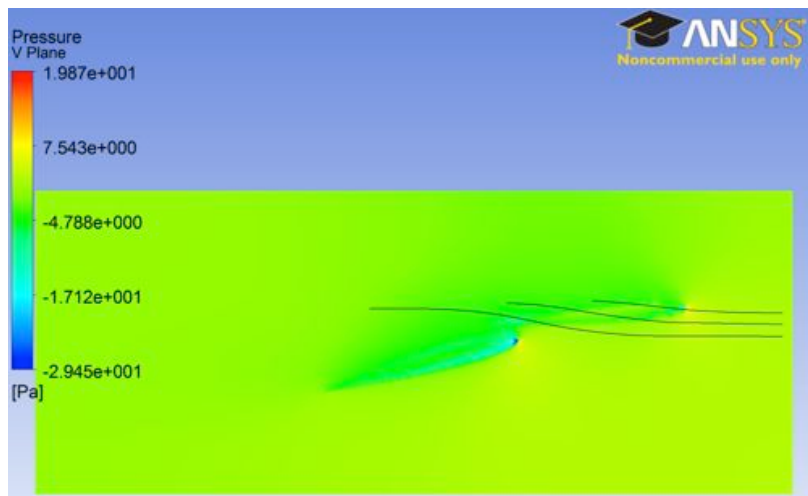


Figure 96: Cross section of pressures at full span, configuration 1

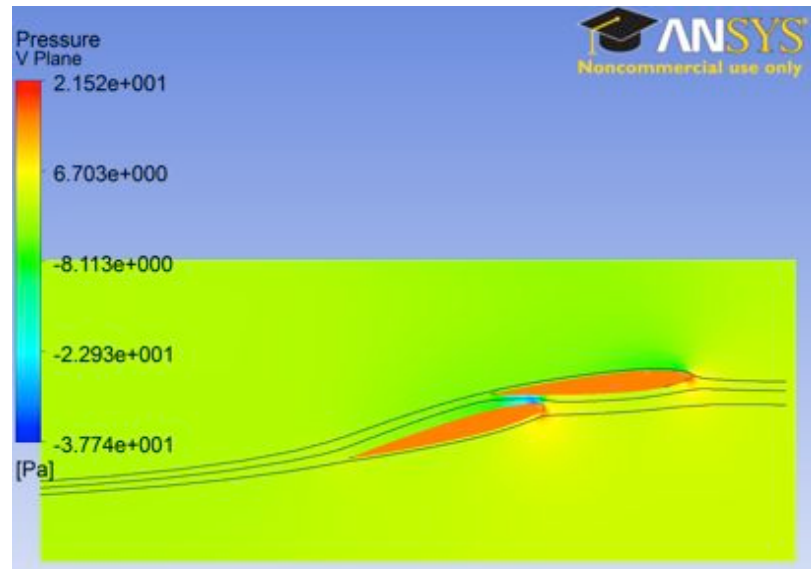


Figure 97: Cross section of pressures at mid span, configuration 2

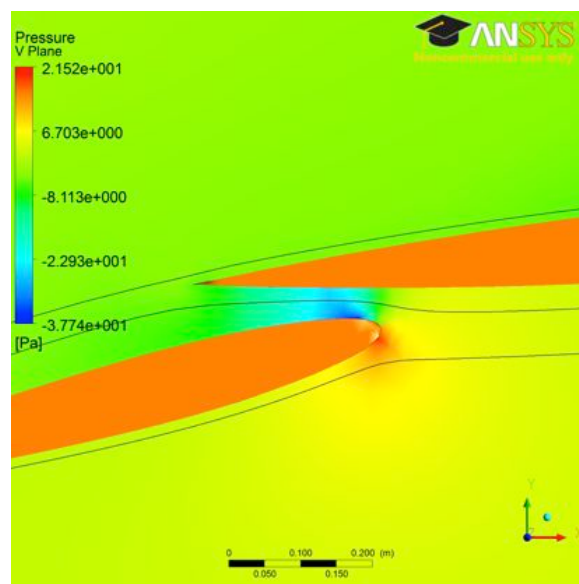


Figure 98: Slot detail of pressures at mid span, configuration 2. Note the strong exaggeration of low pressure due to the slot

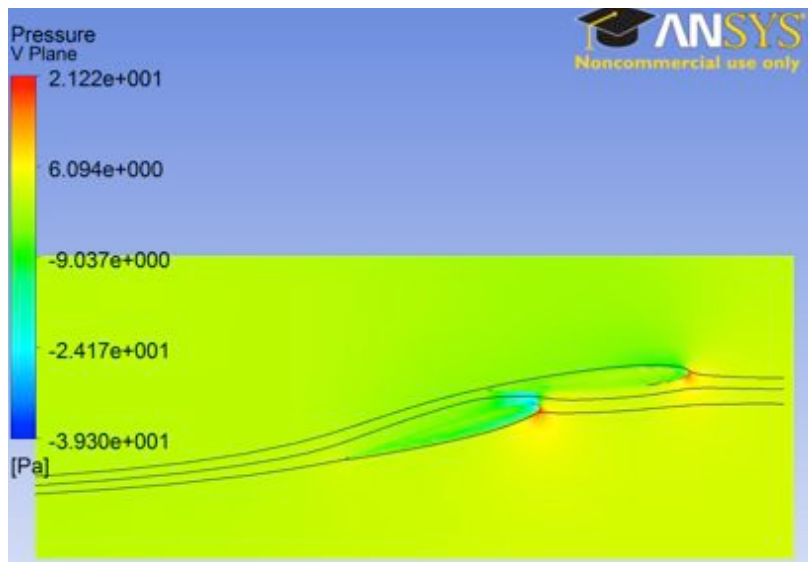


Figure 99: Cross section of pressures at full span, configuration 3

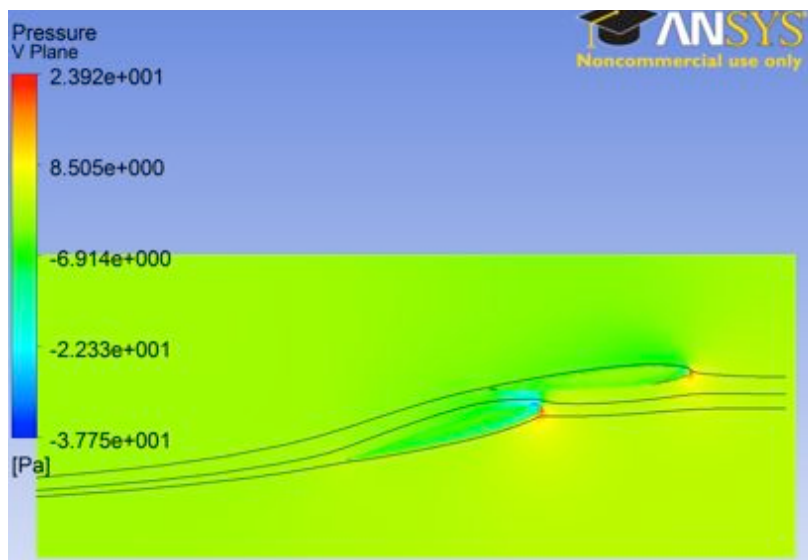


Figure 100: Cross section of pressures at full span, configuration 4

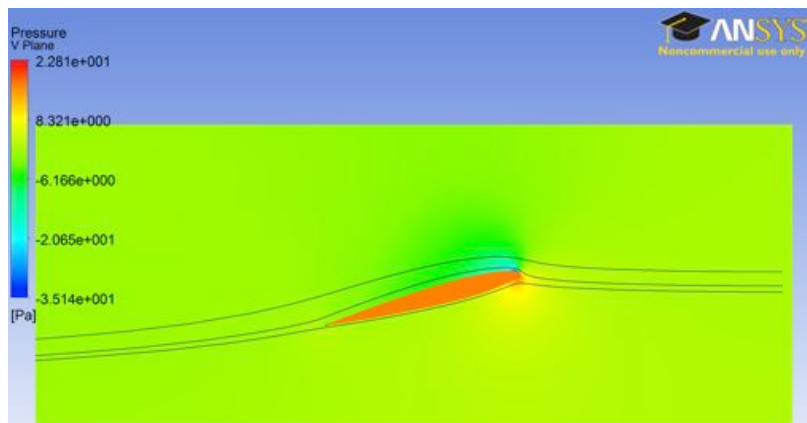


Figure 101: Cross section of pressures at mid span, control configuration

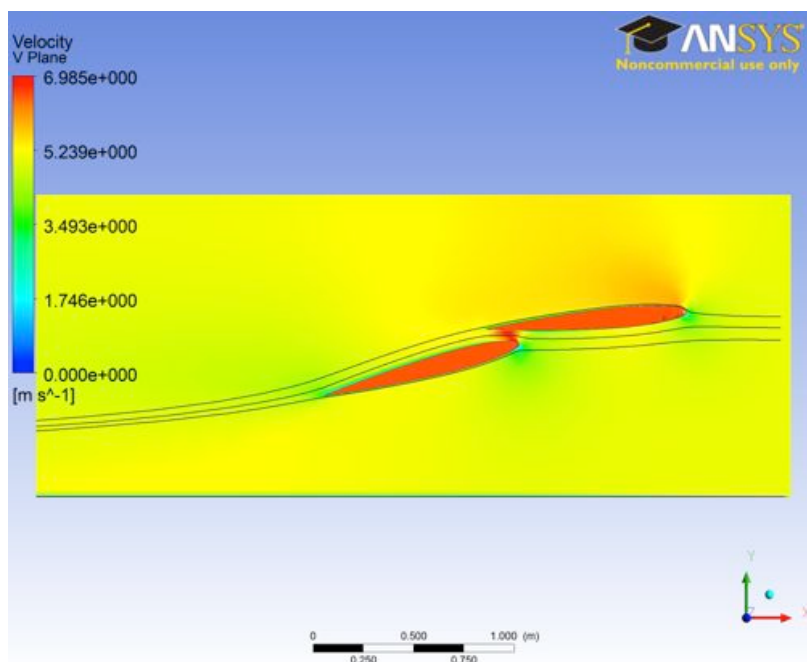
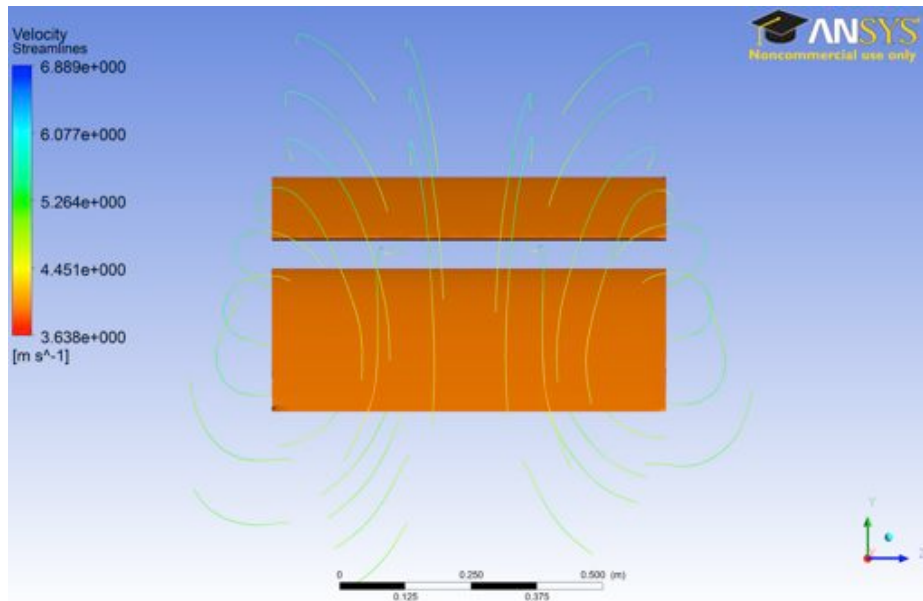
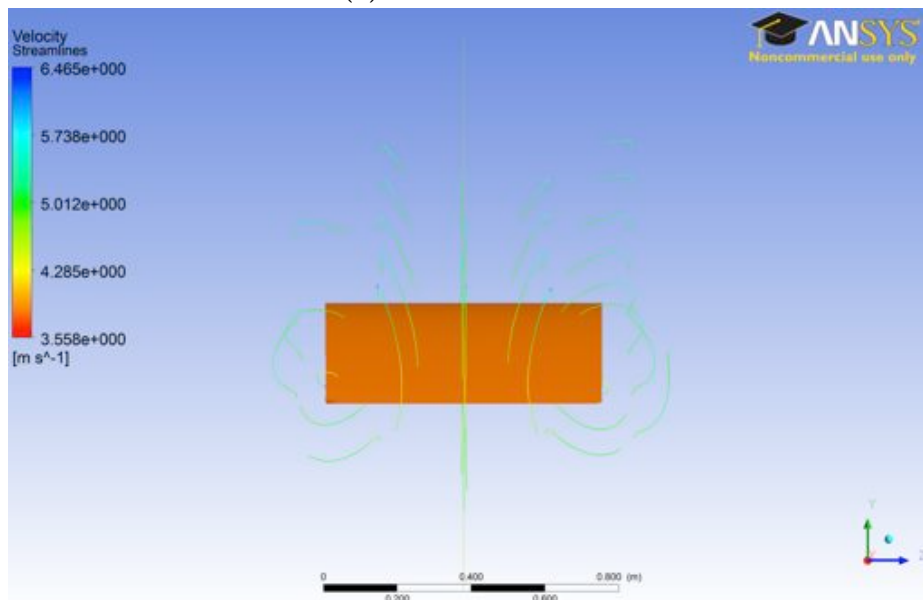


Figure 102: Cross section of velocities at mid span, configuration 1

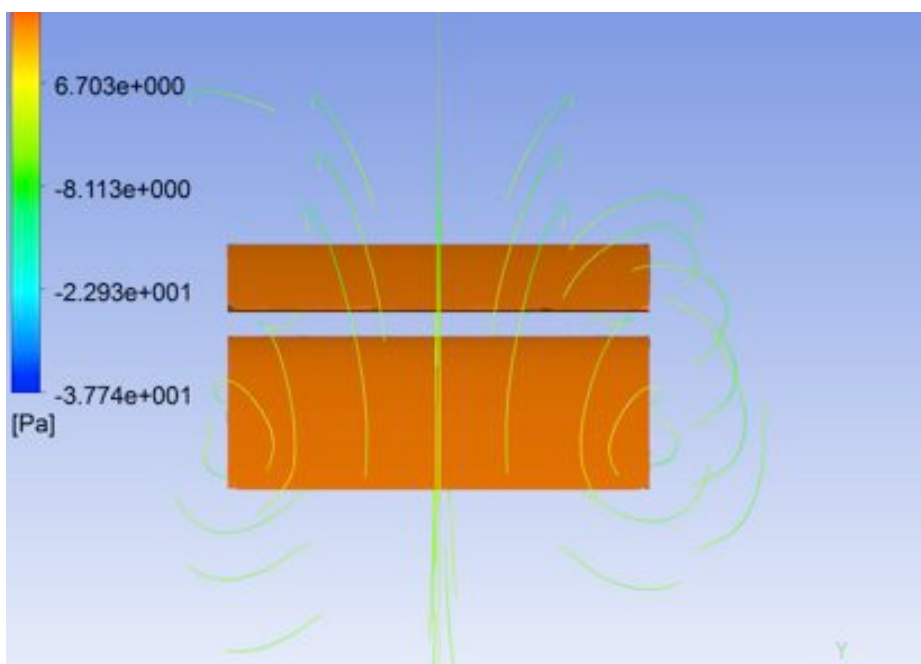
Vortices



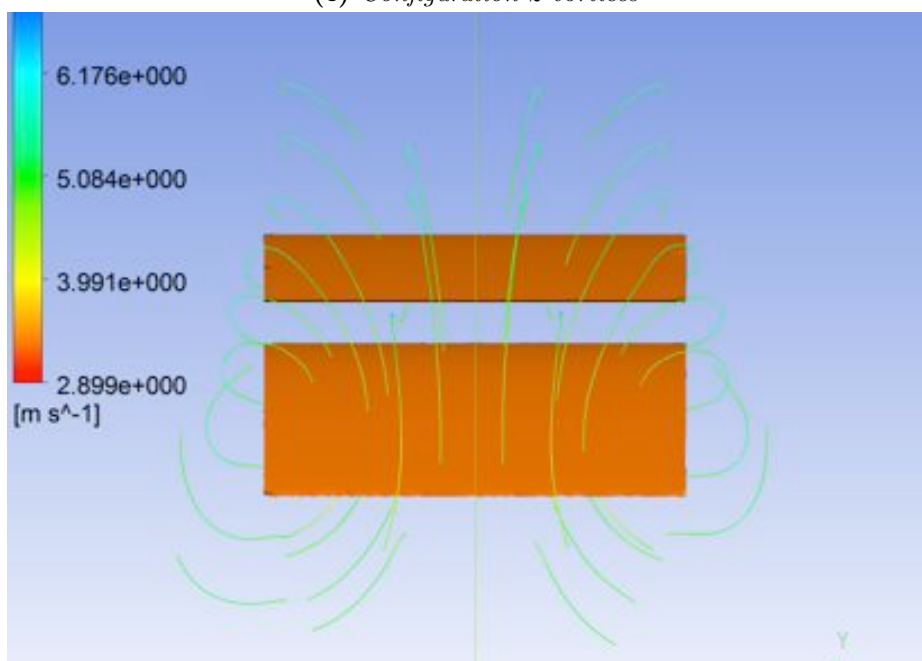
(a) Base case vortices



(b) Control case vortices



(c) Configuration 2 vortices



(d) Configuration 4 vortices

Figure 103: Comparison of wing tip vortices visualised using streamlines for various configurations

Transverse velocity plots

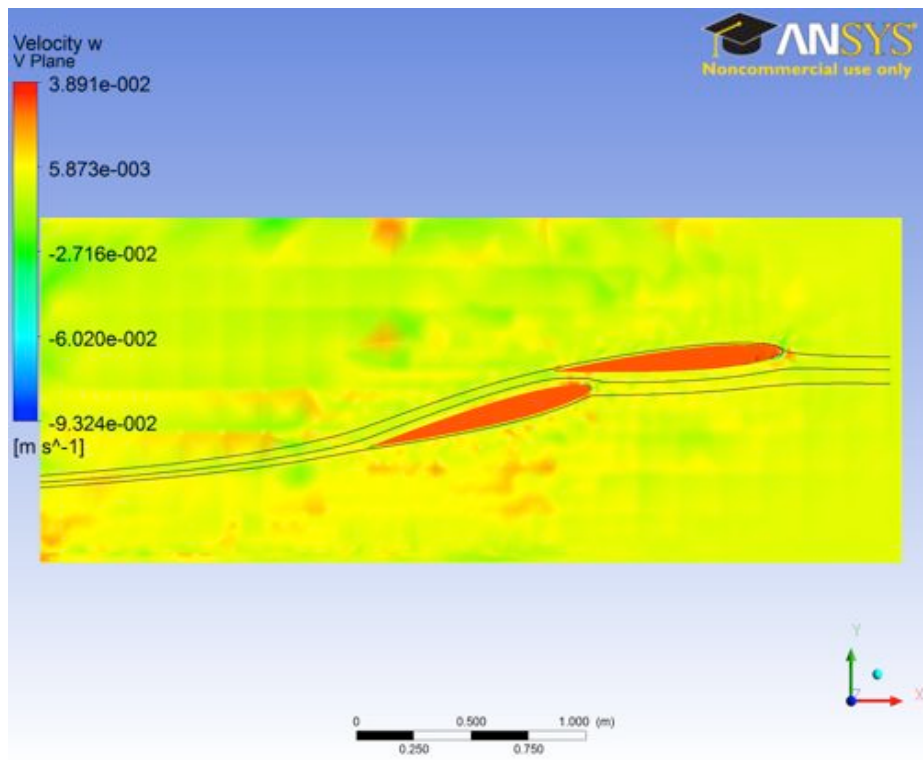


Figure 104: Cross section of transverse velocities at mid span, configuration 1

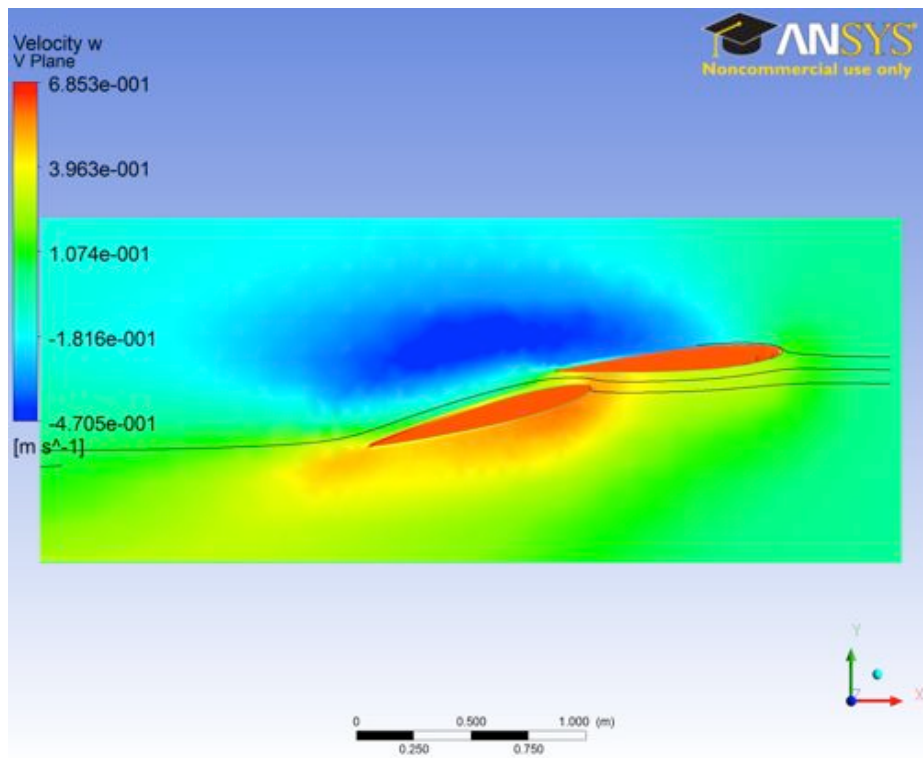


Figure 105: Cross section of transverse velocities at half span, configuration 1

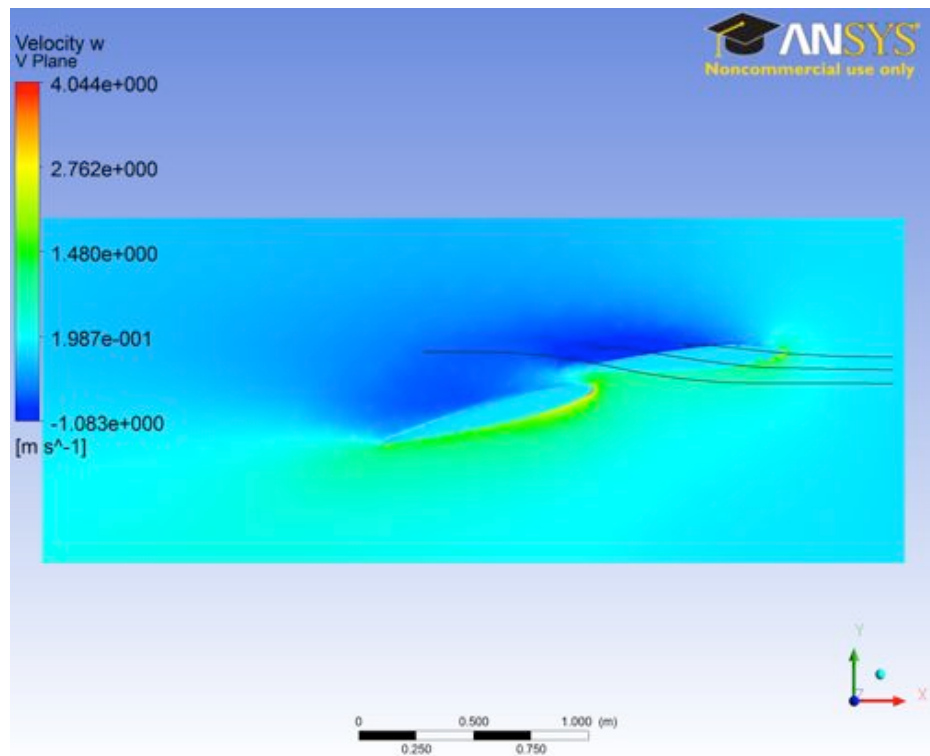


Figure 106: Cross section of transverse velocities at full span, configuration 1

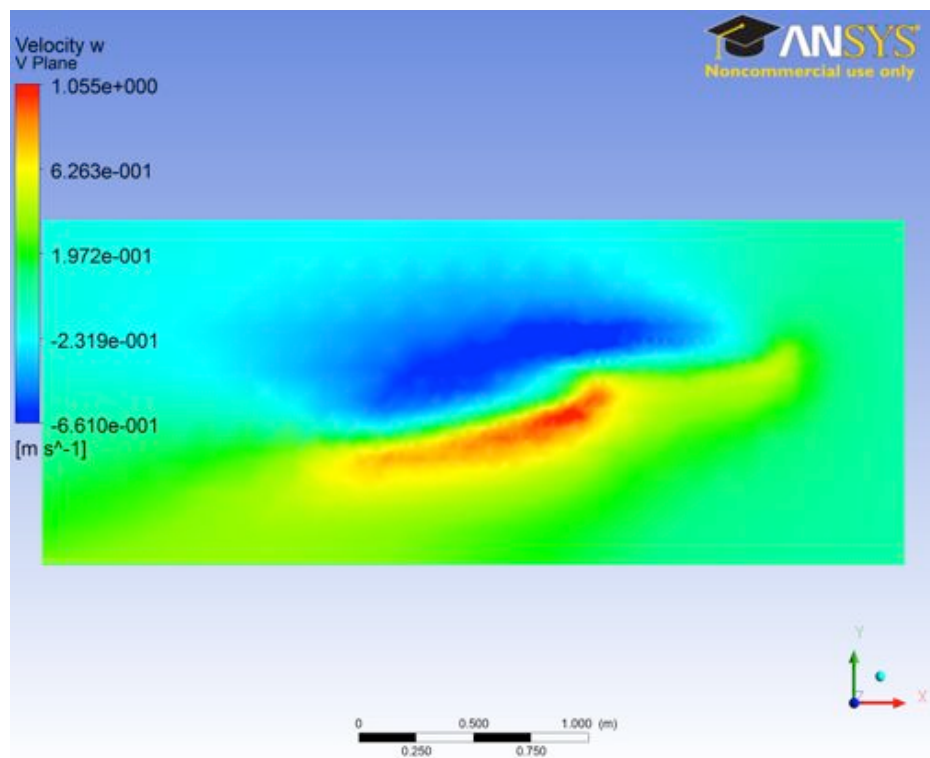


Figure 107: Cross section of transverse velocities at 120% of full span, configuration 1

A.5.1 Notes on conducting experiments using computational fluid dynamics

In attempting to produce an accurate simulation of the flow regime within the wind tunnel two meshing techniques, unstructured 3D tetra meshing and 3D block meshing, were attempted. The sail plan was modelled accurately using Maxsurf as a ‘.igs file’ surface, using the sail plan provided by Westbrook (2012). Had meshing been successful, the camber of the sails would have been accurately replicated using photographs of the sails taken during testing. Software from UKsails, ‘Accumeasure’, is available free online for this purpose. The geometry used to create the unstructured mesh is shown in Fig.108. The interior of the wind tunnel was accurately modelled, although it was considered that the effect of the octagonal, rather than square cross section modelled, was negligible.

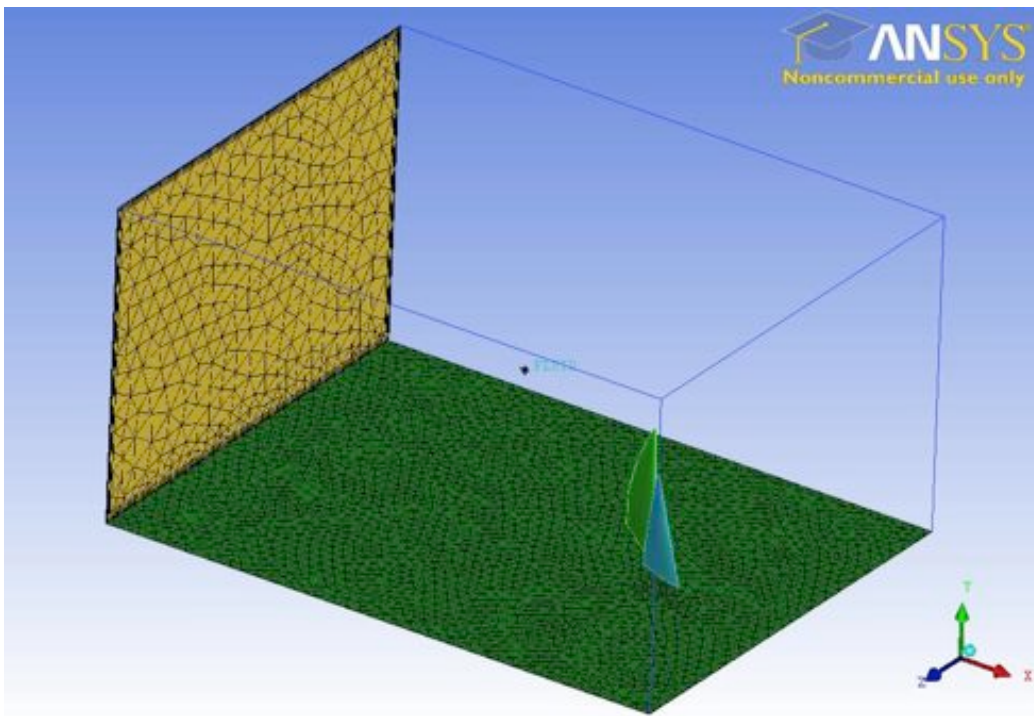


Figure 108: *Isometric view of the unstructured mesh geometry, showing sails in their correct position for the upwind condition. Mesh surfaces are shown on the outlet and floor*

A plan of the unstructured mesh showing the prism layers on no-slip walls, and the increased density around the sails is shown in Fig.109.

However, due to the negligible thickness of the sails, it was not possible to produce a mesh fine enough to converge over the geometry without exceeding the licence granted to student users. Consequently, the mesh did not converge over the geometry as shown in Fig.110.

As an alternative, a blocked mesh was attempted, a top view for which is shown in Fig.111. This converged around the geometry, however, due to the author’s in experi-

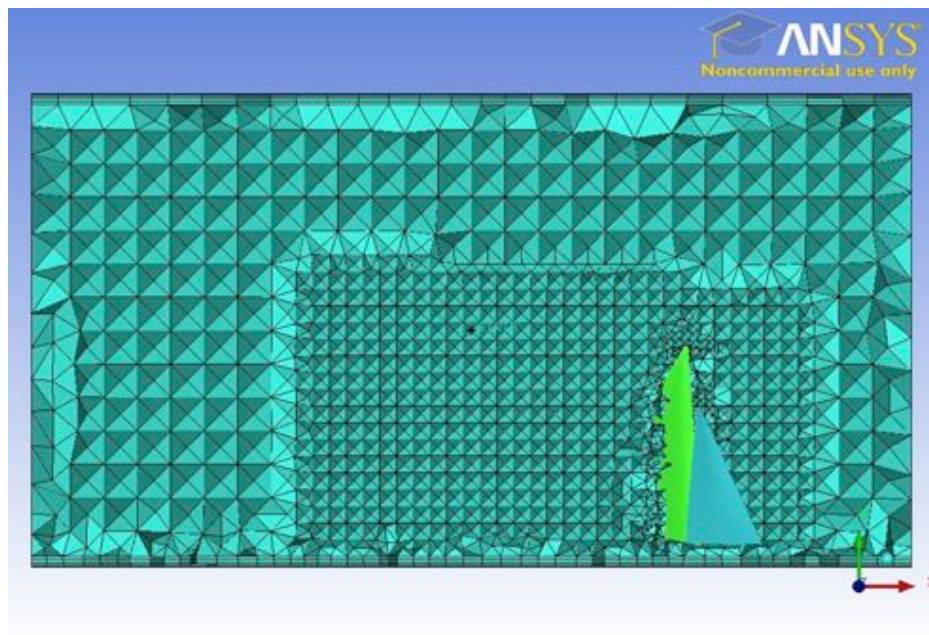


Figure 109: *Cross section of unstructured mesh with sails visible*

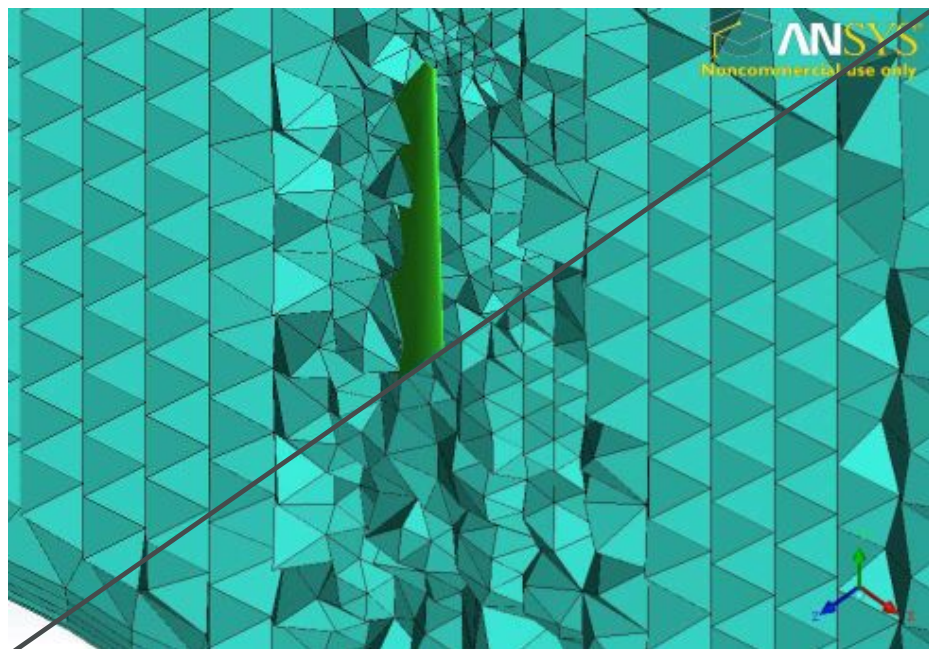


Figure 110: *Two detailed views of the mesh over the mainsail, top half of the image shows the sails visible, the lower half the sails are invisible. It can be seen that the mesh has not converged, and passes through the geometry*

ence at this technique, the coherence of the mesh was poor as shown in Fig.112, and simulation was not successful.

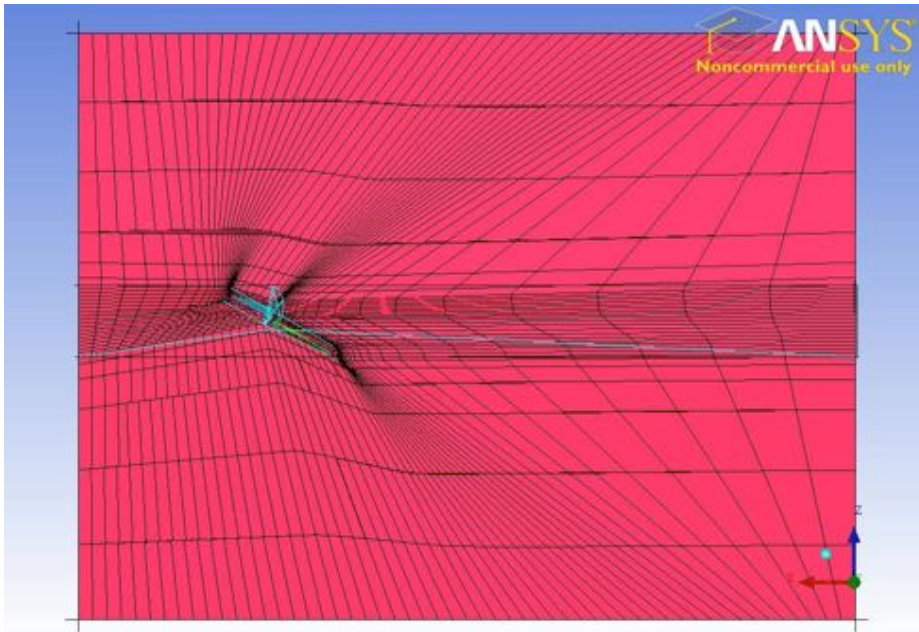


Figure 111: *Top view of the geometry meshed using the blocking technique. Note the high mesh densities around the edges of the sail which enabled convergence. However, these were poorly aligned leading to an incoherent mesh*

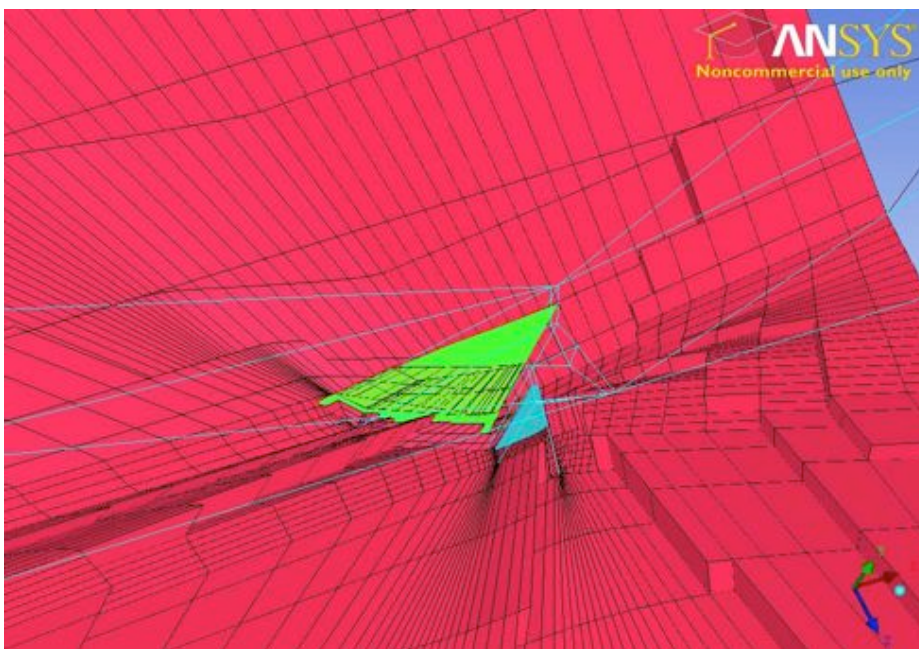


Figure 112: *Detailed view of the mesh around the head of the jib, showing the incoherence*

A.5.2 Global force data

Table 11 shows the global forces on the rig at full scale for each test condition. These forces are for a single wind speed of approximately 17.3 knots, in the upright condition. Where repeat tests were made the resultant force was averaged for ease of interpretation.

Table 11: *Table of average global forces on the rig*

| AWA (deg) | Af (deg) | Am (deg) | Df (N) | Hf (N) |
|-----------|----------|----------|----------|----------|
| 20.0 | 12.5 | 5.0 | 126.825 | 3310.176 |
| 20.0 | 20.0 | 5.0 | 149.200 | 3305.424 |
| 20.0 | 25.0 | 5.0 | -30.256 | 2640.196 |
| 30.0 | 12.5 | 5.0 | 700.928 | 5161.564 |
| 30.0 | 20.0 | 5.0 | 874.058 | 5427.223 |
| 30.0 | 25.0 | 5.0 | 843.175 | 4549.349 |
| 40.0 | 12.5 | 10.0 | 794.062 | 5325.535 |
| 40.0 | 20.0 | 10.0 | 1061.098 | 5513.378 |
| 40.0 | 25.0 | 10.0 | 1524.022 | 5473.863 |
| 50.0 | 20.0 | 10.0 | 1069.723 | 5775.799 |
| 50.0 | 25.0 | 10.0 | 2056.365 | 5529.794 |
| 50.0 | 25.0 | 15.0 | 794.062 | 5325.535 |
| 60.0 | 25.0 | 20.0 | 2145.382 | 5627.535 |
| 60.0 | 35.0 | 30.0 | 2447.733 | 4511.226 |
| 70.0 | 40.0 | 35.0 | 2461.632 | 3920.410 |
| 70.0 | 40.0 | 45.0 | 3207.586 | 3498.640 |
| 80.0 | 30.0 | 45.0 | 2641.162 | 3891.356 |
| 80.0 | 35.0 | 50.0 | 1794.584 | 3137.973 |
| 80.0 | 40.0 | 45.0 | 2148.979 | 3652.966 |
| 80.0 | 40.0 | 55.0 | 2390.267 | 3304.027 |
| 100.0 | 40.0 | 45.0 | 3309.212 | 3441.059 |
| 100.0 | 45.0 | 50.0 | 3439.114 | 2987.503 |
| 100.0 | 50.0 | 55.0 | 3730.598 | 2583.607 |
| 110.0 | 45.0 | 50.0 | 3937.129 | 2895.517 |
| 120.0 | 55.0 | 45.0 | 4672.192 | 2753.987 |
| 120.0 | 60.0 | 60.0 | 3500.045 | 1909.362 |
| 120.0 | 65.0 | 55.0 | 3946.250 | 2354.569 |
| 130.0 | 60.0 | 50.0 | 4407.054 | 2050.893 |

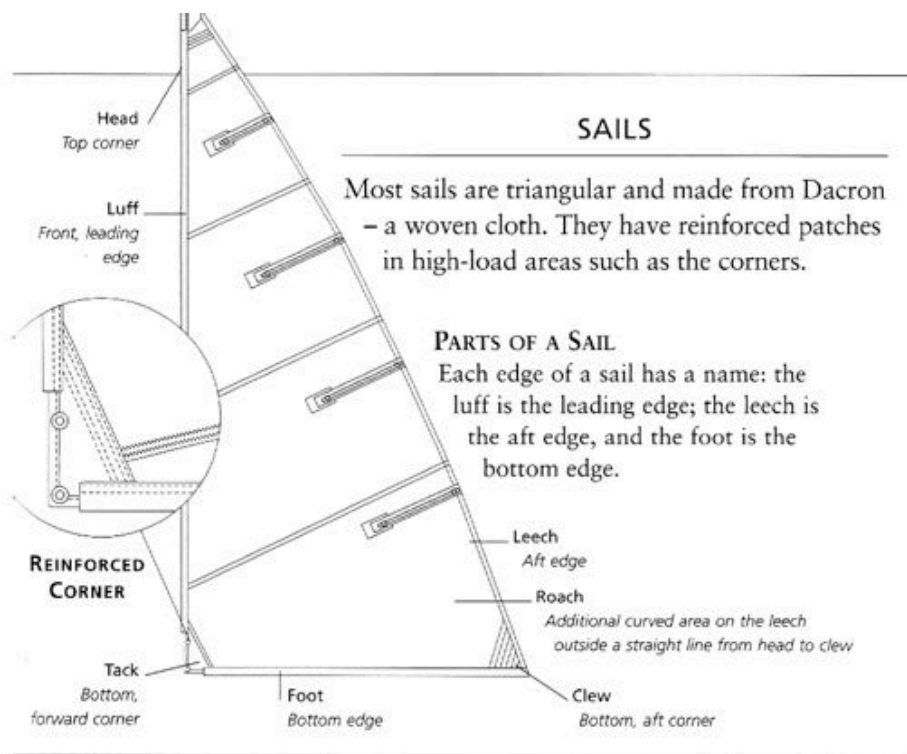


Figure 113: *Diagram of the parts of a sail to aid understanding of the glossary, taken from Slight (1999)*

A.6 Glossary

| | |
|---------------------|--|
| aerofoil | an object designed to produce lift |
| aft |towards the back of a vessel |
| angle of attack |see Fig.4 |
| apparent wind angle | angle between wind and ship as seen from the deck as opposed to true wind angle, as would be seen on a map |
| battens |flexible reinforcements on a sail |
| battens (wishbone) |exterior sail reinforcements, as shown in Fig.31 |
| beam | the width of a ship |
| bermudan | triangular sails |
| boom |horizontal support on the mainsail, holding it out and down |
| boundary layer |region of disturbed flow around an object |
| bow |the front of a vessel |
| camber | the curve or ‘belly’ of an asymmetric aerofoil |
| chord |distance from front to back of a wing |
| couple | two moments acting with or against each other |
| CFD | computational fluid dynamics |
| deck | the surfaces of a vessel on which the crew walk |
| dimensional (non) | a property which is independent of size |
| draft | the depth of a ship below the water |
| drag | force on an object parallel to the direction of flow over it |
| drag (induced) | drag caused by the production of lift |
| drag (parasitic) | drag caused by objects fixed around an aerofoil |
| foil |abbreviation of ‘aerofoil’ |
| fore | towards the front of a vessel |
| fore and aft | orientated along the centreline of a vessel |
| genoa | a sail large forward of the mast |
| gunter | a vertically sliding section at the top of a mast |
| gybe |change of a vessel’s direction while pointing away from the wind |
| heel | an angle of tilt to one side |
| jib | a small sail forward of the mast |
| Junk | a kind of sailing vessel native to the China seas, see Fig.15 |
| keel |an aerofoil beneath the water on a sailing vessel to prevent the vessel being blown sideways |
| kicking strap | diagonal rope holding down the boom, shown in Fig.38d |
| lacing |use of cord to attach sails to supports, shown in Fig.38a |
| leech | the trailing edge of a sail, see Fig.113 |
| leeward |the side of a vessel away from the wind |
| lift |force on an object at right angles to the direction of flow over it |
| luff | the leading edge of a sail, see Fig.113 |

- mainsail the largest sail, positioned aft of the mast
- mast rigid support for a sail
- moment a twisting or lever force
- NACA former national advisory committee for aeronautics, now NASA
- PDE partial differential equation
- rig the entire architecture of a sailing vessel's propulsion, including mast,
sails and all components
- roach sail area additional to a pure triangle, see Fig.113
- RANS Reynolds averaged navier stokes, see Appendix A.1.3
- Reynolds number a property of fluid, see Section 2.4
- sail cloth aerofoil used for the propulsion of sailing vessels
- sailing angle see Apparent Wind Angle
- sheeting angle the angle between a sail and the centreline of the vessel
- sloop one forward and one aft sail
- stay a cable, generally a wire, used to hold a part of the vessel in
position, for example a mast
- stern the back of a vessel
- streamlines theoretical path of a fluid as it moves through space
- tare tests calibrations for the forces on the experimental set up in wind
without sails
- transition see Section 2.4
- VPP velocity prediction program
- windward the side of a vessel from which the wind is blowing